PHILOSOPHICAL
TRANSACTIONS
— OF —

THE ROYAL
SOCIETY

A

MATHEMATICAL,
PHYSICAL
& ENGINEERING
SCIENCES

Stochastic Theory of the Nucleation of Quantized Vortices in Superfluid Helium

R. J. Donnelly

Email alerting service	Receive free email alerts when new articles cite this article - sign up in the box at the top right-hand corner of the article or click **here**

[41]

STOCHASTIC THEORY OF THE NUCLEATION OF QUANTIZED VORTICES IN SUPERFLUID HELIUM

By R. J. DONNELLY†

Department of Physics, University of Oregon, Eugene, Oregon 97403

AND P. H. ROBERTS‡

National Center for Atmospheric Research,§ Boulder, Colorado 80302

CONTENTS

The problem of the appearance of quantized vortex lines and rings in superflow, and the modification of that flow by the vortices, is examined in the light of a suggestion by Iordanskiĭ, namely that thermal fluctuations may play a vital role in the nucleation process. The view is taken that there exists a distribution of quantized vortex rings in liquid helium and that the smallest of these is a roton. The evolution of these rings in a counterflow is examined by means of a Langevin equation. A Fokker–Planck equation is developed, and a number of examples are presented which illustrate the features of such processes. These include nucleation of vortices in an unbounded fluid, nucleation in a finite channel, the thermally activated vortex mill, nucleation of vortices by ions and phonon–roton relaxation times.

1. INTRODUCTION

The problem of critical velocities in liquid helium has been under examination for many years. The first indication of a mechanism for limiting the velocity of pure superflow was Landau's idea that rotons could be produced at a boundary when the velocity of superflow coincided with a certain group velocity for rotons. This indicated a rather high velocity, of order 60 m/s, and such velocities in helium II are approached only in ion experiments well below 1 K. Flow experiments, on the other hand, exhibit critical velocities from centimetres per second to millimetres per second. When quantized vortices were first proposed by Onsager and Feynman, it appeared certain that these vortices, while insignificant thermodynamically, would exhibit dynamical effects which would limit velocities to the lower values more consistent with experimental observation. While there have been qualitative successes with such ideas, the quantitative agreement between theory and experiment has been disappointing, the general experience being that the calculated critical velocities are still too high. It appears, therefore, that the problem is much more complex than had been anticipated, and some key physical ideas are still lacking. For reviews of the subject of critical velocities the reader is referred to Vinen (1963).

Recently, Iordanskiĭ (1965), in an elegant discussion, drew attention to the importance of considering thermal fluctuations as a means of initiating vortex motion which can draw energy from a superflow and subsequently grow to alter that flow. Later, Langer & Fisher (1967) and Fisher (1968), stimulated by experiments on the decay of persistent currents (Kukich, Henkel & Reppy 1968), emphasized the possible role of vortex nucleation by fluctuations in the decay of such supercurrents. An illuminating summary of this point of view has recently appeared (Langer & Reppy 1970).

The purpose of this paper is to develop the theory of fluctuations of quantized vortices from first principles and apply it to a number of suitable problems. The plan is as follows: We examine in §2 the notion of distributions of quantized vortex rings in helium II and discuss the possibility that the roton branch actually represents the low momentum end of the ring spectrum. We develop in §3 a Langevin equation for vortex rings, identify the relevant physical parameters, and from this develop a Fokker–Planck equation. Formulae for the diffusion of rings over a barrier are then developed by analogy to solutions given earlier by us (Donnelly & Roberts 1969 a).

Section 4 is devoted to an examination of spontaneous vortex production in an unbounded fluid, the Iordanskiĭ problem. It is shown that this theory in its simplest form cannot account for the observed features of the decay of persistent currents. There is a possibility that the failure to agree with experiment arises from random lengths of vortex line pinned to protuberances in the channels. The theory of thermal activation of such vortices, first postulated by Glaberson & Donnelly (1966), is examined in §5.

The effect of boundaries on nucleation is developed in §6. This leads to an interpretation of

depressed λ-points in narrow channels or, more properly, to the concept of an onset temperature T_0 for superflow. In an unbounded channel, T_0 coincides with the λ-transition. In a finite channel T_0 may be considerably lower than T_λ owing to fluctuations of vortex rings. When flow is added to the problem, the concept of the onset temperature has to be generalized. An interpretation of some history-dependent effects in superfluidity may be given by speculating the presence of vortex lines on the boundaries, whose density may depend on the preparation of the flow, and which affect the motion far from the walls.

Another important class of nucleation experiment is the formation of vortex rings by ions. We develop in § 7 the notion of localization of rotons near a moving ion and observe that these rotons dramatically increase the drag on the ion. The probability that one of these rotons may grow to critical size and nucleate an ion-ring complex is evaluated and compared extensively with available experimental information. Here, unlike the channel flow problem, agreement with experiment is quite striking.

The conversion of rotons to phonons by means of fluctuations is considered in § 8. This phenomenon is one contributing factor in the attenuation of sound in helium II. The calculations provide an alternative to the well-known collision studies of Khalatnikov.

The numerical work in this paper rests on many parameters, not all known to the accuracy one could desire. We present the values we have adopted in an appendix, together with the source of each estimate.

Throughout this paper we proceed in such a way as to try to minimize the number of new assumptions. We have, for example, specifically not included entropy contributions to vortex nucleation, which may be important, but which are (with the exception of the vortex wave entropy at low temperatures) still a matter of considerable speculation. In the same spirit we have adopted a vortex core radius of $a = 0.128$ nm throughout, even though much evidence is present to tell us that a is a function of temperature, pressure and perhaps even ^{3}He concentration. For example, a model advanced by Glaberson, Strayer & Donnelly (1968) calculates the radius, R_c, at which the energy gap vanishes. This model suggests that R_c increases as T increases and as the pressure P increases, but the details depend upon the magnitude of roton–roton interaction assumed. Values which appear reasonable at the time of writing are $R_c = 0.212$ nm at $T = 0$ K, 0.294 nm at 1.0 K, 0.522 nm at 1.8 K and 1.22 nm at 2.1 K. Larger values of a will lower the free energy barrier for nucleation and tend to improve the agreement with experiment. Nevertheless, the uncertainty in both core entropy and core radius and their specific application to nucleation theory compels us to leave the theory incomplete in these essential aspects.

Preliminary and highly condensed accounts of some of the topics discussed in detail below have appeared elsewhere (Donnelly & Roberts 1969 b, c; Roberts & Donnelly 1970 a, b; Strayer, Donnelly & Roberts 1971).

2. Rotons and quantized vortex rings

(a) Dispersion relations

We postulate that helium II contains a distribution of quantized vortex rings of all shapes and sizes, oriented at random but carried on the moving superfluid. The smallest of these rings will be those whose radius R approaches the radius a of the core. Since this radius is known to be of the order of 0.1 nm, quantum effects are likely to become very important. In particular, since the healing length for the wavefunction of the superfluid is also of order 0.1 nm, further reductions

in R will result in an *increase* in total energy owing to quantum localization effects. If we assume the minimum energy of these rings is E_m, and the momentum corresponding to E_m is p_m, the number of such rings in thermal equilibrium can be computed by elementary statistical methods. The population of states beyond E_m will be filled by thermal collisions. The calculation we have just described is identical to the calculation of the density of rotons in the superfluid if we take $E_m = \Delta$ and $p_m = p_0$ in the usual notation. The idea that the ring spectrum should join the roton dispersion branch is not new, and has been discussed in detail by Feynman (1955). The association of rotons with rings has been taken to be literally true in this paper in order to make numerical estimates quite definite, but no essential changes would result if Δ were replaced by E_m, and p_0 by p_m everywhere. We shall return to this point later.

There is no firm experimental evidence from neutron studies on the evolution of the dispersion relation beyond $p/\hbar \simeq 37\,\mathrm{nm}^{-1}$. The present data are summarized in figure 1, where the neutron measurements are shown as solid lines (cf. Woods 1966; Cowley & Woods 1971). The lower branch is the familiar Landau spectrum with phonons near D and rotons near A. Beyond E the scattered neutron line width becomes too broad to follow. The upper branch appears to belong to free particle excitations. At high energies the data points appear to join the parabolic dashed curve, which represents free particles with the mass of the helium atom (Harling 1970).
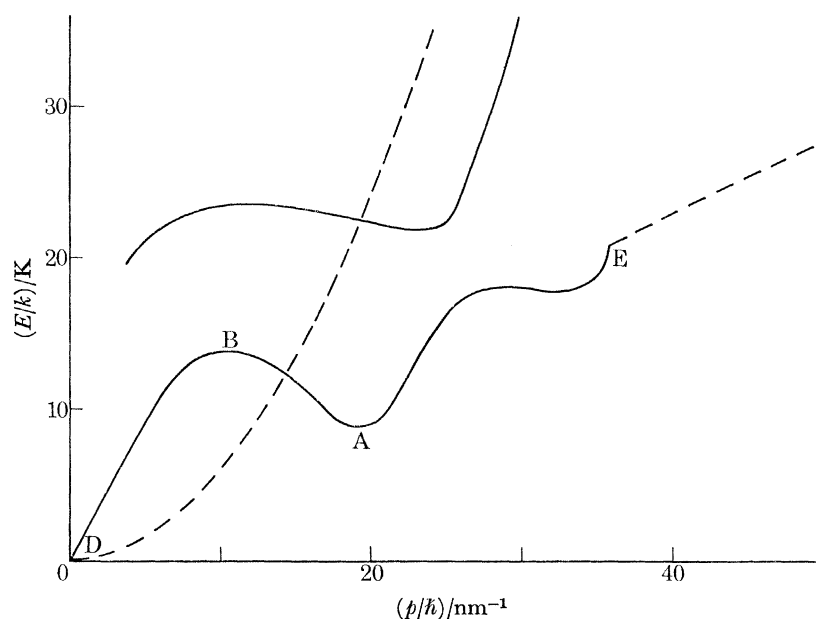
FIGURE 1. Energy-momentum relation for quasi-particles in helium II. The solid lines are determined experimentally by neutron scattering. The dashed line on the left corresponds to free excitations having the mass of a helium atom. The dashed curve on the right corresponds to vortex rings as given by equations (2.1) and (2.2).

Figure 1 presents data on the energy-momentum relation for excitations of the liquid which are microscopic and devoid of thermal content. If we wish to join the branch DAE to a branch of vortex rings, we must decide what quantities to plot on the same diagram. The variable which plays the role of momentum for vortex rings is the impulse, p,

$$p \equiv \rho_s \kappa \pi R^2, \tag{2.1}$$

where ρ_s is the superfluid density, R is the radius of the vortex ring and $\kappa(\equiv h/m)$ is the quantum

of circulation, m being the mass of the ^{4}He atom. An experimental demonstration of the connexion between p and the usual notion of momentum of a particle has been given recently (for large† vortex rings) by Gamota & Barmatz (1969).

The question of the energy and velocity of a vortex ring is more complex, and forms the subject of a paper on vortex structure which will be published separately (Roberts & Donnelly 1971). One problem is that the energy and velocity of vortex rings given by the classical expressions are not, at first sight, connected by the Hamilton equation $v = \partial E/\partial p$ (see, for example, Rayfield & Reif 1964). It turns out that these expressions are correct, but only under the assumption of constant core volume. Experiments in liquid helium, however, are usually carried out at constant pressure, and Roberts & Donnelly (1970a) show in that case that the energy and velocity of a vortex ring of radius R and core radius a are given by

$$E = \tfrac{1}{2}\rho_s\kappa^2 R[\ln(8R/a) - \tfrac{3}{2}], \qquad (2.2)$$

and
$$v = (\kappa/4\pi R)\,[\ln(8R/a) - \tfrac{1}{2}], \qquad (2.3)$$

if we assume that the core is hollow, and that $a \ll R$. Under conditions of constant pressure and temperature, a is a constant, and $v = \partial E/\partial p$. On this model, the energy in (2.2) is made up of the kinetic energy of motion of the superfluid about the core, plus the potential energy arising by displacement of fluid at constant pressure when the radius of the ring, and hence the volume of the core, is changed. This model appears to be the simplest one can adopt, and we have used it throughout this paper unless otherwise stated. If we re-analyse the experimental data of Rayfield & Reif (1964), we find that the core radius on this model should be

$$a = 0.128 \pm 0.013\,\text{nm} \quad (T = 0.28\,\text{K}). \qquad (2.4)$$

The two terms in square brackets in (2.2) may be regarded as the leading terms of an expression in a/R involving both powers and logarithms. Beyond the terms shown, it is not correct to consider the cross-section of the vortex core to be circular. Recently Fraenkel (1970, 1971, private communication) has obtained a rigorous expansion procedure for the flow structure in the small a/R limit, and has shown that (2.3) holds over a larger range of a/R than one might, at first sight, expect.†

We show, by the dashed line on the right of figure 1, the energy and momentum of vortex rings given by (2.2), (2.1) and (2.4). The low momentum part of the ring spectrum joins the neutron data near E just where the neutron experiments show a vanishing scattering cross-section. The vanishing cross-section is, perhaps, not too surprising, for near E we begin a régime of completely different dynamics: to the left of E we have wavelengths given by $\lambda = h/p$, to the right we have a typical dimension R given by $(p/\rho_s\kappa\pi)^{\frac{1}{2}}$. The wavelength of the neutron probe is

---

† Since the core of the vortex is not circular to these higher orders, a and R must be re-defined, it being natural to choose R as the mean of the nearest and furthest point of the core from the axis of symmetry, and a as $\sqrt{(A/\pi)}$ where A is the cross-sectional area of the core. Strictly, the result

$$v = (\kappa/4\pi R)[(\ln 8R/a - \tfrac{1}{4}) - \tfrac{3}{8}(a/R)^2\,(\ln 8R/a - \tfrac{5}{4}) + \dots] \quad (a/R \to 0)$$

obtained by Fraenkel does not refer to the hollow vortex, but to the 'uniform' model in which the vorticity of each core element is proportional to its distance from the axis of symmetry. As a/R increases, the vortex core, Fraenkel showed, becomes increasingly semicircular in shape $[A = \tfrac{1}{2}\pi(2R)^2$, i.e. $a/R = \sqrt{2}]$, and the flow increasingly resembles that of the spherical vortex of Hill (1894) for which $v = 4\kappa/15\pi R \approx 0.267(\kappa/\pi R)$. Even though one might not expect the expansion of v displayed above to be reliable at such large values of $a/R(=\sqrt{2})$, it is in fact found that the first (bracketed) term gives $v = 0.370(\kappa/\pi R)$, i.e. less than 40 % too large while the full expansion shown gives $v = 0.281(\kappa/\pi R)$, i.e. less than 5 % too large. The agreement is remarkable. For smaller values of a/R it is, of course, even better.

decreasing with increasing p and soon becomes less than the interatomic spacing. It would seem that the probability of exciting a vortex ring of size much larger than the neutron wavelength would be small. The coincidence shown at E in figure 1 appears to strengthen the idea that rotons and vortex lines may belong to the same branch. No experimental evidence seems to be in conflict with the idea at present, but we should emphasize that, even if the two branches are disjoint, our calculations are still valid if $|E_m - \Delta|$ is small.

One further problem, of importance above 1 K, should be mentioned here. Glaberson *et al.* (1968) have shown that the core of a vortex in He II likely contains normal fluid, perhaps a material like He I. On changing the length of the vortex core, heat will have to flow from the bath into the newly formed core, implying that there is, effectively, a latent heat associated with the creation of more vortex core. This heat energy will add to the internal energy of a vortex, but since it flows into and out of the core at constant pressure and temperature, it is not connected with changes in energy by outside agents (such as forces which produce an impulse). In the usual way, then, we can speak of a free energy whose changes coincide with the changes in the energy E we have quoted for the hollow vortex. Thus the entropy associated with the core would not appear to affect the regular dynamic behaviour of a vortex ring. It may, however, influence the nucleation process and we shall return to this possibility in § 3. In the context of the present discussion, the energy for vortex rings, plotted as E in figure 1, is the free energy given by (2.2); and the momentum p is the impulse given by (2.1). The group velocity is everywhere $v = \partial E/\partial p$.

So far our discussion has been semi-classical, but it is worth noting here that the structure of the circular vortex in a Bose condensate has recently been examined by Roberts & Grant (1971) in the small a/R limit. They were able to show, in agreement with speculations by Donnelly & Roberts (1969*a*), that the energy of the ring coincided with (2.2) provided the 1.5 was replaced by 1.62. It was also demonstrated rigorously that the Hamiltonian relation $v = \partial E/\partial p$ was obeyed to the same accuracy.

It is important to keep in mind that any experimental determination of a is predicted on the assumption of a particular core structure, and, if another core structure is found more convenient, the same dynamical properties can be secured by changing a appropriately.† In this sense, our findings are not dependent on the choice of a core model. One more precaution should be raised at this point. The theory assumes that the smallest rings (proto-rings) grow by diffusion to a critical size. Since the barrier which is traversed may be as high as $80\,kT$, it takes the cooperation of a large number of excitations to produce the initial fluctuation. The initial stages of growth of a proto-ring must be complex indeed, and there is little chance that we could follow in detail the evolution of a given roton into a ring. This classical uncertainty would appear to reflect the quantum uncertainty which one would expect to find if a wavefunction description could be used throughout. What is important in nucleation theory is the beginning and critical states: the details in between are irrelevant. Our choice of a roton as the beginning state is, as we have remarked above, largely a matter of presenting a definite model.

(*b*) *The effect of superflow*

The free energy surface in momentum space which concerns us is sketched in figure 2*a*, showing the roton minimum and the vortex ring branch joined together with no particular attention paid to the details of the region near E in figure 1. The authors have shown (Donnelly & Roberts 1969*a*)

† This is not, of course, true at higher levels of expansion in a/R, such as, for example, that shown in the footnote on p. 45.

that, for purposes of the escape over barriers, the principal points of interest are the lowest and highest points on the energy surface.

When a steady superflow is applied to the spectrum of excitations shown in figure 2*a*, the energy will shift according to a Galilean transformation. We adopt a frame of reference at rest with respect to the normal component and accordingly the energy of a ring is

$$F = E + \boldsymbol{p} \cdot \mathbf{v}_{\mathrm{s}}, \tag{2.5}$$

where we adopt the symbol F for the transformed free energy which is prevalent in the literature on liquid helium. The group velocity of the ring relative to the normal fluid is $\mathbf{v}$:

$$v_1 = \frac{\partial F}{\partial p_1} = \frac{\partial E}{\partial p_1} + v_{\mathrm{s}1} = v_{\mathrm{L}1} + v_{\mathrm{s}1}, \tag{2.6}$$

where $\mathbf{v}_{\mathrm{L}}$ is the self-induced velocity of the vortex line. The minimum value of F occurs at $\mathbf{v}_1 = 0$ corresponding, of course, to the fact that the corresponding vortex rings are the rotons near A in figure 2*b*. The maximum in F, occurring near C in figure 2*b*, defines *the critical vortex* which is also stationary with respect to the normal fluid ($v_1 = 0$, $v_{\mathrm{L}1} = -v_{\mathrm{s}1}$) and represents a relatively large vortex ring polarized against the superflow. The difference in energies between A and C is *the energy barrier* ΔF. Its magnitude is the primary factor in determining the nucleation rate.
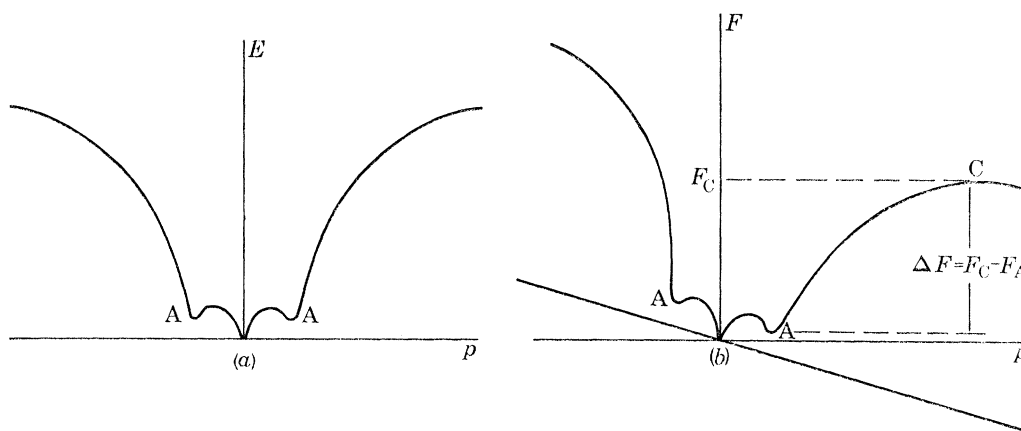

FIGURE 2 (*a*). Section through the free energy surface in momentum space of a dispersion curve with a connected ring branch. The roton 'trough' is at A.   (*b*) Section through the free energy surface in momentum space of a dispersion curve with a connected ring branch, and in the presence of superflow of velocity given by the slope of the straight line through the origin. The critical vortex is at the saddle point C. The free energy barrier for formation of a critical vortex is ΔF.

The growth of a roton which passes from A to C in figure 2*b* is the result of thermal fluctuations. Beyond C, a vortex ring can grow in momentum, i.e. radius, and yet reduce its free energy F. The energy to accomplish this growth must come either from the flow itself or from external fields: we shall encounter examples of each case. The ring will continue to grow until it meets a boundary, or until the frictional forces balance the driving force.

The rate of escape of rotons from A to C may be determined by the theory to be outlined in § 3. This theory, as we have mentioned above, is essentially independent of the shape of the barrier except near A and C. For this reason we make no effort to account for any structure in the potential hill between A and C; we assume only that these points lie on a connected branch and have no minima lower than A. The phonons, of course, have a minimum lower than A; presumably fluctuations over the barrier B (figure 1) adjust the relative populations of phonons and

rotons to their equilibrium values, and in the presence of sound waves these phonon–roton conversions will contribute to the attenuation of sound. We shall consider this in more detail in § 8.

3. The Langevin and Fokker–Planck equations for ring production in a counterflow; calculations of the probability of nucleation

(a) *The Langevin and Fokker–Planck equations*

A vortex ring which serves as a scatterer for another quasi-particle will often suffer a change in its momentum. Since the dimension R of a ring will (except for the smallest rings near A in figure 2) be much greater than the wavelength of the quasi-particle, we expect that the change in ring momentum resulting from the impact will be small compared with the total momentum p of the ring. It is, therefore, permissible to use the formalism of Brownian motion theory to discuss vortex rings (Chandrasekhar 1943). We divide the stochastic effects of collisions of rotons, and indeed all quasi-particles, rotons, phonons and dissolved ^{3}He atoms, into two parts: the systematic 'dynamical friction' created by the preferential direction of quasi-particle impact associated with the ring's persistent motion relative to the quasi-particle gas, and the remaining stochastic force, A_1, which is random in direction. The drag force on a segment of vortex line is supposed to be proportional to the length of line and to the drift velocity relative to the normal fluid. The resulting Langevin equation may be written

$$\frac{\mathrm{d}p_1}{\mathrm{d}t} = -\varLambda(\boldsymbol{p})\frac{\partial F}{\partial p_1} + A_1(\boldsymbol{p}, t), \tag{3.1}$$

where

$$\varLambda(\boldsymbol{p}) = 2\pi DR = 2\left(\frac{\pi}{\kappa\rho_{\mathrm{s}}}\right)^{\frac{1}{2}} Dp^{\frac{1}{2}} = \beta p^{\frac{1}{2}}, \tag{3.2}$$

say, and D is the drag coefficient per unit length of vortex line. The evaluation of β will be described in more detail in the appendix. The coefficient $\varLambda$ has the dimensions MT^{-1} whereas β^2 has the same dimensionality as D, namely, $\mathrm{ML}^{-1}\mathrm{T}^{-1}$.

Let Δt be a time so short that the change $\Delta\boldsymbol{p}$ in $\boldsymbol{p}$ during Δt is small. It is clear that $\Delta\boldsymbol{p}$ will be composed of two parts, corresponding to a systematic deceleration $\varLambda(\boldsymbol{p})\,(\partial F/\partial p_1)\,\Delta t$ due to the dynamical friction, and a diffusive part $\boldsymbol{B}(\Delta t)$, where

$$\boldsymbol{B}(\Delta t) = \int_t^{t+\Delta t} \boldsymbol{A}(\boldsymbol{p}, t)\,\mathrm{d}t, \tag{3.3}$$

is due to the random collisions. Since $\boldsymbol{B}$ is stochastic in origin it is not possible to evaluate it explicitly; all that can be done is to obtain its probability distribution $\varPsi(\boldsymbol{B})$. Even this is impractical unless we suppose that Δt is large compared with the mean collision time of quasi-particles with the ring. In this case $\boldsymbol{B}$ is composed of a large number of random forces which means, therefore, that $\varPsi$ must be Gaussian and isotropic:

$$\varPsi(\boldsymbol{B}) = \frac{1}{(4\pi q\,\Delta t)^{\frac{3}{2}}} \exp\left[\frac{-B^2}{4q\,\Delta t}\right], \tag{3.4}$$

where $q(\boldsymbol{p})$ is a diffusion constant depending on the cross-section presented by the ring, in a way which should be made clearer below. Since by (3.1) and (3.3) the net change $\Delta\boldsymbol{p}$ in $\boldsymbol{p}$ during the interval Δt is

$$\Delta p_1 = -\varLambda(\boldsymbol{p})\,(\partial F/\partial p_1)\,\Delta t + B_1(\Delta t), \tag{3.5}$$

we may obtain directly the probability $\psi(\boldsymbol{p}, \Delta\boldsymbol{p})$ that a vortex ring of momentum $\boldsymbol{p}$ should, during the interval Δt, receive a change in momentum of $\Delta\boldsymbol{p}$: it is

$$\psi(\boldsymbol{p}, \Delta\boldsymbol{p}) = \Psi(\Delta p_1 + \Lambda(p)\,(\partial F/\partial p_1)\,\Delta t). \tag{3.6}$$

The first two moments of this distribution are readily seen to be

$$\langle \Delta p_1 \rangle = -\Lambda(\partial F/\partial p_1)\,\Delta t, \tag{3.7}$$

$$\langle \Delta p_i \Delta p_j \rangle = 2q\,\Delta t\,\delta_{ij} + O(\Delta t)^2. \tag{3.8}$$

Now let $w(\boldsymbol{p}, t)\,\mathrm{d}\boldsymbol{p}$ be the probability per unit volume at time t for the occurrence of a vortex ring in the momentum range $\boldsymbol{p}$ to $\boldsymbol{p} + \mathrm{d}\boldsymbol{p}$. Under the assumptions already made (e.g. that w does not evolve significantly during one collision time) we have

$$\frac{\partial w}{\partial t} = \frac{\partial}{\partial p_1}\left[-\frac{\langle \Delta p_1 \rangle}{\Delta t}w + \frac{1}{2}\frac{\langle \Delta p_i \Delta p_j \rangle}{\Delta t}\frac{\partial w}{\partial p_j} \right] \tag{3.9}$$

(see, for example, Chandrasekhar 1943, ch. 2, §4). From (3.7) and (3.8) this Fokker–Planck equation is, in the present instance,

$$\frac{\partial w}{\partial t} = \frac{\partial}{\partial p_1}\left[\Lambda\frac{\partial F}{\partial p_1}w + q\frac{\partial w}{\partial p_1} \right]. \tag{3.10}$$

Thermodynamics tells us that (3.10) must possess the steady-state Maxwell–Boltzmann solution

$$w = w_0 \exp(-F/kT), \tag{3.11}$$

where w_0 is a normalization constant. On substituting (3.11) into (3.10), we can evaluate the diffusion constant $q(\boldsymbol{p})$, obtaining

$$q = \Lambda kT = \beta(\boldsymbol{p})\,p^{\frac{1}{2}}kT, \tag{3.12}$$

showing that (3.10) may be written as

$$\frac{\partial w}{\partial t} = \frac{\partial}{\partial p_1}\left[\Lambda kT\left(\frac{\partial w}{\partial p_1} + \frac{w}{kT}\frac{\partial F}{\partial p_1}\right) \right]. \tag{3.13}$$

The Einstein equation (3.12) makes physical sense, for the magnitude of the force $-\Lambda\mathbf{v}$ in (3.1) indicates that the cross-section presented by the vortex line to the *directed* collisions associated with the dynamical friction is proportional to Λ. [Note that, according to (3.2), Λ is indeed proportional to $2\pi R$, the length of vortex line.] This suggests that the total number, N, of *random* collisions occurring in the time Δt should be proportional to Λ and, of course, to T. But, since the collisions are random, the net increase they produce in Δp_i should be proportional to the random walk, i.e.

$$(\Delta p_1)_{\mathrm{r.m.s.}} \propto N^{\frac{1}{2}} \propto (\Lambda kT)^{\frac{1}{2}} \propto q^{\frac{1}{2}},$$

as indeed (3.8) implies.

(b) The role of neighbouring states

The derivation of the Fokker–Planck equation (3.9) has implicitly supposed that only circular vortex rings of momentum $\boldsymbol{p}$ and energy F need be considered, and $w(\boldsymbol{p}, t)\,\mathrm{d}\boldsymbol{p}$ has been defined as the probability per unit volume of the occurrence of such a ring in the momentum range between $\boldsymbol{p}$ and $\boldsymbol{p} + \Delta\boldsymbol{p}$. There are, however, a considerable number of neighbouring states which are as effective in nucleation as the circular ring, namely the perturbed states in which a wave motion of small amplitude is superimposed on its circular form. Indeed, one must expect that the random

collisions will continually excite such waves and that the circular ring is the exception rather than the rule. It is also conceivable that the vortex may nucleate at a slow enough rate to acquire a normal core (Glaberson *et al.* 1968). In that case the definition of a neighbouring state may well have to be extended to include standing compressional waves about the normal core. Provided the time scale for relaxation of these internal degrees of freedom is sufficiently short compared with the nucleation time, this multiplicity is easily allowed for by assigning to the circular ring of momentum p a statistical weight $\Gamma(p)$ and including all neighbouring states in the definition of w. It follows that (3.11) must be replaced by

$$w = w_0 \Gamma \exp\left(-F/kT\right), \tag{3.14}$$

which must, in a similar way, be a solution of the new Fokker–Planck equation for the w just defined. It is plausible (and indeed correct, see Iordanskiĭ 1965) that the modified form of (3.10) will now read

$$\frac{\partial w}{\partial t} = \frac{\partial}{\partial p_1}\left[\varLambda \frac{\partial F}{\partial p_1}w + q\Gamma\frac{\partial}{\partial p_1}\left(\frac{w}{\Gamma}\right)\right], \tag{3.15}$$

or, using (3.12)

$$\frac{\partial w}{\partial t} = \frac{\partial}{\partial p_1}\left[\varLambda kT\left(\frac{\partial w}{\partial p_1} + \frac{w}{kT}\frac{\partial \bar{F}}{\partial p_1}\right)\right], \tag{3.16}$$

where

$$\bar{F} = F - TS \quad \text{and} \quad S = k\ln\Gamma. \tag{3.17}$$

If (3.14) is written in the form $\qquad w = w_0 \exp\left(-\bar{F}/kT\right), \tag{3.18}$

it clearly satisfies (3.16).

The question about the validity of combining neighbouring states into the weight Γ involves consideration of time scales. The time scale of the vortex wave on a circular ring which is thermo-dynamically important is $\tau \approx \hbar/kT (\approx 7 \times 10^{-12}\,\mathrm{s}$ at, say, 1.1 K). This corresponds to the period of a vortex wave on the ring of wavelength $(\kappa\tau/4\pi)^{\frac{1}{2}}$, approximately, or a few tenths of a nanometre at 1 K. The time scale τ should be compared with the mean time, τ_d, taken to create a critical ring by collisions. Ignoring the momentum of the proto-ring compared with the momentum p_c of the critical state, τ_d is the time necessary to diffuse a 'distance' p_c in momentum space, namely $p_c^2/q = p_c^{\frac{3}{2}}/\beta(p_c)\,kT$. For a ring of radius 5 nm at 1.1 K, we obtain $\tau_d \approx 1.8 \times 10^{-5}\,\mathrm{s}$, which is indeed large compared with τ.

Note that the presence of entropy modifies some of the conclusions of § 2. The critical fluctuation is now one at which $\bar{F}$ is stationary and since, in general, $\partial S/\partial R$ will not vanish, this will occur at a different momentum from that defined by (2.6). In fact, by (3.17) we replace (2.6) by

$$v_1 = \frac{\partial \bar{F}}{\partial p_1} = \frac{\partial E}{\partial p_1} - T\frac{\partial S}{\partial p_1} + v_{\mathrm{s}1} = v_{\mathrm{L}1} - T\frac{\partial S}{\partial p_1} + v_{\mathrm{s}1}, \tag{3.19}$$

and the critical fluctuation, given by $v_1 = 0$, is characterized by $v_{\mathrm{L}1} = T(\partial S/\partial p_1) - v_{\mathrm{s}1}$. This ring has a velocity $T(\partial S/\partial p_1)$ with respect to the normal fluid.

One should note further that the appearance in (3.17) of the quantity $F - TS$ introduces an extra factor $\exp\left(S/k\right)$ in w, which reflects the density of states at the saddle point C of figure 2 (b) at the moment of nucleation.

(c) Analogies among stochastic equations

Before proceeding to make use of the Fokker–Planck equation for vortex rings, it is profitable to understand the correspondences between quantities such as the diffusivity which enter the equations in configuration space and in momentum space. In doing so we shall refer to the

article by Chandrasekhar (1943) as C., and our earlier paper on ions, Donnelly & Roberts (1969a), as D.R.

Chandrasekhar deals with the velocity $\boldsymbol{u}$, but since impulse is more fundamental to us, we will use $\boldsymbol{p}$. The present probability distribution $w(\boldsymbol{p}, t)$ corresponds to Chandrasekhar's distribution $W(\boldsymbol{u}, t)$. The dynamical friction is defined in C. by saying that $\langle \Delta u_i \rangle$, an average over a period of time short compared with that over which $W(\boldsymbol{u}, t)$ evolves, is $-\beta u_i \Delta t$. [The reader should not confuse the dynamical friction recalled here for comparison with C. and D.R. with the diffusion coefficient $\beta(\boldsymbol{p})$ of the present paper.] We define the corresponding quantity by a similar average, $\langle \Delta p_1 \rangle = -\Lambda (\partial F / \partial p_1) \Delta t$. On the assumption that β is constant, Chandrasekhar obtains

$$\frac{\partial W}{\partial t} = \frac{\partial}{\partial u_1} \left[\beta \left(u_1 W + \frac{kT}{m} \frac{\partial W}{\partial u_1} \right) \right], \tag{3.20}$$

a result which remains true if $\beta = \beta(u_1)$. The coefficient kT/m was determined by saying that $W = \exp(-mu^2/kT)$ must be a steady-state solution. By analogy we have equation (3.12) with kT being fixed by similar considerations. From (3.13), the flux of rings per unit 'area' in momentum space per unit time is

$$j_1 = -\Lambda \left[\frac{\partial F}{\partial p_1} w + kT \frac{\partial w}{\partial p_1} \right]. \tag{3.21}$$

Compare now with Smoluchowski's equation [C., (312)]

$$\frac{\partial w}{\partial t} = \frac{\partial}{\partial x_1} \left[\frac{1}{\beta} \left(\frac{\partial V}{\partial x_1} w + \frac{kT}{m} \frac{\partial w}{\partial x_1} \right) \right], \tag{3.22}$$

where Chandrasekhar's $\boldsymbol{K}$, a body force per unit mass, has been replaced by $-\nabla V$. The independent variables in (3.22) are coordinates in configuration space rather than in velocity space (as in 3.20) or momentum space (as in 3.13). The associated flux is therefore [cf. D.R. (105)]

$$j_1 = -\frac{1}{\beta} \left[\frac{\partial V}{\partial x_1} w + \frac{kT}{m} \frac{\partial w}{\partial x_1} \right]. \tag{3.23}$$

The relation between coefficient of diffusion D and β is given by [cf. D.R., (104)]

$$\frac{1}{\beta} = \frac{m}{kT} D. \tag{3.24}$$

The analogous identification is best seen by contrasting the last term of (3.13) or (3.21), namely $\Lambda kT(\partial w/\partial p_1)$, with those of (3.22) or (3.23), namely $(kT/\beta m) \partial w/\partial x_1$. Clearly the correspondence is

or

$$\left. \begin{aligned} \Lambda &\sim \frac{1}{\beta m} = \frac{D}{kT}, \\ D &\sim \Lambda kT. \end{aligned} \right\} \tag{3.25}$$

Another point of comparison is in energy. In our earlier paper V is the potential per unit mass whereas here F is energy. The correspondence is

$$F \sim mV. \tag{3.26}$$

(d) Calculation of the probability of nucleation

We turn now to the calculation of the probability of diffusion of a ring from A to C in figure 2b. This can be done by applying a modified form of the theory developed earlier (D.R., §4) for the escape of Brownian particles over a potential barrier. The modifications required are of two kinds.

First, the case treated in D.R. was a two-dimensional barrier in physical space; here we are considering escape over a three-dimensional barrier in momentum space. As we noted above, the Smoluchowski equation applied in the former corresponds to a very similar Fokker–Planck equation in the latter. Secondly, although our earlier work considers escape from a well in the potential described as $V(r)$, the roton minimum is not, at least for small v_s, a well. If we recognize that p is a vector and plot $F(p)$ as ordinate in a four-dimensional space with the components of p forming a three-dimensional 'abscissa space', we would have a trough near $|p| = p_0$. If $v_s = 0$, we simply have, near p_0,

$$F = \varDelta + (2\mu_0)^{-1}(p-p_0)^2,$$

where μ_0 is the effective mass of the roton, and the effect of superflow is to convert this to

$$F = \varDelta + (2\mu_0)^{-1}(p-p_0)^2 - \mathbf{v_s}.\mathbf{p}, \tag{3.27}$$

where we take $\theta = 0$ to be in the direction of v_s and $\cos\theta = \mathbf{v_s}.\mathbf{p}/v_s p$. In carrying out the integrations which follow we shall use spherical coordinates (p, θ, ϕ) in p-space.

If $v_s \gg kT/p_0$, the fact that (3.27) is a trough is unimportant: it is 'tipped up' so much by v_s that at its lowest point the type of expansion used previously [cf. D.R., (116)], namely

$$V \approx \tfrac{1}{2}\omega_A^2 x^2 + \tfrac{1}{2}s_A^2 y^2,$$

is valid and raises no difficulties. When $v_s \ll kT/p_0$, the curvature s_A (say) becomes nearly zero and the expansion mentioned would be an invalid representation of the minimum. We proceed by considering general values of $v_s p_0/kT$.

According to (3.27) we express w near A in the form

$$w = \sqrt(2\pi)\, w_0 \exp\{g^2(F_C - \varDelta) - g^2(2\mu_0)^{-1}(p-p_0)^2 + g^2 v_s p \cos\theta\}, \tag{3.28}$$

where $g^2 = 1/kT$, and we choose a form for convenience of comparison with D.R., (130). The number of rings, ν_A, in the vicinity of the trough is obtained by integrating θ right around the trough from $\theta = 0$ to $\theta = \pi$ (even though $\theta = 0$ is clearly the lowest point), by integrating p to ∞ in the usual way (since contributions where this is incorrect are exponentially small) and by integrating over ϕ. Thus

$$\nu_A = \sqrt(2\pi)\, w_0 \exp\{g^2(F_C-\varDelta)\}\iiint \exp\{-g^2(2\mu_0)^{-1}(p-p_0)^2 + g^2 v_s p \cos\theta\}p^2 \sin\theta\, \mathrm{d}p\, \mathrm{d}\theta\, \mathrm{d}\phi, \tag{3.29}$$

which becomes, after integration over θ and ϕ,

$$\nu_A = (2\pi)^{\frac{3}{2}} g^{-2} v_s^{-1} w_0 \exp\{g^2(F_C-\varDelta)\}\int_{-\infty}^{\infty}[\exp\{-g^2(2\mu_0)^{-1}(p-p_0)^2 + g^2 v_s p$$
$$-\exp\{-g^2(2\mu_0)^{-1}(p-p_0)^2 - g^2 v_s p\}]p\, \mathrm{d}p. \tag{3.30}$$

Now
$$\frac{-g^2}{2\mu_0}(p-p_0)^2 + g^2 v_s p = \frac{-g^2}{2\mu_0}p^2 + g^2\left(\frac{p_0}{\mu_0}+v_s\right)p - \frac{g^2}{2\mu_0}p_0^2$$

$$= \frac{-g^2}{2\mu_0}[p-p_0-\mu_0 v_s]^2 + \frac{g^2}{2\mu_0}(2\mu_0 p_0 v_s + \mu_0^2 v_s^2),$$

i.e.

$$\int_{-\infty}^{\infty}\exp\left\{\frac{-g^2}{2\mu_0}(p-p_0)^2 + g^2 v_s p\right\}p\, \mathrm{d}p = \exp\left\{g^2(p_0 v_s + \tfrac{1}{2}\mu_0 v_s^2)\right\}\int_{-\infty}^{\infty}\exp\left\{\frac{-g^2}{2\mu_0}p'^2\right\}[p'+p_0+\mu_0 v_s]\, \mathrm{d}p'$$

$$= (p_0+\mu_0 v_s)(2\pi\mu_0)^{\frac{1}{2}} g^{-1} \exp\{g^2(p_0 v_s + \tfrac{1}{2}\mu_0 v_s^2)\},$$

where $p' = p - p_0 - \mu_0 v_s$ and the integral over p' vanishes because the integrand is odd. Since $\mu_0 v_s \ll p_0$ for velocities much less than 2×10^5 cm/s, we can ignore that quantity when it appears. Returning to (3.30), remarking that the second integral can be done by reversing the sign of v_s, we obtain

$$\nu_A = (2\pi)^{\frac{3}{2}} w_0 \exp\{g^2(F_C - \Delta)\} p_0 g^{-1} (2\mu_0 \pi)^{\frac{1}{2}} [\exp(g^2 v_s p_0) - \exp(-g^2 v_s p_0)]$$

$$= 8\pi^2 \mu_0^{\frac{1}{2}} w_0 g^{-3} v_s^{-1} \exp\{g^2(F_C - \Delta)\} \sinh(g^2 v_s p_0), \qquad (3.31)$$

and we find for (3.28)

$$w_0 = \frac{g\nu_A}{8\pi^2 \mu_0^{\frac{1}{2}} p_0^2} \exp\{-g^2(F_C - \Delta)\} \left[\frac{g^2 v_s p_0}{\sinh(g^2 v_s p_0)}\right]. \qquad (3.32)$$

The situation at the maximum C differs from that of our earlier paper by being in three dimensions instead of two. The free energy can be written near C in suitable diagonal form as

$$F = F_C - \tfrac{1}{2} w_C^2 (p_x - p_{Cx})^2 + \tfrac{1}{2} s_C^2 (p_y - p_{Cy})^2 + \tfrac{1}{2} t_C^2 (p_z - p_{Cz})^2, \qquad (3.33)$$

x being along $\theta = 0$, the direction of flow.

Defining the flux as $\mathscr{F}$ to avoid confusion with the free energy F, we find that, instead of our earlier result [D.R., (128)],

$$\mathscr{F} = (2\pi)^{\frac{1}{2}} D w_0 (\omega_C / s_C), \qquad (3.34)$$

we have

$$\mathscr{F} = 2\pi D g^{-1} w_0 (\omega_C / s_C t_C). \qquad (3.35)$$

As far as our present application is concerned, we may replace t_C by s_C, and employing the correspondence of (3.25) we have $D \sim \Lambda_C / g^2$, and

$$\mathscr{F} = 2\pi \Lambda_C w_0 g^{-3} (\omega_C / s_C^2). \qquad (3.36)$$

The probability of nucleation comes from (3.32) and (3.36),

$$P = \frac{\mathscr{F}}{\nu_A} = \frac{\Lambda_C}{4\pi g^2 \mu_0^{\frac{1}{2}} p_0^2} \left(\frac{\omega_C}{s_C^2}\right) \left[\frac{g^2 v_s p_0}{\sinh(g^2 v_s p_0)}\right] \exp\{-g^2(F_C - \Delta)\}. \qquad (3.37)$$

Note that whereas the curvatures ω_A, s_A, etc. of our calculations on ions had the dimensions of frequency, the curvatures in this paper have dimensions $F^{\frac{1}{2}}/p$ or (mass)$^{-\frac{1}{2}}$.

It is interesting to compare (3.37) with the corresponding expression given by Iordanskiĭ, who made a calculation for thermal equilibrium without making the explicit assumption that the smallest vortex rings are rotons. To cast (3.37) into a form similar to Iordanskiĭ's, we compute the rate $\nu = P N_r$ of vortex rings created per unit volume per second from rotons. To be precise, we may take N_r to be the expression appropriate to a counterflow between normal and superfluid of magnitude v_s [see, for example, (7.10) below]:

$$N_r = \frac{2(2\pi kT)^{\frac{3}{2}} \mu_0^{\frac{1}{2}} p_0}{h^3 v_s} e^{-\Delta/kT} \sinh\left(\frac{p_0 v_s}{kT}\right). \qquad (3.38)$$

We then have

$$\nu = P N_r = \frac{(2\pi)^{\frac{1}{2}} (kT)^{\frac{3}{2}} \Lambda_C \omega_C}{h^3 s_C^2} e^{-F_0/kT}. \qquad (3.39)$$

Iordanskiĭ's expression (3.13) coincides with our (3.19). His expression below (3.14) can be compared with (3.39) by noting that (omitting entropy) $s_C^2 = v_s/p_C$. For some reason not clear to us there is a discrepancy of $\sqrt{2}\pi^2$ between the two expressions.

It should be remarked that, if $p_C v_s / kT$ is small, the energy barrier becomes, in our four-dimensional space introduced above (3.27), a 'rim' which is at much the same height and

location for all $|\boldsymbol{p}|$. The expansion (3.33) then becomes too crude for reliably estimating the pre-exponential factor of (3.37). The correct result is

$$P = \frac{\varLambda_{\mathrm{C}}\omega_{\mathrm{C}}}{2\pi\mu_0^{\frac{1}{2}}}\left(\frac{p_{\mathrm{C}}}{p_0}\right)^2 \mathrm{e}^{-\Delta F/kT}. \tag{3.40}$$

It is interesting to note that this result can be obtained from (3.37) by setting

$$s_{\mathrm{C}}^{-1} = \sqrt{(2)}\,gp_{\mathrm{C}}. \tag{3.41}$$

The p_{C} on the right reflects the fact that the 'width' of the lip is here of the same order as the perimeter of the rim. We use the result (3.40) in §8.

On writing $\mu_0 = 1/\omega_{\mathrm{A}}^2$ we find that (3.40) differs from Kramer's (1940) one-dimensional result [Donnelly & Roberts 1969a, (115)]

$$P = \frac{\varLambda_{\mathrm{C}}\omega_{\mathrm{A}}\omega_{\mathrm{C}}}{2\pi}\mathrm{e}^{-\Delta F/kT} \tag{3.42}$$

only by the 'geometrical factor' $(p_{\mathrm{C}}/p_0)^2$, which reflects the fact that in momentum space the rings must diffuse through successive spherical shells of increasing radius p.

In (3.42) we have recorded the one-dimensional escape probability which we have used in §§6 and 7 below. In (3.37) and (3.40) we have set down two forms for the three-dimensional escape probability which are basic to the theory of §§4 and 8 respectively. For completeness, we record here the two-dimensional result [given by Donnelly & Roberts 1969a, (133)] converted to the present notation as described in §3(c) above. It is

$$P = \frac{\varLambda_{\mathrm{C}}\omega_{\mathrm{A}}s_{\mathrm{A}}}{2\pi}\left(\frac{\omega_{\mathrm{C}}}{s_{\mathrm{C}}}\right)\mathrm{e}^{-\Delta F/kT}. \tag{3.43}$$
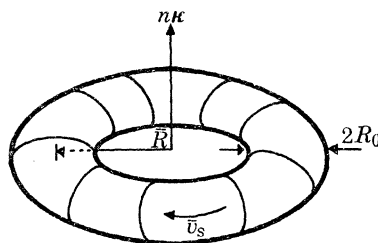
We shall use this form in §5.

FIGURE 3. Superflow consisting of n quanta in a closed tube of radius R_0 and mean radius of curvature $\bar{R}$. ($\bar{v}_s = n\kappa/2\pi\bar{R}$.)

4. Spontaneous vortex production in an unbounded fluid

Suppose we have a persistent current in a circular tube of the form shown in figure 3. If the circulation contains n quanta, $n \gg 1$, then the average superfluid velocity will be given by

$$\bar{v}_s = \frac{n\kappa}{2\pi\bar{R}}, \tag{4.1}$$

where $\bar{R}$ is the mean radius of the curved tube. The flow in this tube now has an associated de Broglie wavelength of magnitude $\lambda = h/m\bar{v}_s = \kappa/\bar{v}_s$. Thus $n\lambda = 2\pi\bar{R}$, and there are n nodes in the flow about the tube.

The flow of a persistent current is one of the most convincing demonstrations of the nature of superfluidity. The presence of such a current can be demonstrated by either destroying the

current by a pulse of heat (Clow & Reppy 1967) and observing the resulting change in the angular momentum of the container, or by suspending the channel so that it forms a superfluid gyroscope, in which case the current is detected in a non-destructive way by tilting the plane of rotation and observing the resulting force of precession (Reppy 1965; Mehl & Zimmerman 1968).

Let us consider the flow of such a current at finite temperatures. At absolute zero a persistent current would correspond to the flow of the entire fluid, i.e. $j = \rho \bar{v}_s$. As the temperature is raised, phonons and rotons will appear which will be stationary with respect to the walls of the container, owing to their viscosity. These excitations will, however, be polarized predominantly against the superflow as suggested by the arguments of §2. The magnitude of this opposing momentum per unit volume may be calculated by a procedure similar to the standard calculation of the normal density (see, for example, Donnelly 1967, p. 82) and has the value $\rho_n \bar{v}_s$. Thus the net momentum density is $\rho \bar{v}_s - \rho_n \bar{v}_s = \rho_s \bar{v}_s$, and the angular momentum density of the circulation will be $L = \rho_s \bar{v}_s \bar{R}$. Suppose a persistent current is prepared by rotating the entire apparatus above the λ-point, cooling to a temperature just below, and stopping rotation. If the angular momentum is measured, it will have a certain value, say $L(T)$, dependent upon the details of the apparatus and the procedure of the preparation of the persistent current. As the temperature is lowered quasi-particles will disappear giving up their momenta to the container. This appears to the observer as an increase in angular momentum of the superflow corresponding to the accompanying increase in ρ_s. This spectacular phenomenon has been experimentally demonstrated by Clow & Reppy (1967), and the explanation suggested above was first given by Feynman (1955).

Now suppose one of the rotons, polarized in the manner suggested above, is expanded by means of collisions to become a critical fluctuation and then expands further until it reaches the walls of the tube. This action will change the phase of the associated de Broglie waves in the flow by 2π. This change in phase is illustrated in figure 1 of Langer & Fisher's paper (1967). The change in phase means, in turn, a decrease in circulation from n to $(n-1)$ quanta. If ν such vortices are nucleated per second per unit volume, then

$$\frac{\mathrm{d}\bar{v}_s}{\mathrm{d}t} = \frac{\kappa}{2\pi\bar{R}}\frac{\mathrm{d}n}{\mathrm{d}t} = -\frac{\nu\kappa V}{2\pi\bar{R}}. \tag{4.2}$$

If each roton in the volume V of the tube is a potential vortex ring, then $\nu = N_r P$ where N_r is the roton density at the temperature of the experiment. One can show that the decay represented by (4.2) is very slow at long times. In most cases P decreases rapidly with v_s typically as $\exp(-v_0/v_s)$ where v_0 is a constant velocity. The rate of decrease of v_s is therefore extremely small when v_s is small; indeed, if this were not true the phenomenon of superfluidity would not exist. To progress further we must now calculate P using equation (3.37). This problem was considered first and most thoroughly by Iordanskiǐ (1965).

Suppose a roton at A in figure $2b$ begins to grow because of random collisions. The critical fluctuation is given by $\partial F/\partial p_1 = 0$, i.e. by $\theta = 0$ and $R = R_C$, where R_C satisfies $\partial F/\partial R = 0$, where by the considerations of §2 we find

$$F = \tfrac{1}{2}\rho_s \kappa^2 R[\ln(8R/a) - \tfrac{3}{2}] - \kappa\pi\rho_s R^2 v_s, \tag{4.3}$$

and this ring is at rest with respect to the walls of the tube. The second derivatives of F needed to provide the factors ω_C and s_C of (3.37) yield

$$\omega_C^2 = -\frac{v_s}{p_C} - \frac{1}{4\pi\kappa\rho_s p_C}\left(\frac{\partial^2 E}{\partial R^2}\right)_C. \tag{4.4}$$

$$s_C^2 = v_s/p_C. \tag{4.5}$$

The probability, P, does not depend very sensitively on the precise evaluation of the pre-exponential factors in (3.37), and in order to simplify (4.4) we may ignore the $O(1)$ terms, after differentiating (4.3) twice, in comparison with the remainder. Straightforward differentiation then yields

$$\omega_{\mathrm{C}}^2 = v_{\mathrm{s}}/2p_{\mathrm{C}} = \tfrac{1}{2}s_{\mathrm{C}}^2, \tag{4.6}$$

and we will use this estimate generally in what follows. The velocity (2.3) may be written as

$$v_{\mathrm{s}} = \frac{\kappa}{4\pi R} \ln \frac{cR}{a}, \tag{4.7}$$

with $c = 8/\sqrt{e}$, or as

$$x = \ln \lambda x, \tag{4.8}$$

where

$$x = \frac{4\pi R v_{\mathrm{s}}}{\kappa}, \quad \lambda = \frac{c\kappa}{4\pi v_{\mathrm{s}} a}. \tag{4.9}$$

For $\lambda < e$, or

$$v_{\mathrm{s}} > \left(\frac{c}{4\pi e}\right)\frac{\kappa}{a}, \tag{4.10}$$

(4.8) possesses no solutions, i.e. F has no well or barrier. This indication of spontaneous ring production corresponds evidently to a rather large Landau condition on v_{s}. For larger values of λ, x has a single maximum, x_{C}, and a single minimum, x_{A}, given approximately for $\lambda \to \infty$ by

$$x_{\mathrm{C}} = \ln \lambda + \ln \ln \lambda + \ln \ln \ln \lambda + \dots, \tag{4.11}$$

$$x_{\mathrm{A}} = \frac{1}{\lambda} + \frac{1}{\lambda^2} + \frac{3}{2\lambda^3} + \frac{8}{3\lambda^4} + \dots. \tag{4.12}$$

(The latter series is asymptotic; the former should be terminated at the term less than e to obtain an upper bound for x and at an earlier term to provide a lower bound.) It is, of course, not strictly correct to use expression (4.12) for the roton well, since (4.7) is really not applicable for these small values of R. Indeed, any solution with $\lambda x < c$ [such as (4.12) implies for large λ] is meaningless since it implies that $R_{\mathrm{A}} < a$. Instead we will replace (4.3) by (3.27) in what follows, implying a hypothetical connexion between the two in the manner already described in § 2.

Experiments on the decay of persistent currents use small v_{s} and large kT, hence we may regard $v_{\mathrm{s}}p_0/kT$ as small (typically 0.01) and replace the expression in square brackets in (3.37) by unity. Using (3.37), (4.6), (4.9) and (4.11), and on discarding a $\ln \ln \lambda$ term in ΔF, as the approximation $x_{\mathrm{C}} = \ln \lambda$ to (4.11) demands, we find

$$P = f \mathrm{e}^{-\Delta F/kT}, \tag{4.13}$$

where

$$f = \frac{\beta_{\mathrm{C}} \rho_{\mathrm{s}} \kappa^3 kT}{64\pi^2 p_0^2 \sqrt{(2\mu_0 v_{\mathrm{s}}^5)}} \left[\ln\left(\frac{c\kappa}{4\pi v_{\mathrm{s}} a}\right)\right]^2, \tag{4.14}$$

and

$$\frac{\Delta F}{kT} = \frac{\rho_{\mathrm{s}} \kappa^3}{16\pi kT v_{\mathrm{s}}} \left[\ln\left(\frac{c\kappa}{4\pi v_{\mathrm{s}} a}\right)\right]^2 - \frac{\Delta}{kT}. \tag{4.15}$$

The appearance of a new critical velocity is evident in (4.15). The velocity

$$v_{\mathrm{th}} = \rho_{\mathrm{s}} \kappa^3 / 16\pi kT \tag{4.16}$$

might be termed the *thermal characteristic velocity*. Typical values are shown in table 1. It may be noted that the high velocities shown there contain the essence of the difficulty of vortex nucleation. Unless v_{s} is comparable with v_{th}, or effects omitted here such as density of neighbouring states are significant, appreciable nucleation rates will not occur. Actually the estimate (4.15) for ΔF is

pessimistic. A more precise solution of (4.8) (and continuing the use of 4.6) leads to the values listed in table 2. These have been computed for the illustrative temperature of 2.1 K for parameters listed in the appendix. It will be observed that ν is a very sensitive function of temperature and that the critical value of v_s, for which $\nu = 1$, say, is almost an order of magnitude too large to agree with the experiments of Kukich *et al.* (1968) and Notarys (1969). It may be noted that the values of fN_r given are of the order of those estimated by Langer & Fisher (1967) and Fisher (1968), and stated by them to be a characteristic atomic frequency. The analysis just given suggests, however, that fN_r should be extremely temperature dependent, and it provides a means of estimating this dependence and also that created by pressure variations, ^{3}He concentrations, etc.

TABLE 1. TYPICAL VALUES OF THE THERMAL CHARACTERISTIC VELOCITY

T/K	1.1	1.7	2.0	2.1	2.14	2.16	2.17
v_{th}/m s^{-1}	186	93.4	46.0	24.5	14.0	7.2	2.2

TABLE 2. NUMERICAL MAGNITUDES IN IORDANSKIĬ'S THEORY OF NUCLEATION IN AN UNBOUNDED FLUID; HERE $T = 2.1$ K AND $a = 0.128$ nm

v_s/cm s^{-1}	200	300	387.7	400	500	600	700
R_C/nm	27.7	17.2	12.7	12.2	9.34	7.49	6.21
$p_0/\hbar$nm^{-1}	8.24×10^4	3.18×10^4	1.73×10^4	1.60×10^4	9.39×10^3	6.04×10^3	4.15×10^3
$\Delta F/kT$	251	129	82.4	77.8	50.9	35.0	24.8
fN_r/cm^{-3}s^{-1}	4.01×10^{36}	1.26×10^{36}	6.04×10^{35}	5.52×10^{35}	2.89×10^{35}	1.70×10^{35}	1.08×10^{35}
ν/cm^{-3}s^{-1}	2.90×10^{-73}	9.41×10^{-21}	1.03	89.6	2.23×10^{13}	1.07×10^{20}	1.89×10^{24}

We may now assess how the persistent current will decay with time, using (4.2) and the simple form of the probability of nucleation summarized in (4.13) to (4.16).

If we write
$$z = c\kappa/4\pi a v_s,\qquad(4.17)$$
and define A and B by
$$A = \frac{\beta_C\rho_s N_r VkT}{p_0^2 \bar{R}}\left(\frac{a}{c}\right)^{\frac{7}{2}}\left(\frac{\pi\kappa}{2\mu_0}\right)^{\frac12}e^{A/kT},\quad B = \frac{\rho_s\kappa^2 a}{4ckT},\qquad(4.18)$$
we find
$$dz/dt = Az^{\frac92}(\ln z)^2 e^{-Bz(\ln z)^2}.\qquad(4.19)$$
It is readily shown from this equation that, in the limit $t\to\infty$,
$$z\sim\frac{\ln t}{B(\ln\ln t)^2},\qquad(4.20)$$
or, returning to the original variables,
$$v_s\sim v_{th}\frac{(\ln\ln t)^2}{\ln t},\quad(t\to\infty).\qquad(4.21)$$

It is interesting to observe that this result is completely independent of the form of the pre-exponential factor f, and (4.14) could be modified almost at will (in respect of magnitude and algebraic power of v_s) without affecting (4.21).

A little consideration shows that the time required before the form (4.21) is attained is too large to be physically relevant. When such slow decay processes are at work, the terms in $\ln z$ in (4.19) scarcely change over the time during which the experiments are performed, and can be replaced by average values. It is of some interest to notice that, in this case, the decay law has a universal form. To see this, let $\bar{v}_s$ be a mean value of v_s for the evaluation of the logarithmic terms, and define a dimensionless superfluid velocity, y, and time, τ, by
$$v_s = v_{th}\left[\ln\left(\frac{c\kappa}{4\pi a\bar{v}_s}\right)\right]^2 y,\qquad(4.22)$$

$$\tau = \frac{A}{B^{\frac{7}{2}}} \left[\ln \left(\frac{c\kappa}{4\pi a \bar{v}_s} \right) \right]^{-5} t$$

$$= \frac{64 \beta_C V N_r}{p_0^2 \bar{R}} \left(\frac{2\pi}{\mu_0} \right)^{\frac{1}{2}} \frac{(kT)^{\frac{9}{2}}}{\rho_s^{\frac{5}{2}} \kappa^{\frac{13}{2}}} \frac{e^{A/kT}}{\left[\ln \left(\frac{c\kappa}{4\pi a \bar{v}_s} \right) \right]^5} t. \tag{4.23}$$

We then obtain
$$\mathrm{d}y/\mathrm{d}\tau = -y^{-\frac{5}{2}} \mathrm{e}^{-1/y}. \tag{4.24}$$
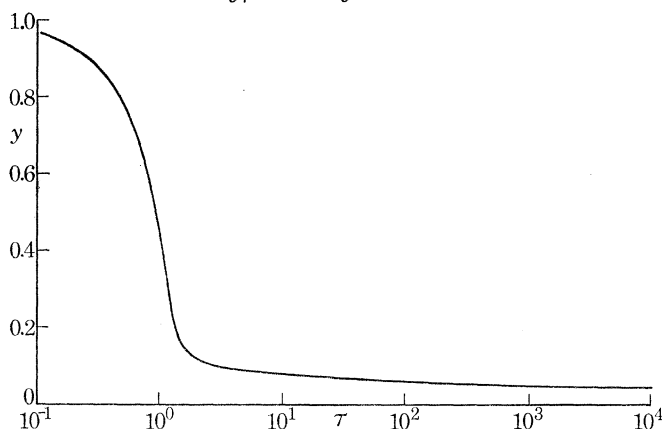

FIGURE 4. 'Universal' decay curve for superflow in a closed channel. The curve is the solution of the differential equation $\mathrm{d}y/\mathrm{d}\tau = -y^{-\frac{5}{2}} \mathrm{e}^{-1/y}$, where the variables y and τ are defined by (4.22) and (4.23).

The form of $y(\tau)$ is shown in figure 4. We can show from (4.24) that, in place of (4.21), we have

$$v_s \sim \frac{v_{\mathrm{th}}}{\ln t} \left[\ln \left(\frac{c\kappa}{4\pi a \bar{v}_s} \right) \right]^2, \quad (t \to \infty). \tag{4.25}$$

5. The thermal vortex mill

The characteristic velocities of table 2 are very much greater than those observed by Kukich *et al.* (1968) and Notarys (1969). Indeed the latter author has observed that the radii of the critical vortex rings implied by the small critical velocities of his experiments are greater than those of his channels! It can hardly be correct, therefore, to model the process by a vortex ring in isolation from solid walls. In the first examination of the effect of walls we study the properties of a vortex mill of the same general type as that envisaged by Glaberson & Donnelly (1966) but with two differences. First, the activation of the mill to the critical state is through thermal fluctuations superimposed on a general superflow past the pinned vortex. Secondly, the vortex line is considered to be pinned on two projections on the opposite sides of the pores or channels in the experiments, rather than on two projections close to each other on the walls. This means that image effects are small and will be ignored. It follows that the estimates of P we will obtain are, if anything, too small. We visualize the vortex line caught on two projections a distance l apart as illustrated in figure 5a, and we visualize it distorted by thermal fluctuations into the mean shape of a circle which we paramatize by the angle θ shown from the centre of curvature to the projection. The change in momentum (impulse) in reaching this state from the straight line state ($\theta = 0$) will be of order $\rho_s \kappa$ times the area between the two, shown shaded in figure 5a. [A further discussion of impulse applied to nucleation problems is given in §6(a).] We therefore take

$$p = \tfrac{1}{4} \rho_s \kappa l^2 (\theta \operatorname{cosec}^2 \theta - \cot \theta). \tag{5.1}$$

In computing the energy, we use the idea of tension in a vortex, that is, that a vortex segment of radius of curvature R has the same energy per unit length as a ring. (We shall encounter this again in §7.) Thus from (2.2) the energy per unit length is $\rho_s \kappa^2 [\ln(8R/a) - \tfrac{3}{2}]/4\pi$ and for the segment in figure $5a$ the corresponding energy may be written approximately as

$$E = (1/4\pi) \rho_s \kappa^2 l\theta \operatorname{cosec}\theta \ln(8\mathscr{R}/a), \tag{5.2}$$

where to overcome a difficulty concerning the form of the logarithmic term we have adopted a cutoff of $\mathscr{R}$, a mean radius of curvature, which we regard as a constant and have dropped the constant $-\tfrac{3}{2}$. [It could equally well be absorbed into the logarithm as in (4.7).] Since the dominant effects are not contained in this term, some such approximation should be tolerable. The expression for the free energy in a superflow now becomes

$$F = \frac{1}{4\pi} \rho_s \kappa^2 l \ln\left(\frac{8\mathscr{R}}{a}\right) \theta \operatorname{cosec}\theta - \tfrac{1}{4}\rho_s \kappa l^2 v_s(\theta \operatorname{cosec}^2\theta - \cot\theta). \tag{5.3}$$

The equilibrium states are given by

$$\frac{\partial F}{\partial \theta} \equiv -\rho_s \kappa l^2 \frac{(\sin\theta - \theta\cos\theta)}{2\sin^3\theta}\left[v_s - \frac{\kappa}{2\pi l \operatorname{cosec}\theta}\ln\left(\frac{8\mathscr{R}}{a}\right)\right] = 0, \tag{5.4}$$

which implies

$$v_s = \frac{\kappa}{2\pi l \operatorname{cosec}\theta}\ln\left(\frac{8\mathscr{R}}{a}\right). \tag{5.5}$$
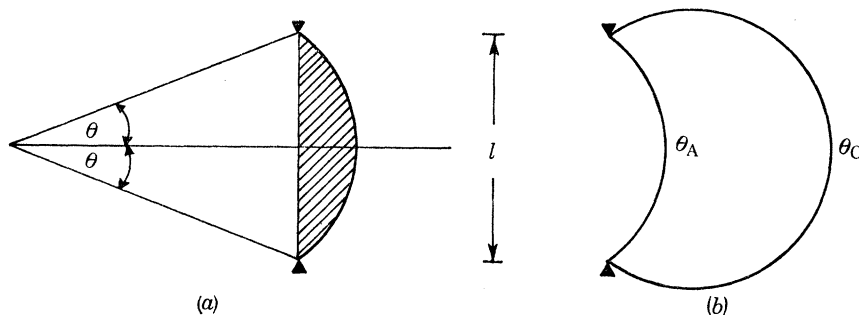

FIGURE 5. Vortex line (heavy curve) attached to two projections. (a) Initial stage, flow is into the page, the change in impulse from the state of zero flow is proportional to the shaded area. (b) The configuration of the line corresponding to the well, θ_A, and to the critical vortex, $\theta_C = \pi - \theta_A$.

An expression of this form is, of course, expected from the Arms & Hama theory (1965). The two roots are a minimum θ_A ($< \tfrac{1}{2}\pi$) corresponding to the well, and a maximum $\theta_C = \pi - \theta_A$ corresponding to the critical fluctuation. These are illustrated in figure $5b$. The corresponding values of F are

$$F_A = \tfrac{1}{4}\rho_s \kappa l^2 v_s(\theta_A \operatorname{cosec}^2\theta_A + \cot\theta_A), \tag{5.6}$$

and

$$F_C = \tfrac{1}{4}\rho_s \kappa l^2 v_s[(\pi - \theta_A)\operatorname{cosec}^2\theta_A - \cot\theta_A], \tag{5.7}$$

so that

$$\frac{\Delta F}{kT} = \frac{F_C - F_A}{kT} = \frac{\rho_s \kappa l^2 v_s}{4kT}[(\pi - 2\theta_A)\operatorname{cosec}^2\theta_A - 2\cot\theta_A]. \tag{5.8}$$

The computation of the pre-exponential factor f (cf. (4.14)) is quite complicated since, to allow for the width of the well and the lip, we must consider cases in which the plane of the loop in figure $5a$ is oblique to the plane normal to v_s. These two degrees of freedom, corresponding to tilting the loop, and increasing its radius, suggests that the escape calculation should be a two-dimensional one. A tedious argument indicates that, at least for small θ_A and $(\pi - \theta_C)$, (4.6) will

continue to apply, while both ω_A^2 and s_A^2 are given approximately by v_s/p_A. Using the result (3.43) quoted above, we find that P is still given by (4.13), but with ΔF decided by (5.8) and with

$$f = \frac{\Lambda_C v_s}{2\pi\sqrt{2}\,p_A} = \frac{\beta_C v_s[(\pi-\theta_A)\cosec^2\theta_A + \cot\theta_A]^{\frac{1}{2}}}{\pi l(2\rho_s\kappa)^{\frac{1}{2}}(\theta_A \cosec^2\theta_A - \cot\theta_A)}, \tag{5.9}$$

(see (3.2)). Here p_A is given by (5.1) with θ_A replacing θ. It is not obvious what value for $\mathscr{R}$ should be adopted. Its effect on P lies mainly in its influence on the height of the barrier and this, in turn, is influenced most by the value of $\mathscr{R}$ for $\theta = \theta_c$. It is therefore natural to take $\mathscr{R}$ to be the radius of curvature when the ring is in the circular extended position denoted by θ_C in figure 5b, i.e.

$$\mathscr{R} = \tfrac{1}{2}l \cosec\theta_A, \tag{5.10}$$

which is, of course, the same as when it is in its unextended position θ_A. Given (5.10), equation (5.5) again takes the form

$$x = \ln\lambda x, \tag{4.8}$$

but with

$$x = \frac{2\pi l v_s \cosec\theta_A}{\kappa}, \quad \lambda = \frac{2\kappa}{\pi v_s a}, \tag{5.11}$$

in place of (4.9). Much of the discussion given below that equation holds true with obvious amendments, e.g. if $\lambda < e$, or

$$v_s > \left(\frac{2}{\pi e}\right)\frac{\kappa}{a}, \tag{5.12}$$

there are no equilibrium states, and the vortex nucleates spontaneously. Also, since $\cosec\theta_A > 1$ for all θ_A, only one branch of the solution of (4.8) is relevant, namely that which reduces to (4.11) in the limit of large λ. Even this branch fails to have meaningful solutions if $\lambda x < 4l/a$, a condition which implies spontaneous nucleation after the manner of Glaberson & Donnelly (1966).

The case $\lambda \gg 1$ is comparatively simple. Then by (4.11) we have

$$\cosec\theta_A = \frac{\kappa}{2\pi l v_s}\ln\left(\frac{2\kappa}{\pi v_s a}\right), \tag{5.13}$$

and (5.1), (5.8), and (5.9) provide the necessary expressions for p, f and ΔF. The limits imposed by (5.13) and the consideration that $\cosec\theta_A > 1$ are shown in table 3 for a number of values of l.

TABLE 3. LIMITING VALUES OF l AND v_s IMPLIED BY EQUATION (5.13)

l/nm	1	5	10	50	100	500
v_s/cm s^{-1}	5366	1483	833	210	115	28

If lv_s/κ is small, so is θ_A, and the solution becomes even simpler. By (5.8)

$$\frac{\Delta F}{kT} = \frac{\rho_s\kappa^3}{16\pi kTv_s}\left[\ln\left(\frac{2\kappa}{\pi v_s a}\right)\right]^2, \tag{5.14}$$

(cf. (4.15)) and by (5.9)

$$f = \frac{3\beta_C\kappa^2}{8(2\pi^5\rho_s\kappa)^{\frac{1}{2}}l^3v_s}\left[\ln\left(\frac{2\kappa}{\pi v_s a}\right)\right]^2, \tag{5.15}$$

(cf. (4.14)). It is interesting to note that in this case, P is (apart from the pre-exponential factor which affects P insensitively) independent of l, the length of line. It is also evident from (5.14) that the characteristic velocity, v_{th}, defined by (4.16), again plays a crucial role in determining ΔF, and therefore P.

To obtain a feeling for the numerical magnitudes, we again consider $T = 2.1$ K and the constants given in the appendix, and take $l = 50$ nm. The results are shown in table 4.

TABLE 4. RESULTS FOR A THERMALLY ACTIVATED PINNED VORTEX OF LENGTH
$l = 50$ nm AT $T = 2.1$ K.

$v_s/\text{cm s}^{-1}$	50	100	150	190	200
θ_A/deg	11.3	25.3	42.7	62.8	70.6
$\Delta F/kT$	2420	634	166	25.6	8.84
f/s^{-1}	2.86×10^9	1.04×10^9	4.93×10^8	2.50×10^8	1.96×10^8
P/s^{-1}	1.0×10^{-1041}	4.0×10^{-267}	3.5×10^{-64}	2.0×10^{-3}	2.8×10^4

It is not entirely straightforward to deduce the rate of vortex production from these values of P. For example, we do not know what value should be adopted for the density of pinned vortices per unit area of container. Also it is not obvious whether a single line stretched across the tube would be a perpetual source of vorticity (a 'mill') such as Glaberson & Donnelly suggested, or would nucleate a vortex ring only once. Another difficulty lies in the fact that, as the vortex passes from the θ_A to the θ_C positions of figure 5b, it will tend to move with respect to the normal fluid either by sliding *in toto* along the walls or, if its ends are firmly rooted on projections on the walls, it must distort considerably and 'pay out' line as it does so. It is difficult to examine these matters quantitatively.

If the projections shown in figure 5b do not lie at opposite sides of the channel, but lie close together on one side of the channel, image effects cannot be ignored. They are discussed more fully in § 6 below. We merely comment here that although image effects appear to increase the energy barrier to be overcome, they do not seem to make P substantially larger. But it is already clear from tables 3 and 4 that fluctuations appear to be an important source of rings at a velocity only 10 % below that at which the Glaberson–Donnelly mechanism is effective ($v_s = 210$ cm/s, from table 3). We therefore continue our search for a more efficient source of vorticity.

6. NUCLEATION IN A FINITE CHANNEL

(a) The temperature of the onset of superflow

We now consider the effect of a wall on the spontaneous nucleation process of Iordanskiĭ described in § 4 above. Although experiments are often carried out in highly irregular channels such as compacted rouge or Vycor glass, or in nearly two-dimensional situations such as an unsaturated film, we shall suppose the fluid is confined to a circular tube of radius R_0, and is at rest. We imagine a ring to nucleate, from a roton at the centre of the tube polarized along its axis, to a circular ring whose plane is perpendicular to the axis of the tube on which it is centred. This model is common to studies of the Feynman critical velocity mechanism by Fineman & Chase (1963) and Gopal (1963). Although we will follow the analysis of the latter author assuming, as he did, that the rings are classical 'solid core' rings, when their radius, R, is large compared with their cross-sectional radius, a, our conclusions are not sensitive to core structure. Following the philosophy of § 2, that the roton and vortex branches are part of the same dispersion curve, we imagine that, for $R \lesssim a$, the spectrum has a roton well. Also, by analogy, for $R \gtrsim R_0 - a$, the quantum pressure effects associated with healing at the wall and the image of the ring will produce an analogous minimum which we will call 'the image well'. Following Gopal, we assume this occurs at $R_I = R_0 - a$, and evaluate the energy, E_I, and momentum, p_I, of that state accordingly. Since we expect quantum pressure effects for the core near a wall to be similar to those producing

the roton minimum, we will take the curvature $\partial^2 E/\partial p^2$ to be the same as that in the roton well, namely, μ_0^{-1}. These considerations lead to the curve sketched in figure 6. While the arguments given here apply strictly only to the evolution of a ring from the axis of the tube, we apply the theory as if every available roton were a candidate for nucleation. One suspects, in any case, that this represents the lowest energy situation, and that a ring growing to finite dimensions under a fluctuating force might well centre itself in the potential well denoted by ΔE_R in figure 6.
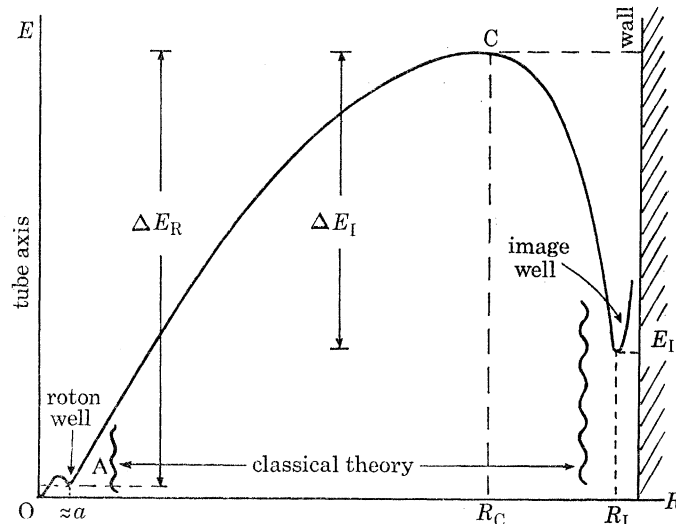

FIGURE 6. Schematic diagram of the dependence of the energy of a vortex ring, centred on the axis of a tube, as a function of the radius R of the ring. The curve is also, parametrically, a dispersion curve since $p \propto R^2$. The region in which classical theory is applied is indicated, and the roton and image wells are greatly exaggerated for clarity.

It might be argued that the probability of a ring in the image well making a quantum transition into the wall may be large. It is difficult to see how such a relatively macroscopic wavefunction could suddenly and coherently make such a transition, and we are not aware of any estimates having been made of the relevant matrix elements. It is, however, important to point out that, even if the matrix elements are large and hence our estimates of vortex line density on the wall are too high, many of our arguments [particularly our estimates of $T_0(R_0)$ and $T_0(R_0, v_s)$ below] will still apply, since they depend, in no essential way, on the vortices at the wall.

In the absence of superflow, E is, in an unbounded fluid, a monotonically increasing function of R, and there is no possibility of creating a permanent ring of large radius (although there will statistically always be some present in the Maxwell tail). The situation in a tube, as may be seen from figure 6, is crucially different. The confinement of the vortex flow to the tube depresses E at large R, and creates a single maximum between the roton and image wells, and nucleation can occur in either direction over this barrier. By 'nucleation outwards', we will mean the nucleation of vortex rings in the image well from rotons in the interior, by 'nucleation inwards', we will mean the reverse process of the collapse of rings from the well into rotons in the interior. In either process, the probability of nucleation is independent of the sense of circulation. Once, however, a nucleation has taken place, a flow is created in the tube and this, as we shall see in the following section, enhances the probability that a nucleation of the opposite sense will take place subsequently. The mechanism is, then, self-correcting and maintains, on the average, the original state of superfluid at rest. The time scale, τ, of this process is, for nucleation outwards, of

order $1/\nu V$ where V is the volume of helium in the apparatus and ν is the rate parameter, PN_r, of the type introduced in §4. For nucleation inwards, it is of order $1/\nu_\mathrm{s} S$, where S is the surface area of the tube, ν_s is a rate parameter $p_\mathrm{V} S_\mathrm{V}$ which will be discussed presently, and S_V is the density of vortex line on the walls. The image well could be populated initially by a vigorous stirring of the fluid—for example making it flow at speeds beyond the critical velocity. It is intuitively clear (and indeed it will be demonstrated in the next section) that in the presence of a superflow the rate of production of vortices by either of these processes adjusts itself in such a way as to always reduce the superflow. The nucleation rate tending to destroy the superflow will be increased beyond the value $1/\tau$ obtained above, while that of the reversed sense will be decreased. We may infer that if τ is 'sufficiently small', say 1 sec, the phenomenon of superflow will be greatly inhibited. This is the well known 'suppression of the λ-point'. We now set about the task of evaluating it as a function of R_0 and T.

TABLE 5

R_0/nm	x_C	$E_\mathrm{C}/k\rho_\mathrm{s}$	$E_\mathrm{I}/k\rho_\mathrm{s}$	$10^{-8}\omega_\mathrm{C}\rho_\mathrm{s}^{\frac{1}{2}}$
1.0	0.733	379	298	204
1.2	0.742	513	366	158
1.6	0.754	809	503	106
2.0	0.763	1 130	640	78.1
2.4	0.770	1 480	776	60.6
3.0	0.777	2 040	981	44.4
4.0	0.787	3 050	1 320	29.8
5.0	0.794	4 130	1 660	21.8
7.0	0.803	6 470	2 340	13.6
10.0	0.813	10 300	3 370	8.25
15.0	0.822	17 300	5 080	4.67
20.0	0.829	24 800	6 740	3.11
30.0	0.837	40 800	10 200	1.76
40.0	0.842	58 000	13 600	1.17
50.0	0.846	75 900	17 000	0.855

In an unbounded fluid, the momentum, p, of a ring of radius R coincides with the classical hydrodynamic expression $\rho_\mathrm{s}\kappa\pi R^2$ for its impulse. In a bounded fluid, the correct choice of impulse leaves room for argument (Vinen 1966; Gopal 1963; Huggins 1966; Kawatra & Pathria 1966). There seems to be no compelling reason, for example, why $-\rho_\mathrm{s}\kappa\pi(R_0^2-R^2)$ should not be as appropriate a definition of p as $\rho_\mathrm{s}\kappa\pi R^2$; indeed, when nucleation occurs from the walls, Vinen (1966) has argued that the former definition may be physically more plausible. Although these questions must be faced whenever the absolute magnitude of the free energy is thought to have significance, they appear to be of no moment here. For, when computing the probability of escape over a barrier such as that indicated in figure 6, we require only the free energy difference between A and C and the corresponding curvatures. This requires a knowledge of only the momentum difference of these states, and the constant difference $\rho_\mathrm{s}\kappa\pi R_0^2$ in the two definitions of p just given plays no part. This conclusion remains true when there is plug flow of superfluid down the tube, which will be considered in the next section. We may therefore adopt the classical expression for p given in equation (2.1). The free energy, F, is the kinetic energy of superflow of the vortex, and can, in the classical range, be obtained from Gopal's analysis. Gopal presents two forms of solution, one (the inner) is valid for small $x = R/R_0$; the other (the outer) for small $1-x$. There is a common range of x in which the expansions agree well with each other. Its location depends in detail on the value of R_0/a. In what follows we have used the inner and outer forms of

the solution as appropriate. For the value of E_I, the energy of the image well, we have taken Gopal's estimate

$$E_I = \tfrac{1}{2}\rho_s \kappa^2 R_I (\ln 2 + \tfrac{1}{4}), \tag{6.1}$$

where $R_I \equiv R_0 - a$ as shown in figure 6. It is clear that, since $E_I \gg \Delta$, the energy difference ΔE_I between the image well and the critical fluctuation is much less than ΔE_R, the energy difference between roton well and critical fluctuation. It follows that the probability of nucleation inwards greatly exceeds that of nucleation outwards and that, in statistical equilibrium, the population at the E_I energy level is correspondingly less than N_r, the roton density at the energy level Δ.

Table 5 displays values of E_C, the energy maximum, its location $x_C = R_C/R_0$, its curvature ω_C, and E_I as functions of R_0 (k is the Boltzmann constant and a is taken to be $0.128\,\mathrm{nm}$).†

In evaluating the probability P we will adopt the simple one-dimensional theory of Kramers (cf. Chandrasekhar 1943). This is not strictly accurate since we should consider states adjacent to the lip. These states refer to vortices (no longer quite plane-circular) slightly off-centre and slightly oblique to the tube section. The investigation of these neighbouring states would be an intricate matter and would result only in corrections to the pre-exponential factor f. Such corrections influence P but slightly and there seems no justification for undertaking such an elaborate analysis for such a small refinement in P. We therefore take (3.42):

$$P = \frac{\Lambda_C \omega_A \omega_C}{2\pi} \exp\left(-\Delta E_R/kT\right). \tag{6.2}$$

We can now use (6.2) to evaluate T_0, the temperature of the depressed λ-point. We define this temperature by saying that it is that temperature at which, on the average, one vortex per unit volume per second is fluctuating over the barrier at C, i.e. $\tau^{-1} = \nu = N_r P = 1$. We have ignored inward nucleations in this definition, but it is easily shown that, were they added, the change in the estimate of T_0 would be negligible.

One should note carefully that T_0 is not, strictly speaking, a depression of the λ-point in the sense that the superfluid is destroyed. Indeed one assumes the superfluid, and the quasi-particles, have the same properties as are appropriate to this temperature, but that the fluctuations of rings over barrier C in figure 6 would cause rapid decay of any attempted superflow in the range $T_0 < T < T_\lambda$. Moreover, oscillatory flow such as that accompanying third or fourth sound will disappear at only a slightly higher temperature. To see this, note that at $2.14\,\mathrm{K}$ the value of R_0 associated with $\nu = 1$ is $8.34\,\mathrm{nm}$, while that associated with $\nu = 10^3$ is $7.79\,\mathrm{nm}$. Thus temperatures only slightly above T_0 correspond to rapidly increasing values of ν. It is likely that fourth sound of frequency f, for example, will become strongly damped at a temperature such that $f \approx \nu$. Thus T_0 should increase slightly with increasing frequency, but the change is so small it may well be beyond experimental resolution. Evidence that direct flow and fourth sound are extinguished at nearly the same temperature is presented in figure 7. The data in this figure, given by Guyon &

---

† It may be noted that, in one minor respect, we have departed from Gopal's analysis. The critical fluctuation is one in which the vortex is at rest with respect to the tube, i.e. is such that $v_i = \partial F/\partial p$ is zero. Indeed, Roberts & Donnelly (1970a) have noted that the expression for the velocity of the classical circular vortex ring with solid core can be obtained in this way, provided explicit recognition is made of the conservation of vorticity in a ring during the differentiation with respect to p. This requires that a is considered to be a function of R and that $R\,\mathrm{d}a/a\,\mathrm{d}R = -\tfrac{1}{2}$. It may be objected that, if the same procedure of differentiating Gopal's expression (2.14) for image energy is adopted, the contribution (2.15) to the ring velocity is not recovered. It appears, however, that there is a small discrepancy in Gopal's method of obtaining the ring velocity: his statement below (2.14) is not strictly correct in the order to which he is working. Thus we retain our result $v_i = \partial F/\partial p_i$ in the present analysis and, in locating the maximum of F in this and the following sections, we allow a to vary in the manner just indicated. It should be observed that the dominant terms are unaffected by the considerations of this footnote.

Rudnick (1968), represent experiments on the same packed powder sample (Carbolac II). The results of direct flow measurements are indicated by the solid line and the amplitude of a low frequency ($f \approx 100\,\mathrm{Hz}$) component in the fourth sound resonator is shown by the dashed line.
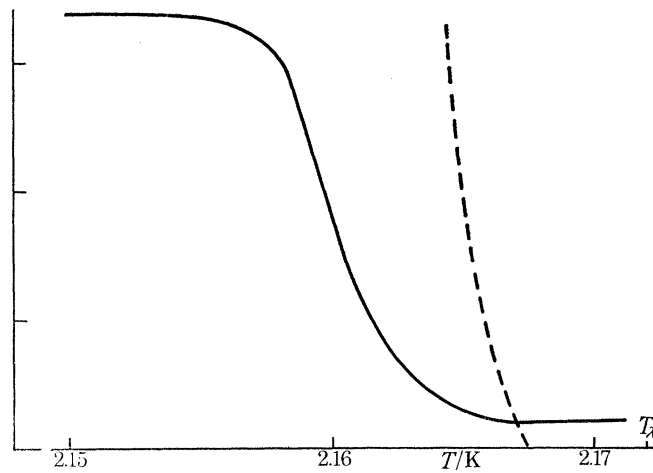

FIGURE 7. Flow rate (solid line) and low-frequency resonance amplitude in a fourth sound cavity (dashed line) as a function of temperature. Both disappear near $2.167\,\mathrm{K}$ (after Guyon & Rudnick 1969)
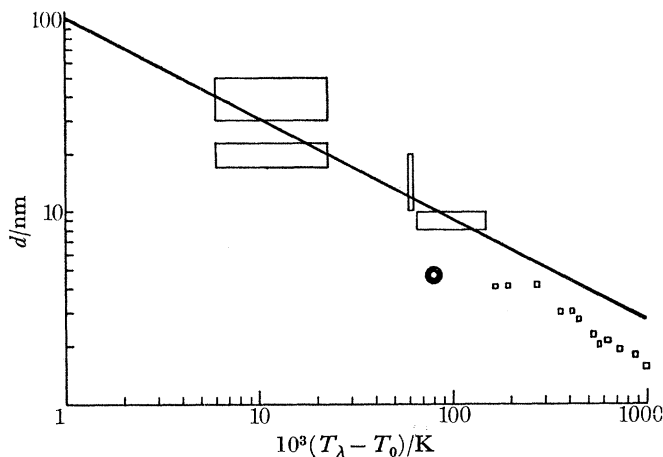

FIGURE 8. Calculation of the temperature of onset of superflow, T_0, as a function of $d = 2R_0$, from the condition $\nu = 1\,\mathrm{s}^{-1}$ and $a = 0.128\,\mathrm{nm}$. The experimental onset temperatures indicated by rectangles and one circle were obtained by Guyon & Rudnick (1969). The squares indicate unsaturated film measurements by Fokkens et al. (1966).

Accepting the definition of T_0 by $\nu = 1$, and adopting $a = 0.128\,\mathrm{nm}$ for the core radius, we find the results shown by the solid line in figure 8, where we have taken $d = 2R_0$. The experimental data, assembled by Guyon & Rudnick (1968), refer to their fourth sound measurements, and the unsaturated film experiments of Fokkens, Taconis & de Bruyn Ouboter (1966). With the reservation mentioned in § 1 that a is a function of temperature, the onset curve in figure 8 is in gratifying agreement with experiments. The fluctuation model for the onset temperature developed here (which as we have remarked, is independent of the concept of inward nucleation) offers an alternative to the Ginsburg–Pitaevskii approach discussed by Guyon & Rudnick (1968).

We now estimate the surface density of vortex line S_V (dimensions cm^{-1}) on the wall in thermal

equilibrium. In the present model, S_V is also the number of circular vortex rings per unit length of tube. These will nucleate inwards at the rate

$$S_V \Lambda_C \omega_A \omega_C (2\pi)^{-1} \exp(-\Delta E_I/kT).$$

If we regard all rotons in the tube as capable of nucleation outwards, the reverse process proceeds at the rate

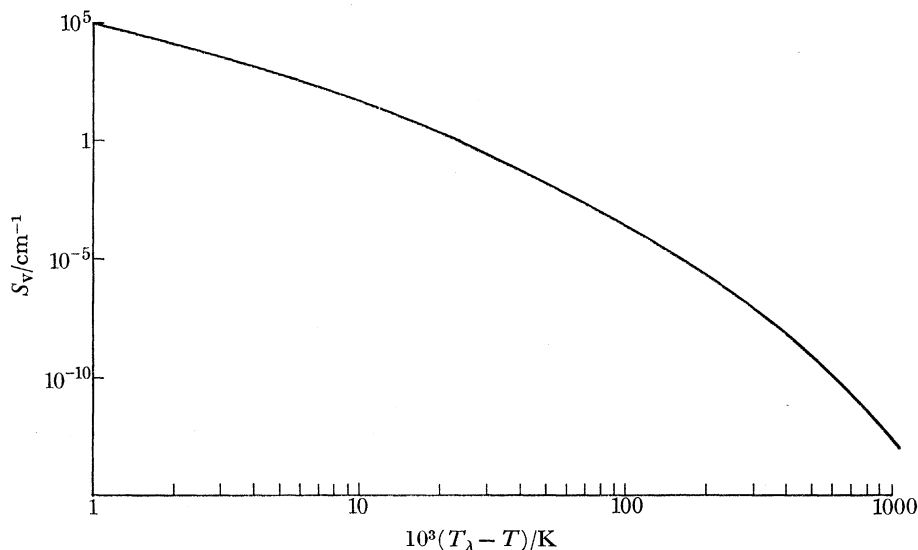$$N_r \pi R_0^2 \Lambda_C \omega_A \omega_C (2\pi)^{-1} \exp(-\Delta E_R/kT).$$

FIGURE 9. Relationship between S_V and T_0 given by equation (6.4). The curve was derived by computing T_0 for a given R_0, then computing S_V using the T_0 and R_0 so obtained.

(It will be recalled that we assumed that the curvatures of roton and image wells are the same, namely ω_A). Thus in thermal equilibrium, where the two rates balance, we have

$$S_V = \pi R_0^2 N_r \exp(-(E_I - \Delta)/kT), \tag{6.3}$$

or, using the theoretical expression for N_r [cf. equations (A 2) and (A 3) below],

$$S_V = \left(\frac{\mu k T}{2\pi}\right)^{\frac{1}{2}} \frac{(p_0 R_0)^2}{\hbar^3} \exp(-E_I/kT). \tag{6.4}$$

Figure 9 displays the vortex ring density S_V at the onset temperature T_0 appropriate to a given tube diameter R_0. This was done by first computing T_0 for a given R_0, then computing S_V from equation (6.4) using the T_0 and R_0 so obtained. This balance does not take into account the possibility that the vortex may be annihilated on the wall, as discussed at the beginning of this section. The physical pictures which emerge appear sufficiently close to laboratory experience that we are encouraged to believe that finite amounts of vortex line may actually exist on boundaries.

Whether, in fact, the wall possesses the above equilibrium population of vortex line probably depends very much on the way the fluid is prepared. If helium II were condensed directly from the vapour, it is probable that S_V would be much smaller than the value suggested by (6.4) and might even be zero. The rate τ^{-1} at which the population would grow is fantastically small because of the height of the barrier compared with kT. If, on the other hand, the fluid is set into supercritical motion after it is cooled, it may well acquire a population of this magnitude and, moreover,

because of the height of the barrier compared with kT, there is little subsequent exchange between rotons in the fluid and rings in the well. It would now be correct to regard these rings as being trapped by their own images. Note that $\partial E/\partial R = 0$ at the bottom, $R_{\rm I}$, of the ring well, and that rings trapped there will have, on the average, no motion along the tube although thermal agitation will produce drifts back and forth from time to time. Finally it should be admitted that the procedure described for fixing the well at $R_{\rm I}$ is somewhat arbitrary. More careful considerations may well call for a revision of the magnitudes of $E_{\rm I}$ and the curvature there in the future.

Experimentally, the specific heat at the depressed λ-point shows a maximum reminiscent of that which gives the true λ-point its name, but more diffuse. The question we may now ask is whether the existing theory can explain the specific heat anomaly. The creation of each vortex ring on the wall from the main body of the fluid by outward nucleation requires the random energy of the fluid to be converted into the ordered energy of hydrodynamical motion. When considered as one of a population on the walls, each of which is partnered by a vortex ring of opposite circulation, the ordered energy of motion becomes less significant. (Consider, for example, the fact that the hydrodynamical energy per unit length of a line vortex is of order $\rho_{\rm s}\kappa^2 \ln(\mathscr{L}/a)$, where $\mathscr{L}$ is a large distance cutoff, whereas that for a pair of such vortices of opposite circulation separated by a distance $2d$ is at most of order $\rho_{\rm s}\kappa^2$. In any case, a uniform distribution of vortices of each type over the wall will not create hydrodynamic flow inside.) There remains, however, the fact that entropy flows into a vortex core either from the fluid which gave it birth, or from the walls, if they are conducting. The entropy associated with a vortex line is influenced by several factors which are not yet completely understood. The most important contribution at relatively high temperatures is probably the entropy of the normal core (Glaberson et $al.$ 1968). In evaluating this we liken the interior of the core to an He I-like material and compute the entropy excess of this over the entropy of the same volume of He II. In this way we obtain the estimate

$$S_l = \left[8.10^6 \rho T - k N_{\rm r}\left(\frac{3}{2} + \frac{\varDelta}{kT}\right) \right] \pi R_{\rm c}^2 \text{ erg K}^{-1}\text{cm}^{-1} \tag{6.5}$$

for the entropy per unit length of vortex line. The constant 8×10^6 is chosen so that the excess falls to zero at T_λ and to agree with the entropy of He I ignoring the λ-anomaly. The radius of the normal core, $R_{\rm c}$, is given approximately by

$$R_{\rm c} \approx \frac{0.32}{\sqrt{(T_\lambda - T)}} \text{ nm}, \tag{6.6}$$

according to the analysis of Glaberson et $al.$ (1968). The entropy of the array of vortices on the walls of the tube is now seen to be $2\pi R_0 S_{\rm V} S_l$ per unit length of tube or $2S_{\rm V} S_l/R_0$ per unit volume of contained fluid. Thus the specific heat per unit volume is

$$C_l = T\frac{\mathrm{d}}{\mathrm{d}T}\left(\frac{2S_{\rm V}S_l}{R_0}\right) = \frac{2p_0^2 R_0}{\hbar^3} T\frac{\mathrm{d}}{\mathrm{d}T}\left[\left(\frac{\mu kT}{2\pi}\right)^{\frac{1}{2}} \mathrm{e}^{-E_{\rm I}/kT} S_l\right]. \tag{6.7}$$

The heat capacity given by (6.7) gives an excess which must be added to the heat capacity of the rotons and phonons. Presumably the normal λ-anomaly may be suppressed in narrow channels. Since the vortex cores are not present above T_λ, the excess determined here vanishes at T_λ. Further information on the latent heat of vortices is needed to see how well (6.7) or a similar expression agrees with experiment.

(b) The effect of superflow

We now extend the theory of § 6 (a) to the case in which the normal fluid in the tube is at rest and the superfluid is moving everywhere with the uniform velocity v_s (> 0) down the tube (plug flow). The difference, $F(R)$, between the free energy of this state and one in which superimposed on it there is a vortex of radius R coaxial with the tube, is related to $E(R)$ the expression for $v_s = 0$, by (2.5), which may be written in one dimension as

$$F(R) = E(R) + v_s p(R), \tag{6.8}$$

where we put $p(R) = \rho_s \kappa \pi R^2$, as before. For $\kappa < 0$, the last term of (6.8) is negative so that $F(R) < E(R)$, the probability of outward nucleation is therefore increased (relative to its value for $v_s = 0$). Since, however, $|p(R)|/|E(R)|$ increases monotonically with R, the probability of inward nucleation is decreased. Conversely, for $\kappa > 0$, these conclusions are reversed: outward nucleation becomes less probable. We have, therefore, four different rates of fluctuation, inward and outward nucleation for rings of positive and negative circulation. The dominant processes, the outward nucleation of rings of negative κ and the inward nucleation of rings of positive κ, act in a sense to destroy the flow v_s, which will, ultimately, cease unless an agency acts to maintain it (i.e. a source of thermodynamic potential). If, on the other hand, the flow is maintained, a statistical balance will be struck in which the number, S_V^-, of vortex rings per unit length of tube having negative circulation exceeds that, S_V^+, of rings of positive circulation. Hydrodynamically, the population of vortices on the wall now resembles a vortex sheet of strength $\mathscr{S} = \kappa(S_V^+ - S_V^-)$. It is, strictly, not consistent to suppose, as we have done, that v_s is uniform throughout the tube, for there must be a discontinuity of $\mathscr{S}$ cm/s across the image wells. (The effect of this different superfluid velocity in the healing region between image vortices and the wall does not, however, appear to be particularly significant.)

If we compare the present nucleation process with that for an infinite fluid (§ 4), we see that the energy barrier implied by (6.8) is always lower for outward nucleation of rings of negative κ than it is at the same v_s in the Iordanskiï process. The barrier is therefore overcome with greater frequency. Nevertheless, if v_s is large compared with the Feynman velocity, $\kappa/4\pi R_0$, the critical ring size $R_C(v_s)$ is small compared with R_0 and, since image effects are negligible, it is asymptotically the same as the theory in § 4 would predict. The same is true for the values of ν and P. If, however, v_s is small compared with $\kappa/4\pi R_0$, the critical ring size, $R_C(v_s)$, lies close to $R_C(0)$ the maximum of $E(R)$ on the Gopal theory propounded in § 6 (a). The energy and ring diameter of the critical fluctuation are now considerably less than that arising in the Iordanskiï process at the same v_s. This fact is illustrated in figure 10 which shows, for the two values of 0 and 700 cm/s for v_s, the flow $V_I(R_0)$ which would be required on the Iordanskiï theory to give the same energy barrier. [The corresponding ring size $R_I(R_0)$ always exceeds $R_C(v_s)$ and may well exceed R_0, as Notarys (1969) has observed.] If crude estimates of the energy barrier are required, one can, in this case of small $R_0(v_s)$, ignore the displacement of $R_C(v_s)$ from the value $R_C(0)$ of the Gopal theory, and evaluate (6.8) from the E_C displayed in table 5. As before, interesting nucleation rates occur when E_C/kT, is about 80. We may further, in extension of our definition of an onset temperature for superfluidity, define a T_0, which is now a function of v_s as well as R_0, to be that temperature at which $\nu = 1$. Figure 11 illustrates this generalization with $d = 2R_0$ and $a = 0.128$ nm. The curve for $v_s = 0$ coincides with that of figure 8. The curves for $v_s = 350$ and 700 cm/s asymptotically agree with the Iordanskiï theory, and in this region of relatively large channels it is correct to speak of an 'instrinsic' critical velocity, i.e. one independent of channel

size. Channel sizes smaller than *ca.* 80 nm begin to show definite effects of boundaries. Since the pores of most gyroscope experiments are very small, they are almost always operating under conditions where boundaries are important and where, in consequence, the concept of an 'intrinsic' critical velocity has no meaning. For fixed channel size T_0 tends to zero as v_s becomes infinite.
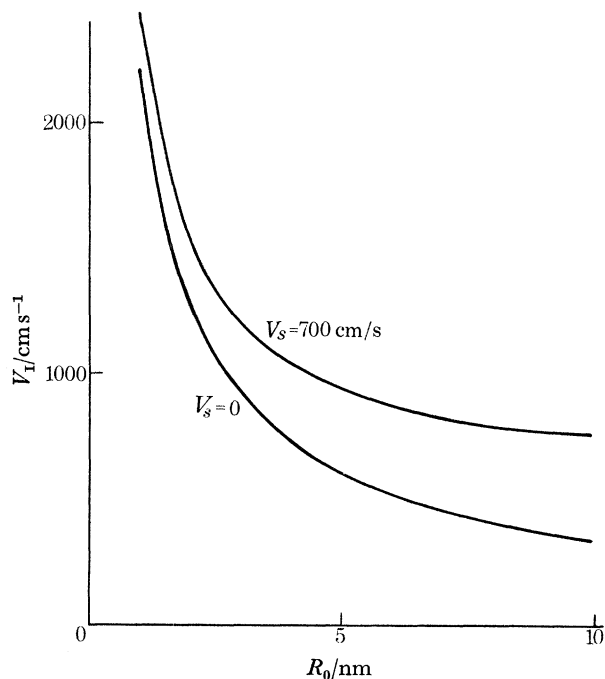

FIGURE 10. The flow, V_I, which would be required on the Iordanskiĭ theory to give the same energy barrier as we find for a finite channel of radius R_0 with flows of 0 and 700 cm/s. The profound effect of finite channel size is readily appreciated.
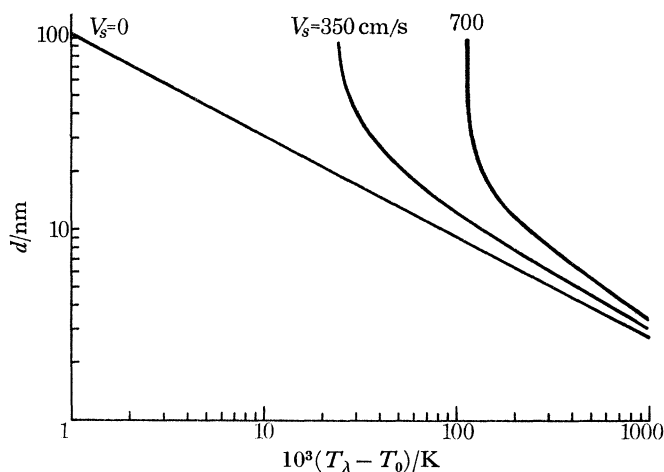

FIGURE 11. Generalized onset temperatures for $v_s = 0$, 350 and 700 cm/s as a function of channel size. The whole family of curves $T_0(R_0, v_s)$ may be thought of as a map of critical velocities. Note that only at the largest values of d do we begin to find T_0 independent of d, i.e. the 'intrinsic' or Iordanskiĭ limit.

Turning our attention to inward nucleation of rings of positive κ, we find that the energy barrier for this process does not decrease as rapidly with v_s as the outward nucleation of negative κ rings just described. This is illustrated in table 6. Although the results shown there are clearly

dependent on our assumptions concerning E_I, they indicate that, apart from very small tubes, or temperatures very close to T_0, inward nucleation will not be as potent a means of reducing superflow as outward nucleation, unless the population of vortices of positive κ on the walls is, for some reason, abnormally high. (We should observe that Δ has not been subtracted from the energies for outward nucleation shown in the table.)

TABLE 6. EFFECT OF SUPERFLOW ON THE ENERGY BARRIERS
FOR INWARD AND OUTWARD NUCLEATION

	$v_s = 0$		$v_s = 700 \text{ cm/s}$	
R_0/nm	$E/k\rho_s$ outward	$E/k\rho_s$ inward	$E/k\rho_s$ outward	$E/k\rho_s$ inward
1	379	80.8	298	48.9
2	1 130	494	791	335
3	2 040	1 060	1 260	698
4	3 050	1 730	1 670	1 190
5	4 130	2 470	2 020	1 610
6	5 280	3 270	2 300	2 050
7	6 470	4 130	2 520	2 490
8	7 710	5 020	2 690	2 930
9	8 990	5 960	2 820	3 380
10	10 300	6 930	2 910	3 840

Let us now consider the process of 'cooling through the onset temperature T_0'. While T exceeds T_0, the processes of creation and destruction of vortices occurs so rapidly that the fluid can adjust continuously to the changing temperature. As T approaches T_0, the relaxation process becomes slower, and, at temperatures only slightly below T_0, ν becomes so small that further cooling is adiabatic (no matter how slowly it is carried out on the laboratory time scale), and the populations of vortices on the walls are now 'frozen' to their values at T_0 as roughly estimated by (6.4). While we have already explained in § 6 (a) that there is a very effective mechanism to ensure that, on cooling liquid helium at rest, we shall obtain equal values of S_V^+ and S_V^-, non-equilibrium conditions in cooling, or statistical fluctuations in these populations may well lead to a situation where T_0 has been passed leaving one sign of vortex predominant. Under these circumstances a test would reveal a spontaneous persistent current, as indeed Mehl & Zimmermann (1968, p. 226) have reported. If the apparatus has been cooled through T_0 with $S_V^+ = S_V^-$, rotation will fail to alter the population unless one rotates so rapidly as to reach the $T_0(R_0, v_s)$ belonging to the channel size and temperature in question. Then the populations can adjust, and on stopping rotation a persistent current will be seen of the same magnitude as would have been observed by cooling down rotating with velocity v_s. This point resolves a question raised by Mehl & Zimmermann (1968, p. 228), who noted experimentally the coincidence in magnitude of persistent currents prepared by the two methods described here.

Now suppose one prepares a persistent current by cooling through the onset temperature $T_0(R_0, v_s)$ corresponding to the rate of rotation of the apparatus and stops, leaving a persistent current of magnitude v_s. If one now raises the temperature of the apparatus to some temperature $T > T_0(R_0, v_s)$, fluctuations will cause a decay of the persistent current, which is rapid at first, but becomes slower as the critical value of v_s corresponding to that temperature is reached and passed. This decay has been observed experimentally by Kukich et al. (1968) under the general conditions described. As one would expect, the rate of decay reported by them is greater the higher the temperature.

While the qualitative effects described here have been successful, the quantitative agreement is not satisfactory. Comparison with the velocity data of Mehl & Zimmermann (1968), and Kukich *et al.* (1968) shows that the calculated critical velocities are still higher than those observed experimentally. Corrections to the value of a, entropy considerations and density of states arguments can close this gap. For example, if the temperature is so high that a is comparable with R_0, the wavefunction for the superfluid will be unable to reach its equilibrium value, and the average superfluid density will be reduced to a value below ρ_s. The lowering of the energy barrier will reduce the critical velocity. We leave further discussion until these considerations can be made more quantitative.

7. Nucleation of quantized vortex rings by ions

(a) The nucleation problem

The mechanism by which an ion produces and becomes bound to a quantized vortex ring is interesting for a number of reasons. First, the ion is so small that it produces almost no macroscopic disturbance of the liquid: the flow about the ion may be taken to be laminar (the Reynolds number is of order one or less). Secondly, the situation is reminiscent of the famous problem of the drag on a moving sphere in hydrodynamics. The notions of the boundary layer and its separation from the sphere were developed over a period of years as an explanation both of the shape of the drag curve and for the 'drag crisis'. In this chapter we shall endeavour to account for the shape of the drag curve for ions in helium II and the subsequent growth of a ring. Indeed the nucleation of a quantized vortex ring from an ion is the quantum analogue of the drag crisis, for not only does the drag on an ion-ring complex differ markedly from the drag on an ion, but the entire dynamics of the complex is different also.

Early speculations on this problem have been advanced by Huang & Olinto (1965). More recently, however, experiments by Rayfield (1967) have led him to make a suggestion in sharp variance with the discussions of Huang and Olinto, namely that the vortex ring is somehow 'peeled' from the ion in such a way that it is not necessary for the vortex ring to capture the ion in a discontinuous manner.

One might at first try to enlarge on Rayfield's idea by supposing that the ion is slowed down at the moment of nucleation and that the vortex ring is formed by the impulse imparted to the surrounding liquid by this braking action, the necessary energy coming from the accompanying decrease in kinetic energy of the ion. For simplicity suppose the ion is idealized as a point with mass m_i. If the velocity of the ion initially is v_i, and after nucleation v_f, then the statement that the momentum lost to the ion is converted to the impulse of the ring reads

$$m_i(v_i - v_f) = \rho_s \kappa \pi R^2. \tag{7.1}$$

The change in kinetic energy of the ion may appear as energy of the ring when

$$\tfrac{1}{2} m_i(v_i^2 - v_f^2) \geqslant \tfrac{1}{2} \rho_s \kappa^2 R L, \tag{7.2}$$

where $L = (\ln(8R/a) - \tfrac{3}{2})$. Dividing (7.2) by (7.1) we obtain

$$v_i + v_f \geqslant \kappa L/\pi R. \tag{7.3}$$

If we require that the ion move at the self-induced velocity of the ring at the moment of nucleation, then

$$v_f = \frac{\kappa}{4\pi R} [\ln(8R/a) - \tfrac{1}{2}] \simeq \frac{\kappa}{4\pi R} L. \tag{7.4}$$

Equations (7.3) and (7.4) give $\qquad v_1 \gtrsim 3 v_r.$ $\qquad\qquad$ (7.5)

This means that, in order to induce vortex rings, ions must be accelerated to about three times the speed of the most rapidly moving rings in an experiment. Experiments at the University of Oregon, discussed in § 7 (f) below, tend to show that the most rapidly moving ion-ring complexes have about the same velocity as the ions which produce them. Furthermore, since these velocities are in the range 30 to 40 m/s, we would need $v_1 = 90$ to 120 m/s to produce rings (i.e. about twice the Landau velocity for roton emission). Since no ion velocities this high have been observed we are forced to abandon the argument given above and are led to examine the role of thermal fluctuations as a means of acquiring sufficient energy and momentum to produce vortex rings.
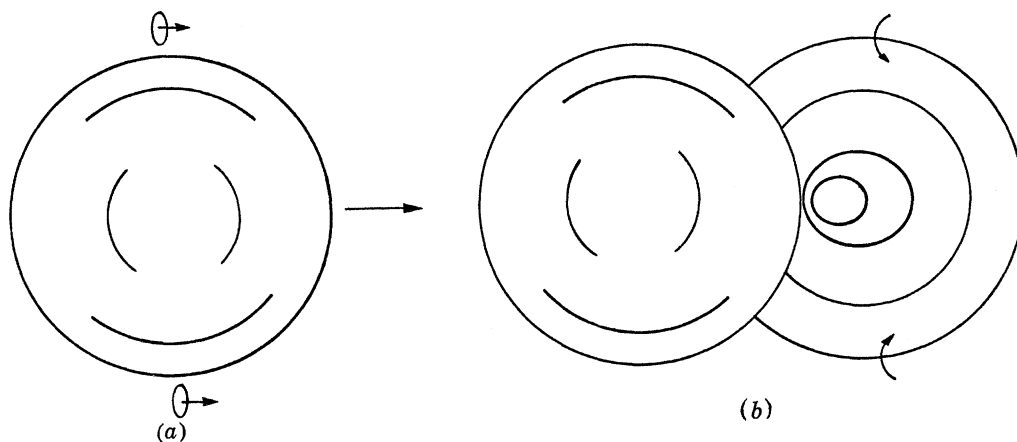

FIGURE 12 (a). Ion moving to the right with rotons localized near the equator predominantly polarized in the direction of motion. (b) Ion moving into the page, suggesting successive stages in the nucleation of a critical ring from a localized proto-ring. Circulation of ring is indicated by arrows.

The theory presented here takes the view that a roton, localized near the equator of an ion, and polarized so as to face the oncoming flow of superfluid, acts as a nucleus, or proto-ring, for the growth of a macroscopic vortex ring [cf. figure 12a]. Roton localization will be discussed in § 7 (b) and an estimate of the number of localized rotons, n_r, will be obtained. It is sufficient to suppose that collisions cause the proto-ring to grow until finally it is large enough to have a self-induced velocity equal to that of the ion, that is, it is a critical vortex ring [or more properly vortex segment as suggested by figure 12b]. The critical vortex ring is supposed to be attached to the sphere. While details of how this attachment occurs are not known, there is a natural attraction experienced by an ion near the core of a vortex which has been extensively studied by the authors (Donnelly & Roberts 1969a). If we assume, then, that the critical ring has the appearance illustrated in figure 12b, we can make quantitative estimates of its velocity, shape, energy and momentum which allow a calculation of the free energy barrier ΔF. This is carried out in § 7 (d). One can now calculate the probability P that a localized roton will grow to critical size. Thereafter the ring expands spontaneously, deriving the energy to do so from the electric field producing the ion motion. The final radius of the ring will be determined by the condition that the drag on the ring [cf. equation (A 5)] is balanced by the electric force:

$$eE = \alpha[\ln(8R/a) - \tfrac{1}{2}]. \qquad\qquad (7.6)$$

The P determined in this way will be a function of v_1 for a given set of conditions on pressure, temperature and ³He concentration. The actual nucleation rate ν per ion will be the product

$n_r P$ of the number of localized rotons and P. From ν we can calculate the probability $\exp\left(-\nu\tau\right)$ that an ion will survive for τ seconds without nucleating a ring. Experimentally, this means that if N ions enter a drift space of length L moving at velocity v_1, a fraction $N_1/N = \exp\left(-\nu L/v_1\right)$ of those ions will arrive at the collector. The remainder $(1-N_1/N)$ will have nucleated a vortex ring. We shall find that N_1/N decreases from unity only at quite large velocities [see § 7 (f) below].

We can make the following experimental predictions: at velocities for which $\exp\left(-\nu\tau\right) \simeq 1$, all the ions entering the drift space will pass through at velocity v_1 without nucleating a ring. If v_1 is so large that $\exp\left(-\nu\tau\right) \simeq 0$, then all ions entering the drift space will emerge attached to quantized vortex rings. In the relatively narrow range of velocities between, both ions and ion-ring complexes will be observed. If the experiment is carried out by pulse techniques, we would expect the ion pulse to be reduced in amplitude in this range of velocity, but to have a definite arrival time. The rings, however, being nucleated according to a probability law, will have a range of arrival times depending on their distance from the collector at the moment of nucleation. Experiments testing these predictions will be described in § 7 (f).

(b) Localized roton states; the drag force on a moving ion

This section is concerned with the calculation of the number of rotons which can act as nuclei for the growth of a quantized vortex ring. We must first try to understand how a roton manages to be in the neighbourhood of an ion and in the correct orientation to act as a nucleus for ring growth; for at $0.6\,\mathrm{K}$ the probability of a roton being found within a volume the size of a negative ion is 3.7×10^{-4}, its orientation being, of course, random. We shall show that we can calculate the required number using the concept of localized roton states, and that direct experimental evidence for their existence comes from examining the drag on an ion at high velocities.

The connexion between localized roton states and drag can be appreciated from the following discussion (Strayer *et al.* 1971). Suppose we wished to compute the drag on an ion by solving the Landau equations (see, for example, Donnelly 1967, ch. 4). At low speeds the velocity field for the normal fluid with respect to the ion would be given, at a radial distance r from the ion small compared with ν/v_1 (where ν is now the kinematic viscosity of the normal fluid), by the Stokes flow:

$$v_{nr} = -v_1 \cos\theta \left[1 - \frac{3R_1}{2r} + \frac{R_1^3}{2r^3}\right], \qquad (7.7a)$$

$$v_{n\theta} = v_1 \sin\theta \left[1 - \frac{3R_1}{4r} - \frac{R_1^3}{4r^3}\right], \qquad (7.7b)$$

and for the superfluid by the potential flow:

$$v_{sr} = -v_1 \cos\theta \left[1 - \frac{R_1^3}{r^3}\right], \qquad (7.8a)$$

$$v_{s\theta} = v_1 \sin\theta \left[1 + \frac{R_1^3}{2r^3}\right], \qquad (7.8b)$$

where $\theta = 0$ is the direction of motion and R_1 is the radius of the sphere. At finite velocities the variables, including ρ_n, are functions of $\boldsymbol{w} = (\mathbf{v_n} - \mathbf{v_s})$ (see, for example, Donnelly 1967, pp. 112–113) so that from (7.7) and (7.8) one could calculate $\boldsymbol{w}$, then $\rho_n(w)$, solve anew for $\mathbf{v_n}(\boldsymbol{w})$ and $\mathbf{v_s}(w)$ and so on. One would hope that this iterative procedure would converge. We shall attempt to make some progress by means of a single interation, and by the use of the localized roton scheme first introduced by Glaberson *et al.* (1968), for calculating the properties of a vortex core. We cannot expect a very good solution from a single iteration, nor from using a continuum model

when the mean free paths of the excitations are much greater than the size of the ion. We can hope, nevertheless, to identify the governing physical processes.

The roton density in the presence of relative velocity of normal and superfluid is

$$N(T, w) = h^{-3} \int [\exp\{(\varDelta + (p - p_0)^2/2\mu_0 - pw\cos\phi)/kT\} - 1]^{-1} \, \mathrm{d}^3 p, \tag{7.9}$$

where ϕ is the angle between w and p. The integral in (7.9) can be evaluated by noting that the effect of w is to depress the roton minimum to $\varDelta_m = \varDelta - \frac{1}{2}\mu_0 w^2 - p_0 w$ and locate it at $\phi = 0$ and $p_m = p_0 + \mu_0 w$ [cf. figure 2b]. The principal contribution to the integral arises from the neighbourhood of the minimum $(\varDelta_m, p_m)$. Since in the present application we find $\varDelta_m/kT$ may still be considered significantly greater than unity, we drop the 1 in (7.9) and, observing that $p_0 \gg \mu_0 w$, we obtain

$$N(T, w)/N(T, 0) = [\sinh(p_0 w/kT)]/(p_0 w/kT), \tag{7.10}$$

where $N(T, 0)$ is the usual roton density, N_r. The number of rotons, n_r, trapped in the well about the ion should come by integrating $N(T, w) - N_r$ over all space outside the ion, using (7.7) and (7.8) to compute w. One finds that this quantity diverges, and that the origin of the divergence is the Stokes approximation which leads to (7.7). This divergence may be removed by a proper discussion of the Oseen flow which occurs at distances from the ion large compared with v/v_1, and by considering the incipient wake present at these distances. It would appear however that,
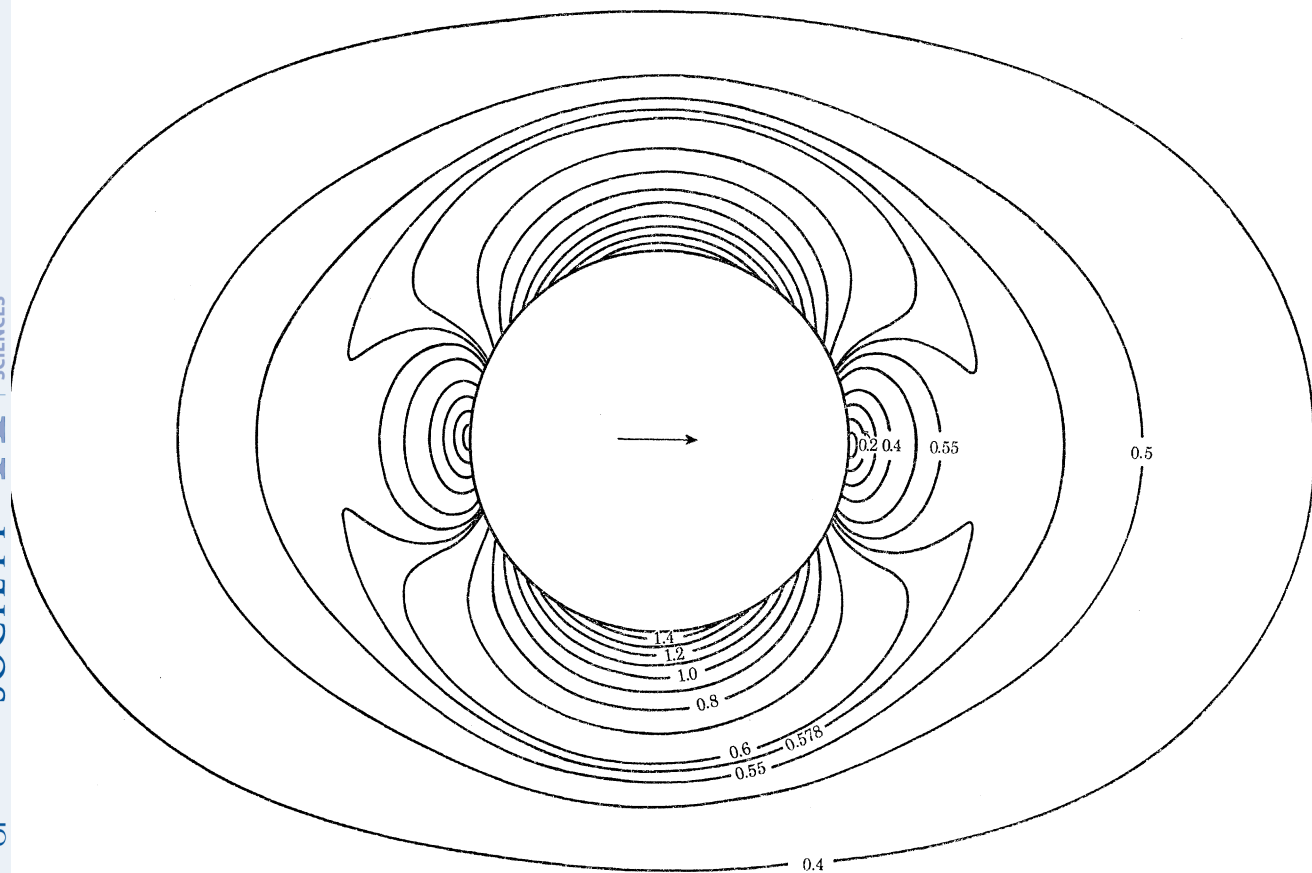

FIGURE 13. Lines of $|w| = $ constant near a moving ion. The curves are labelled with the corresponding value of $|w|$ measured in the unit v_1. The direction of motion ($\theta = 0$) is indicated by the arrow.

although the integrated enhancement in roton density from these regions is large, it does not correspond to oriented rotons trapped in the sense to be described presently. For this reason, a finite value of n_r was obtained by cutting off the integration. The choice of cutoff may be appreciated by reference to figure 13 which shows contours of constant $|w|$ plotted in the unit v_1. These contours can be seen from (7.9) to be contours of constant well depth for trapped rotons, and hence turning points for the motion of rotons whose energy is $p_0 w$ less than Δ. Those surfaces which intersect the ion surround the deepest energy well (at the equator), and we have chosen to integrate only to the last such surface, characterized by $|w| = v_1/\sqrt{3}$. This provides a finite estimate for n_r the number of localized, polarized rotons. It also introduces a new length in the problem, the distance l over which trapping occurs, and figure 13 shows that this is broadly of the order of the radius of the ion.

The calculation just described assumes the roton is a point particle. Actually the roton wavelength is about 0.4 nm, compared to the presently accepted ion radii $R_i^- = 1.6$ nm, $R_i^+ = 0.5$ to 0.8 nm. We shall allow for this situation by making a first-order correction to the energies by an uncertainty principle argument, as did Glaberson et al. (1967). If V is the volume available to a trapped roton as estimated from figure 12 and the argument above, the spread of momenta is of order $\Delta p \approx \hbar/V^{\frac{1}{3}}$ and the spread in energies $\Delta E \approx (\Delta p)^2/2\mu_0$. This energy spread is added to the argument of the exponential in (7.9). Final values of n_r come from integration by Simpson's one-third rule.

The detailed numerical results are temperature-dependent, and are not represented over the entire range of the natural variable

$$K = p_0 v_1/kT, \tag{7.11}$$

by any simple function we have examined. We find however that, in the temperature range $0.6\,\mathrm{K} \leqslant T \leqslant 1.0\,\mathrm{K}$ and the velocity range $3 < K < 8$, the following formulae approximate the results:

$$n_r = N_r R_i^3 \mathscr{E}_r, \tag{7.12}$$

where

$$\mathscr{E}_r = C\left[\frac{\sinh mK}{mK} - 1\right], \tag{7.13}$$

and m and C are chosen to fit best the numerical results (see table 7). Note that (7.13) is not a good approximation outside the range indicated. We consider these results to be more reliable than those we derived earlier [Donnelly & Roberts 1969c, equation (11)] on the simpler approximation that $\mathbf{v}_n$ is zero near the ion.

TABLE 7. NUMERICAL VALUES OF CONSTANTS USED TO CALCULATE n_r AND THE DRAG ON AN ION AT FINITE VELOCITIES.

T/K	m_+	m_-	C_+	C_-	f_+	f_-	$\mu^+/\mathrm{cm^2\,V^{-1}\,s^{-1}}$	$\mu^-/\mathrm{cm^2\,V^{-1}\,s^{-1}}$
0.6	0.9	1.0	4.94	7.97	0.060	0.012	1700	155
0.8	0.9	1.0	6.08	8.33	0.060	0.012	66	26
1.0	0.9	1.0	6.94	8.56	0.060	0.012	7.4	4.2

Let us now observe the ion from the laboratory frame. Noting first that $n_r \ll 1$, we see that the ion is usually bare: a roton which approaches the ion is localized for a time which may be estimated from equation (115) of Donnelly & Roberts (1969a). For example, at $T = 0.6$ K and $v_1 = 30$ m/s, the mean lifetime of a roton localized near a negative ion is about 3×10^{-5} s, whereas the interval between collisions with rotons of the bath is approximately 2×10^{-7} s. The trapped roton has a thermal velocity of order $\langle v \rangle = \sqrt{(kT/\mu_0)} \approx 91$ m/s and hence fluctuates back and

forth in its well at a frequency of order $\langle v \rangle / R_i = 6 \times 10^{10} \, \text{s}^{-1}$. During the time the trapped roton remains, the ion will experience about 150 collisions with the rotons of the bath and the trapped roton will fluctuate in its well perhaps 1000 times between each of these collisions. We have in addition, of course, phonon collisions, which will be more numerous.

One might, at first, believe that the relative occupation time of a roton localized near an ion is not long enough to be significant. We shall find, however, that these rotons have three important effects on the motion of the ion. First, they act as momentum transfer agents between the moving ion and the stationary normal fluid outside. Second, they increase the fluctuation rate near the ion by increasing the coefficient α_r (see the appendix, equation A 7) by the factor $\mathscr{E}_r$. Third, the rotons are in the precise position and polarization to act as 'proto-rings' for the growth of a macroscopic vortex ring. Our calculations will show that reasonable agreement with experiment results when all these considerations are taken together.

The experimental study of vortex-ring nucleation involves measurements of the velocity of an ion as a function of applied electric field. Let us, therefore, examine the way in which localized rotons influence the velocity-field relationship, changing it significantly from the simple mobility law which prevails at low velocities.

On a continuum picture, each time the roton fluctuates outward, it encounters the stationary normal fluid outside; some ion momentum is lost on every return trip, the exact amount depending upon the constitution of 'normal fluid' outside, i.e. rotons, phonons and ^{3}He atoms. The effective mass associated with a roton is $m = p_0^2 / 3kT$ [cf. Donnelly 1967, (3.73)]. The amount of momentum transmitted from the ion by the fluctuating roton will be written as fmv_i, where f (the only free parameter in this theory) is empirical and in general would be expected to be a function of the temperature, pressure, ^{3}He concentration and ion species. The resulting drag on the ion, F_r, is the product of the number of trapped rotons, the fluctuation rate, and the momentum exchange per fluctuation:

$$F_r = f(p_0^2 / 3kT) \, v_i \sqrt{(kT/\mu_0)} \, R_i^{-1} n_r$$

$$= f \rho_{nr} \mathscr{E}_r v_i \sqrt{(kT/\mu_0)} \, R_i^2. \tag{7.14}$$

Note that $p_0^2 N_r / 3kT = \rho_{nr}$ is the roton contribution to the normal fluid density evaluated far from the ion (cf. Donnelly 1967, p. 86), and the factor $\mathscr{E}_r$ is a measure of the local enhancement of this quantity owing to the flow about the ion. The mechanism of momentum transport described here resembles ordinary viscous transport as discussed in the kinetic theory of gases with the length l replacing the free path, and Strayer et al. (1971) have referred to the process as 'quasi-viscous'.

Equation (7.14) may be obtained a different way. Let us calculate the viscous stress

$$\mathscr{F} = \eta \, \partial v / \partial r$$

on the surface of the ion. The shear $\partial v_n / \partial r$ is approximately v_i / R_i and the coefficient of viscosity is $\eta = nm \langle v \rangle l$ [cf. Donnelly 1967 (3.97)], where $n = n_r / R_i^3$ is the number density, and we have taken $l \approx R_i$. The drag on the ion is then a product of the stress and the area of the surface, which recovers equation (7.14). Thus the quasi-viscous drag operates over the trapping length l about the ion. Because l acts in place of the free path, the coefficient of viscosity employed here contains a density, which is absent for an ideal gas.

When experiments on ion motion are performed, an arrangement is generally chosen which allows the ion to traverse a path at constant velocity, that is the drag force F on the ion is balanced by the electric field E; i.e. $F = eE$. Thus the field E required is the dependent variable, being the

force per unit charge necessary to maintain the ion drift velocity v_1. At low velocities the necessary field is given by the mobility relation $E = v_1/\mu$ where μ is composed of contributions from phonons, rotons and ^{3}He atoms:

$$\mu^{-1} = \mu_{\rm r}^{-1} + \mu_{\rm p}^{-1} + \mu_3^{-1}. \tag{7.15}$$

The hypothesis we make is that the quasi-viscous drag which occurs as a result of roton localization may be added to the low velocity contribution to give simply

$$E = \frac{v_1}{\mu} + v_1\left(\frac{f}{e}\right)\rho_{\rm nr}\sqrt{\frac{kT}{\mu_0}} R_1^2 \mathscr{E}_{\rm r}. \tag{7.16}$$

Equation (7.16) reduces to the usual mobility law at small velocities, since $\mathscr{E}_{\rm r} \to 0$ as $v_1 \to 0$. This means that the mobility of ions in helium II should strictly be defined as

$$\mu^{-1} = (\partial E/\partial v_1)_{v_1 = 0}. \tag{7.17}$$

At very high velocities ($K \gg 10$) the drag increases as $\exp\left(\frac{3}{2}K\right)$, reflecting the tendency of rotons to concentrate in the deepest part of the well at the equator where $|\boldsymbol{w}| \to \frac{3}{2}v_1$. Ring nucleation occurs before the asymptotic law begins to be valid, so that we must work in the intermediate range $3 < K < 10$, where $\mathscr{E}_{\rm r}$ is given approximately by (7.13).
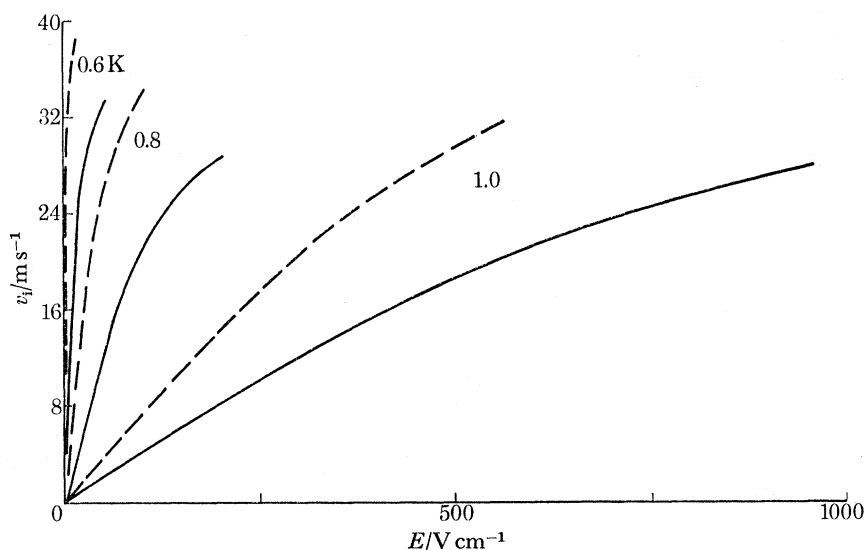

FIGURE 14. The drift velocity of positive ions (dashed lines) and negative ions (solid lines) at $T = 0.6$, 0.8, and $1.0\,\mathrm{K}$ calculated from equation (7.16) and the constants of table 7.

A family of drag curves for $T = 0.6$, 0.8 and $1.0\,\mathrm{K}$ for positive and negative ions is shown in figure 14. The curves are calculated from equation (7.16) using the values of m, C, f and μ listed in table 7. These calculated drag curves show a number of features of interest. The fields required to bring ions up to the nucleation velocity (the end-points of the curves) are highly temperature-dependent, whereas the velocities at which the quasi-viscous drag becomes apparent are *not* dramatically temperature-dependent (they range from 20 to 30 m/s in figure 14). The curves shown are in general agreement with experiment, considering the relatively large uncertainties in mobilities which still exist, and indicate that our empirical parameter f is independent of T in the temperature range indicated, and at the vapour pressure.

A more detailed comparison of equation (7.16) with experiment will be given in §7 (f) below. We shall see that the shapes of positive and negative ion drag curves are given quite accurately.

The results of the calculations of this section, then, provide evidence that the magnitude and temperature-dependence of n_r is reasonable, and provide strong corroboration for the present theory of ion nucleation which assumes that localized rotons are the origin of macroscopic vortex rings.

(c) Localized helium-3 states

Andreev (1966) has suggested that when small amounts of ^{3}He are added to ^{4}He to produce a dilute isotopic solution, some of the ^{3}He atoms may concentrate on the free surface of the liquid. Rayfield (1968) and Dahm (1969) have suggested that this may be true also for the microscopic free surface of a negative ion. This effect may be important in the production of rings by fluctuations because the localization of ^{3}He atoms increases the collision rate near the site of vortex nucleation.

Andreev gives an estimate for the number of ^{3}He atoms per unit area of surface, namely

$$N_s = \frac{n_3}{n_4} \frac{\hbar}{m} \rho \left(\frac{\mu}{m*}\right) \left(\frac{2\pi}{m*kT}\right)^{\frac{1}{2}} e^{\epsilon_0/kT}, \tag{7.18}$$

where μ is the effective mass of the impurity atom in the surface, $m*$ is its effective mass in the bulk solution and ϵ_0 is the binding energy of the surface state. Experiments by Zinovyeva & Bolarev (1968) give $\mu/m* = 0.9 \pm 0.1$ and $\epsilon_0/k = 1.8 \pm 0.2\,\mathrm{K}$, but there is, of course, no assurance that these parameters apply, without substantial modification, to the surface of a microscopic negative ion bubble.

The effect of the condensed ^{3}He atoms will be to increase α_3 [see the appendix, equation (A 8)]. We estimate this effect as follows. The number of ^{3}He atoms near the growing vortex ring is $n_3 V$, where V is the volume in which fluctuations are important. The discussion above shows this to be roughly a shell between $r = R_1$ and $r = 2R_1$; we will in fact take it to be 3 ion volumes. Thus the enhancement of ^{3}He atoms can be described by a factor $\mathscr{E}_3$, where

$$\mathscr{E}_3 = \frac{4\pi R_1^2 N_s}{3(\frac{4}{3}\pi R_1^3) n_3} = \frac{N_s}{R_1 n_3}. \tag{7.19}$$

We shall see that this will influence nucleation by changing α_3 to $\alpha_3 \mathscr{E}_3$, thus increasing the effective total value of α.

(d) Specification of the critical vortex; the free energy barrier and the curvatures

We suppose that a roton, in a localized state near an ion, as described in § 7 (b), acts as a proto-ring, which by diffusion in momentum space becomes a critical vortex, as envisaged in figure 12. We need not, as we have noted before, be too concerned with states between these limits, but the initial and final states should be carefully characterized in order to compute the free energy difference $\Delta F = F_C - F_A$ shown in figure 2. This should be done in the presence of the rather complex superfluid velocity field of equation (7.8).

The velocity of an element of vortex line depends on several factors: the presence of other vortex elements, of boundaries, of applied flow, and on the structure of the core itself. Provided the radius of curvature, R, of the element is large compared with its core diameter, the dominant term in its velocity is the self-induced velocity, which is

$$v = \frac{\kappa}{4\pi R} \ln \frac{1}{\epsilon}. \tag{7.20}$$

It is directed perpendicular to the osculating plane at the point of the element considered. This observation was first made by Arms & Hama (1965) who did not, however, give a value to the small parameter ϵ appearing in (7.20). To make a theory consistent with equation (2.3) we should take $\epsilon = \sqrt{e}\, a/8R$. Equation (7.20) should be modified to include the effects of distant vortex elements, boundaries and core structure. These have the effect of modifying the constant $\sqrt{e}/8$ in the value of ϵ just quoted. When the vortex is placed in a flow we can, ignoring dissipative effects, assume that there is added to the velocity above, the velocity of flow at the axis of the element: shear in the applied velocity only distorts the cross-section of the core. It follows, then, that provided $v_s \ll \kappa/a$ we may obtain the shape of the critical vortex by equating the velocity in (7.2) to the (reverse of the) local stream velocity.
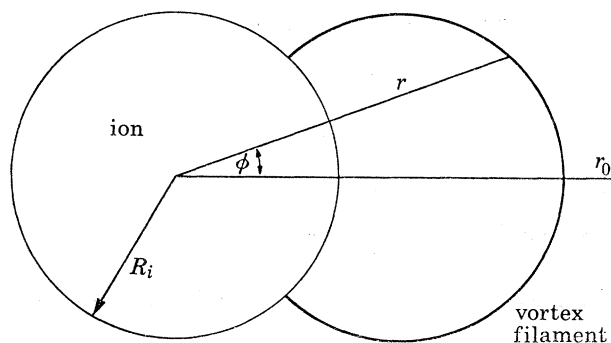

FIGURE 15. Geometry for calculating the shape of the critical vortex.

We set up spherical polar coordinates (r, θ, ϕ), in which $r = R_i$ is the ion surface, $\theta = 0$ is the direction of motion of the ion and $\phi = 0$ is directed towards the point $r = r_0$ on the vortex line farthest from the ion (cf. figure 15). Since the lowest energy state arises when the vortex lies in the equatorial plane, we write the equation of its axis in the equilibrium state as

$$r = r(\phi), \quad \theta = \tfrac{1}{2}\pi; \tag{7.21}$$

and the objective now is to use (7.20) above to compute $r(\phi)$. In doing so we shall assume that ϵ is constant. Although this is strictly inconsistent, the error is small since it will emerge that the radius of curvature in the solution changes slowly with ϕ. Equation (7.20) now gives

$$\frac{1}{R} \equiv \frac{-r(\mathrm{d}^2 r/\mathrm{d}\phi^2) + r^2 + 2(\mathrm{d}r/\mathrm{d}\phi)^2}{[(\mathrm{d}r/\mathrm{d}\phi)^2 + r^2]^{\frac{3}{2}}} = \frac{4\pi}{\kappa}\frac{v_z(r)}{\ln(1/\epsilon)}, \tag{7.22}$$

where $v_z(r)$ is the superfluid velocity defined by (7.8b) for $\theta = \tfrac{1}{2}\pi$. If we measure r in units of R_i and $v_z(r)$ in units of v_i, the velocity of the ion in the laboratory, this may be written in the dimensionless form

$$r\frac{\mathrm{d}V}{\mathrm{d}r} = 2V - \frac{V^2}{\lambda}f(r), \tag{7.23}$$

where

$$V^2 = \left(\frac{\mathrm{d}r}{\mathrm{d}\phi}\right)^2 + r^2, \quad f(r) = \frac{v_z}{v_i}, \tag{7.24}$$

and

$$\lambda = \frac{\kappa}{4\pi v_i R_i}\ln\frac{1}{\epsilon}. \tag{7.25}$$

Let

$$g(r) = \int_1^r r f(r)\,\mathrm{d}r. \tag{7.26}$$

For any axisymmetric body with fore-aft symmetry, we would have on the equatorial plane

$v_z = \partial\psi/r\,\partial r$ where ψ is a stream function. Essentially $g(r)$ in (7.26) is the stream function difference (i.e. the flux) between the surface and the radius concerned. Then (7.23) gives at once

$$\frac{r^2}{V} = \frac{g+C}{\lambda}, \tag{7.27}$$

where C is a constant, and hence

$$\phi = \pm \int_{r_0}^{r} \frac{\mathrm{d}r}{r\sqrt{\left[\left(\frac{\lambda r}{g+C}\right)^2 - 1\right]}}, \tag{7.28}$$

which determines $\phi = \phi(r)$, i.e. the form of the required curve.

In the case of interest, v_z is the potential flow (7.8b) past the sphere, i.e. in dimensionless units,

$$f(r) = 1 + \tfrac{1}{2}r^{-3}, \tag{7.29}$$

so that by (7.26)

$$g(r) = (r^3 - 1)/2r. \tag{7.30}$$

To determine C we note that a vortex core must meet a boundary normally. Otherwise the vortex together with its image would have a cusp associated with infinite energy and velocity. When $r = 1$, we must therefore have $\mathrm{d}r/\mathrm{d}\phi = \infty$. Thus by (7.24) and (7.27) we have $C = 0$. It is also clear by (7.24) and (7.27) that, at $r = r_0$ (where $\mathrm{d}r/\mathrm{d}\phi = 0$), $g = \lambda r$, i.e. by (7.30),

$$r_0^3 - 2\lambda r_0^2 - 1 = 0, \tag{7.31}$$

giving

$$r_0 = \tfrac{2}{3}\lambda + (c + \tfrac{1}{2})^{\frac{2}{3}} + (c - \tfrac{1}{2})^{\frac{2}{3}}; \quad c = (\tfrac{1}{4} + \tfrac{8}{27}\lambda^3)^{\frac{1}{2}}. \tag{7.32}$$

Figure 16 shows the results of numerical integrations of (7.28) for four values of λ. It is clear that the larger λ the more the vortex is pulled from the ion.
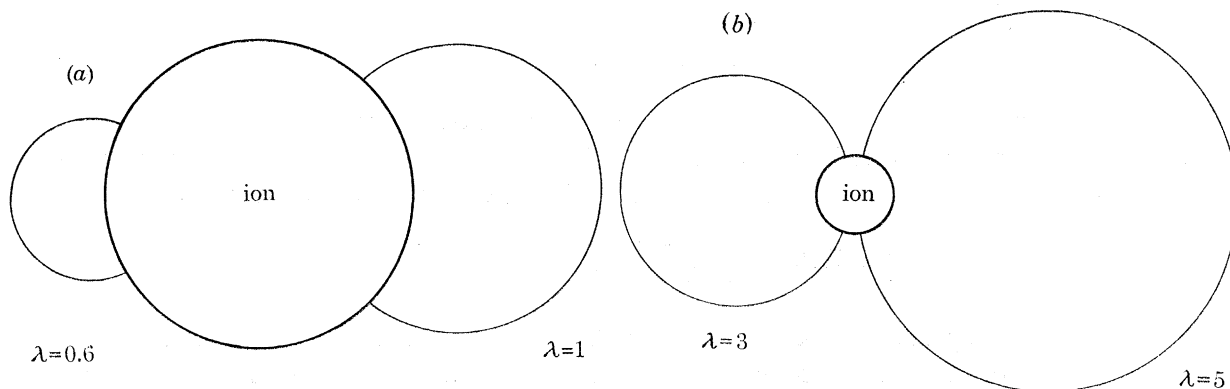

FIGURE 16. Shape of the critical vortex on Arms's 'localized induction' concept shown for four values of the dimensionless velocity λ. (a) and (b) are shown on different scales of the ion radius for convenience in display.

A corollary of the Arms–Hama concept is the idea, due to Feynman (1965), that the hydrodynamical energy E of the vortex flow can be computed to the same logarithmic accuracy by multiplying its arc length by an energy per unit length, or tension, of $(4\pi)^{-1}\rho_s \kappa^2 \ln(1/\epsilon)$. We are therefore interested in computing the arc length $S(\lambda)$ of the vortex and also, because of the impulse p, its area $A(\lambda)$. We find, still in dimensionless units,

$$S = 2\int_{1}^{r_0} \frac{2\lambda r^2\,\mathrm{d}r}{[(2\lambda r^2)^2 - (r^3 - 1)^2]^{\frac{1}{2}}}, \quad A(\lambda) = \int_{1}^{r_0} \frac{(r^2 - 1)(r^3 - 1)\,\mathrm{d}r}{r[(2\lambda r^2)^2 - (r^3 - 1)^2]^{\frac{1}{2}}}. \tag{7.33}$$

The necessary integrations were performed numerically, the singularities of the integrands at $r = r_0$ being carefully allowed for. It should be evident from an inspection of figures 16a and 16b that no violence is done to the truth by neglecting the variation of v_z with r, obtaining then a circle of radius χR_1 (say). Assuming that this curvature is that consistent with v_z at $r = r_0$ (and $\phi = 0$) and reapplying the Arms–Hama result (7.20), we quickly obtain the results listed in table 8, which also gives the corresponding quantities obtained from the more precise theory. Clearly, the agreement between the two theories is good at any λ: in fact they are identical in both the limits $\lambda \to 0$ and $\lambda \to \infty$. We use this circle theory to find P and hence $\nu\tau$. We take E_C to be that appropriate to a segment of vortex of length $R_1\chi(\pi + 2\tan^{-1}\chi)$, namely

$$E_C = \frac{1}{4\pi}\rho_s\kappa^2 R_1\left[\ln\left(\frac{8R_1\chi}{a}\right) - \frac{3}{2}\right]\chi(\pi + 2\tan^{-1}\chi), \tag{7.34}$$

which is consistent with Feynman's tension idea and with equation (2.2). The momentum p_C is taken to be that corresponding to the area lying between the vortex and the ion, viz.

$$p_C = \rho_s\kappa R_1^2[\tfrac{1}{2}\chi^2(\pi + 2\tan^{-1}\chi) + \chi - \tan^{-1}\chi], \tag{7.35}$$

and we set the velocity

$$\frac{\partial E}{\partial p} = \frac{\kappa}{4\pi R_1\chi}\left[\ln\left(\frac{8R_1\chi}{a}\right) - \frac{1}{2} - \frac{2\chi}{(1+\chi^2)(\pi + 2\tan^{-1}\chi) + 2\chi}\right], \tag{7.36}$$

equal to the velocity v_z at $(r_0, 0)$, namely

$$v_1\left[1 + \frac{1}{2(\sqrt{(1+\chi^2)}+\chi)^3}\right]. \tag{7.37}$$

This, for given χ, determines v_1.

We should recall that, since R_1 is so small for helium ions, the radius of curvature χR_1 of the critical fluctuation is only a few multiples of a. Although classical vortex theory is surprisingly

TABLE 8

λ	ϕ_0	r_0	$\dfrac{E_C}{\rho_s\kappa R_1^2 v_1}$	$\dfrac{p_C}{\rho_s\kappa R_1^2}$	$\dfrac{E_C - p_C v_1}{\rho_s\kappa R_1^2 v_1}$
			Circle		
0.1	4.07	1.074	0.02334	0.00845	0.0149
0.2	8.63	1.163	0.1045	0.0408	0.0637
0.4	18.65	1.393	0.5121	0.2281	0.2840
0.6	28.49	1.681	1.347	0.6549	0.6923
0.8	36.90	2.005	2.671	1.365	1.306
1.0	43.92	2.351	4.501	2.364	2.138
1.5	55.93	3.264	11.30	6.072	5.227
2.0	63.28	4.211	21.26	11.44	9.82
3.0	71.53	6.150	50.64	27.01	23.63
5.0	78.68	10.094	147.1	77.16	70.00
			More exact theory		
0.1	4.0	1.07	0.0228	0.00806	0.0148
0.2	8.4	1.15	0.0994	0.0371	0.0623
0.4	18.1	1.35	0.470	0.194	0.276
0.6	28.2	1.59	1.23	0.549	0.678
0.8	37.7	1.88	2.46	1.17	1.29
1.0	45.7	2.21	4.22	2.09	2.13
1.5	59.4	3.10	10.9	5.70	5.23
2.0	67.2	4.06	20.9	11.1	9.82
3.0	75.1	6.03	50.3	26.7	23.6
5.0	81.2	10.0	147	76.9	70.0

good for quite small values of R/a (see footnote on p. 45), the expression for E, and therefore v_1, becomes rather sensitive to the value of a assumed or, equivalently, to the constant $\frac{3}{2}$ taken in (7.34). For example, if the constant is omitted entirely, the critical velocity is more than doubled for each ion, taking it generally beyond the Landau velocity for emission of rotons.† Since this is the case, we should also expect that image effects neglected in the present calculation should affect E significantly. Fortunately, in the limit $\chi \to 0$, it appears that images should have no effect on our results whatever, since the critical fluctuation resembles a semi-circular arc on an infinite wall. The image is also a semicircle which completes the circular ring. In computing the kinetic energy of flow, however, the integration must be taken over only half the volume, and therefore gives only half the classical expression, in agreement with (7.34) above. At other values of χ, the image of each element of the vortex is an element of strength $\kappa R_1/r$ at the inverse point, and directed in the obvious way (see, for example, Basset 1888 art. 311). For $\chi \to \infty$ this image coincides with the diameter of the ion joining the points at which the vortex meets it. The strength of the vortex is not, however, constant along this diameter, falling from its value κ on the ion surface to zero at its centre. In this limit, however, the corrections described extend over only a tiny volume near the ion, and vanish in the limit $\chi \to \infty$. At intermediate values of χ, the position is neither clear nor easy to assess, but we would surmise that, since the image effects do not influence E in either limit, they would not affect it greatly under any circumstance.

(e) Calculations and results

For simplicity, we have adopted again the one-dimensional form (3.42) of the escape probability P:

$$P = (2\pi)^{-1} \omega_A \omega_C \Lambda_C \exp\{-(F_C - F_A)/kT\}. \tag{3.42}$$

By the reasoning of § 7 (b) below equation (7.9),

$$F_A = \Delta - p_0 v_z(r_0), \tag{7.38}$$

where $v_z(r_0)$ comes from (7.37). On the assumption that the roton is the proto-ring,

$$\omega_A^2 = \mu_0^{-1}. \tag{7.39}$$

The free energy

$$F_C = E_C - p_C v_z(r_0), \tag{7.40}$$

is given directly by (7.34) and (7.35). The curvature ω_C comes by differentiating (7.36) once more:

$$-\omega_C^2 \equiv \frac{\partial^2 E}{\partial p^2} = \frac{-(\ln(8R_1\chi/a) - \frac{5}{2})}{4\pi R_1 \chi^2} \left\{ \rho_s R_1^2 \left[\chi\left(\pi + 2\tan^{-1}\chi + \frac{2\chi}{1+\chi^2}\right) \right] \right\}^{-1}, \tag{7.41}$$

and the vortex diffusivity is given by

$$\Lambda_C = 4\alpha(\pi/\rho_s \kappa^3)^{\frac{1}{2}} p_C^{\frac{1}{2}}. \tag{7.42}$$

The nucleation rate is determined by the product of the number of trapped rotons and the probability of nucleation:

$$\nu = n_r P, \tag{7.43}$$

where n_r is given by (7.12) and (7.13). Given (7.13), the probability that an ion will traverse a drift space of length L without nucleating a ring is given (as we have remarked before) by

$$N_i/N = e^{-\nu\tau}, \tag{7.44}$$

where

$$\tau = L/v_1, \tag{7.45}$$

† The theory of the onset of superflow of § 6 (a) also becomes sensitive to these constants as the diameter of the tube decreases. We there adopted the constant $-7/4$ in (2.2) in order to follow Gopal's analysis and results.

and we have used $L = 5.2$ cm for purposes of comparison with experiments performed at the University of Oregon.

The core parameters have been included in the calculations simply by writing the logarithmic factor $[\ln (8R/a) - \frac{3}{2}]$ as $\ln (\xi R/a)$, where $\xi = 1.785$. Other core sizes or models can easily be included by changing ξ or a.

Calculations have been carried out numerically using a Hewlett Packard 9100 A desk calculator system equipped with an X–Y recorder output. The procedure is to look up all the constants for the temperature and pressure of interest from § 7 (b) and the appendix: these are entered appropriately in the program. Execution is obtained by guessing an initial value of χ, computing v_1 from (7.36) and (7.37) and N_i/N from (7.38 to 7.45). As the value of χ is incremented, N_i/N is plotted out as a function of v_1. The appearance of a representative calculation is shown in figure 17, together with indications of the various velocity regions discussed above. At low velocities the ions are bare and obey a mobility relation. At larger velocities, the ions begin to localize rotons forming the ion–roton complexes described in § 7 (b). The ratio N_i/N decreased from unity when the ion–roton complexes begin to nucleate macroscopic rings in noticeable numbers. We define the characteristic velocity, v_{1c}, for nucleation as that velocity for which $\nu\tau = 1$, or $N_i/N = e^{-1}$. At higher velocities nearly all ions have nucleated vortex rings.
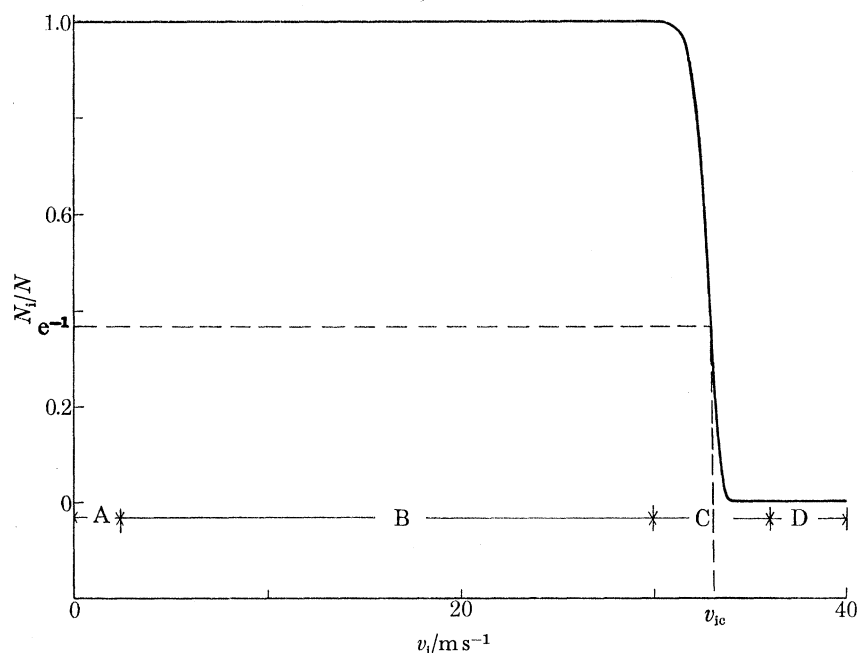

FIGURE 17. Appearance of a representative calculation of N_i/N as a function of v_i. We can distinguish four regions, A to D. Region A corresponds to very low velocities, and to 'bare' ions. Region B is the régime of ion–roton complexes. Region C is a mixed region of ion–roton and ion–ring complexes. Region D is all ion–ring complexes. The characteristic velocity, v_{ic}, is determined by the condition $N_i/N = 1/e$.

The rapid cutoff of N_1/N in the neighbourhood of v_{1c} is due to the finite lifetime of ion–roton complexes in a manner analogous to the escape of ions from quantized vortex lines which was studied earlier by us (see Donnelly & Roberts 1969 a, figures 9 and 10). This similarity to our previous calculations prompts us to refer to the cut-off characteristic of figure 17 as a 'lifetime edge'.

The ion radii to be used require some discussion. The negative ion radius estimated by Parks &

Donnelly [cf. figure 9b of Donnelly & Roberts 1969a] is $R_i^- = 1.6$ nm, a value independently confirmed by Zipfel & Sanders (1968). The radius of the positive ion, 0.79 nm, has been considered to be somewhat too large. Dahm & Sanders (1966) estimate 0.67 nm, whereas Schwarz & Stark (1969) quote 0.5 nm. We note that 0.65 nm is within a healing length of all estimates, and hence is a reasonable compromise. We adopt, therefore, $R_i^+ = 0.65$ nm and $R_i^- = 1.6$ nm for the calculations of this paper.

We show in table 9 the results of calculations of v_{1c} for positive and negative ions at the vapour pressure. Values of χ_C which determine the size of the critical vortex are also quoted.

TABLE 9. TEMPERATURE DEPENDENCE OF v_{1c} AND χ_C FOR POSITIVE
AND NEGATIVE IONS ($P = 0$, $a = 0.128$ nm)

T/K	0.3	0.4	0.5	0.6	0.7	0.8	0.9	1.0	1.2	1.4
$v_{1c}^+/\text{m s}^{-1}$	45.5	44.3	42.5	39.8	37.3	35.2	33.4	31.9	29.3	26.8
χ_C^+	0.64	0.67	0.73	0.83	0.92	1.02	1.11	1.20	1.38	1.58
$v_{1c}^-/\text{m s}^{-1}$	38.7	37.3	35.5	33.1	31.1	29.4	28.0	26.8	24.6	22.7
χ_C^-	0.29	0.31	0.34	0.39	0.44	0.48	0.53	0.57	0.65	0.75

Experiments yielding the temperature dependence of positive and negative ion nucleation velocities have been carried out below 1 K by Cunsolo & Maraviglia (1969). They found evidence for two branches of ion-ring complexes. The branch corresponding to the conditions of the present theory is shown in figure 18, the other branch will be discussed presently. Cunsolo & Maraviglia recorded the *threshold field* for ring formation, and the corresponding velocity. We have, therefore, calculated that quantity from the theory by assuming that the threshold would be seen when approximately 10 % of the ion complexes had nucleated rings, that is $N_1/N = 0.90$. These results are plotted as the solid lines in figure 18, and it can be seen that the magnitude and temperature-dependence of the onset velocities are in satisfactory agreement with experiment over the range $0.4\,\text{K} < T < 1.0\,\text{K}$.
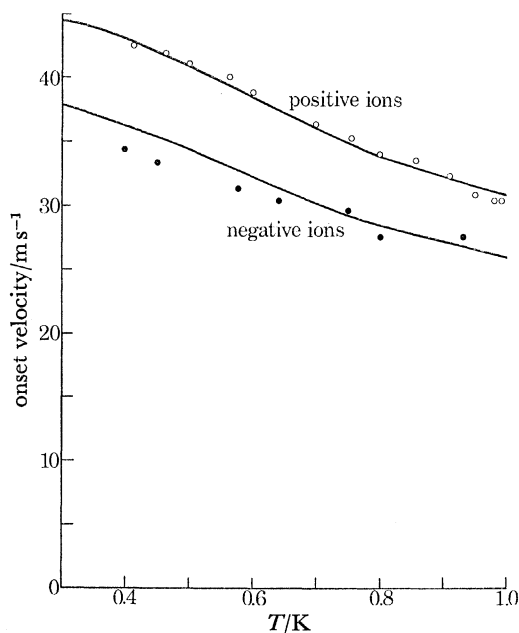

FIGURE 18. Onset velocities determined by Cunsolo & Maraviglia (1969) for positive ions (open circles) and negative ions (closed circles). Solid lines are calculated from the theory for the onset velocity ($N_i/N = 0.90$).

The second branch of rings observed by Cunsolo & Maraviglia (1969) was also observed by Rayfield (1968). It arises in the following way: the determining variable in nucleation is the velocity of the ion; the electric field plays no essential part. At low enough temperatures, where α is small, the formation of fast ions by α-particles at the source gives them sufficient velocity that $v_i > v_{ic}$, and rings are produced directly. These rings will decay unless sufficient field is present near the source to overcome the drag. It is easy to estimate the magnitude of the minimum field, E_{min}, necessary to maintain rings at the critical size by setting $\chi_C \approx 1$, so that

$$E_{min} \cong \frac{\alpha}{e}\left[\ln\left(\frac{8R_i}{a}\right) - \frac{1}{2}\right]. \qquad (7.46)$$

Thus if the experiment is arranged to have a field $E > E_{min}$ between the source and the first grid, source rings will be observed in the rest of the apparatus. At certain temperatures, source rings may be so prevalent that one may have to arrange a region where $E < E_{min}$ to allow source rings to decay away. At very low temperatures it will be nearly impossible to observe bare ions: for example, at $T = 0.1\,\mathrm{K}$, E_{min} is only $5\,\mathrm{mV/cm}$, which can easily be produced by stray potentials. This circumstance has been noted by Neeper & Meyer (1969) and a similar explanation advanced by Gamota & Sanders (1968).
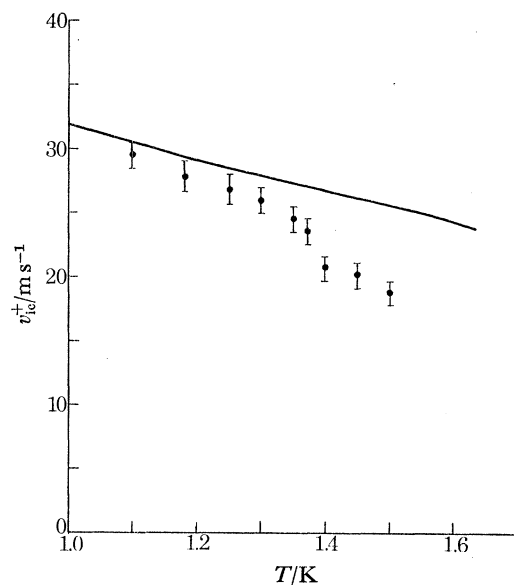

FIGURE 19. Velocities for nucleation of rings as estimated from drag curves for positive ions by Bruschi *et al.* (1968).

The region above $1\,\mathrm{K}$ is very difficult to explore because the field required to maintain ring velocities of this order increases to the order of many kilovolts/centimetre owing to the high energy loss, given by $\alpha[\ln(8R/a) - \frac{1}{2}]$ ergs/cm. Further, the positive ion ceases to be permanently attached to a vortex above $1\,\mathrm{K}$ (cf. Donnelly & Roberts 1969a). Bruschi, Mazzoldi & Santini (1968) were able to observe a high field velocity for positive ions, independent of field, which was interpreted as an equilibrium between creation and detachment of rings from ions, and hence a rough guide to the magnitude of v_{ic}^+. Their results are shown in figure 19 compared with the present theory. The agreement in magnitude is good, considering the uncertainties in the indirect experimental determination. The theory, calculated with constant a, will give a v_{ic}^+ which falls off more rapidly than is shown when the temperature-dependence of the core radius is finally known.

The difference between positive and negative ions on our model reflects several factors. One is the size of the ion. Table 10 shows the dependence of v_{1c} on ion radius at $T = 0.65$ K and at the vapour pressure. The critical velocity falls steadily with increasing ion radius. The effect can be seen on comparing positive and negative ions at the vapour pressure: $v_{ic}^{+} = 38.5$ m/s and $v_{ic}^{-} = 32.0$ m/s. On applying pressure, P, we would expect little effect on the positive ion since its radius is not thought to vary much with pressure. The negative ion, however, being a bubble, will shrink in size (cf. Donnelly & Roberts 1969a, figure 11); at 20 atm (1 atm $\approx$ 100 kPa) it appears to have decreased in size to about 1 nm. On the basis of table 10 the critical velocity would *increase* from 32.0 to 35.2 m/s. There are, however, other effects. The values of Δ/k, μ_0 and p_0 all change as outlined in the appendix. Taking all variations into account we find, at $T = 0.65$ K, $v_{ic}^{-} = 32.05$ m/s at the vapour pressure and 35.26 m/s at 20 atm, a slightly larger increase than suggested by size alone. Rayfield (1968) working between 0.3 and 0.6 K finds nearly a 50 % increase. Indeed his results at high pressures would appear to correspond to an ion radius smaller than that of even the positive ion!

TABLE 10. THE VARIATION OF v_{1c} WITH ASSUMED ION RADIUS R_1 AT $T = 0.65$ K

$R_i/$nm	0.4	0.5	0.6	0.8	1.0	1.2	1.4	1.6	1.8	2.0
$v_i/$m s^{-1}	42.5	40.5	39.0	36.8	35.2	33.9	32.9	32.0	31.4	30.8

The present theory suggests that at low temperatures, adding ^{3}He will increase the fluctuations. The extent of this effect is examined in table 11 at $T = 0.3$ K for positive and negative ions.

TABLE 11. INFLUENCE OF VARYING CONCENTRATIONS OF ^{3}He IN ^{4}He
ON THE CRITICAL VELOCITY

n_3/n_4	10^{-10}	10^{-8}	10^{-6}	10^{-4}	10^{-2}
$v_{ic}^{+}/$m s^{-1}	46.16	46.07	44.71	42.79	41.11
$v_{ic}^{-}/$m s^{-1}	39.17	37.83	36.22	34.83	33.62

There is a difference in the effect of doping—slightly greater reduction in v_{1c} for the negative ion because of localization of ^{3}He atoms on the surface, as described in § 7 (c). The condensed ^{3}He on the negative ion tends to reduce the effect of adding hydrostatic pressure. Rayfield (1968) has observed this effect, but, again, the magnitude of the effect he obtains is larger than we can account for. It is entirely possible, of course, that the concentration of ^{3}He on the surface of a negative ion is much greater than that estimated for a macroscopic free surface by Andreev. Furthermore, the binding energy ϵ_0 may well be a function of pressure. Systematic measurements of nucleation as a function of temperature, pressure and ^{3}He concentration may open the way to understanding these effects.

(f) *Nucleation experiments and comparison with theory*

Although experiments on critical velocities were available at the time this theory was being developed, experiments testing some of the features specifically related to the fluctuation picture were lacking. A series of such experiments were begun by D. M. Strayer and R. J. Donnelly at the University of Oregon, some of which will be summarized here (Strayer 1971).

One characteristic feature of the nucleation picture developed here is the lifetime edge. Observation of this edge requires two separate experiments: a measurement of v_i as a function of electric field E (or in practice the voltage V across the drift region) and measurement of N_i/N,
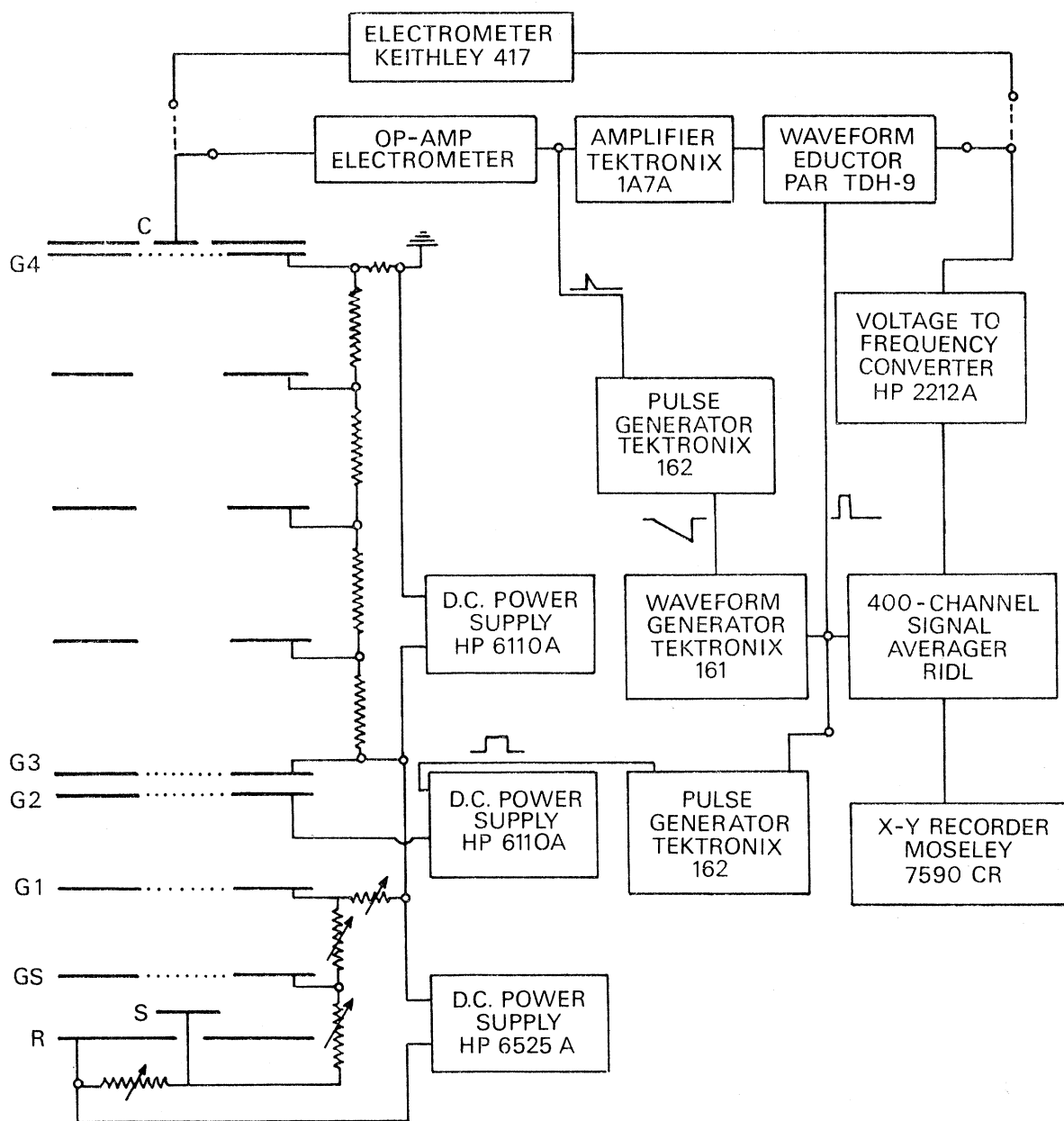
FIGURE 20. Apparatus used at the University of Oregon for studying the nucleation of vortex rings by ions. A representative set of electrode potentials for observing negative ions is shown.

which is proportional to the ion current reaching the collector, as a function of E. An apparatus designed for these measurements is illustrated in figure 20.

The mobility cell was constructed by modifying the apparatus used earlier to measure ion motion along vortex lines (cf. figure 12, Donnelly & Roberts 1969a). The principal change was to put the radioactive source which produces the ions on the bottom of the apparatus. The major improvement required for the nucleation experiment was better time resolution. One can see from figure 14 that velocities greater than 30 m/s must be measured in this experiment to a relative accuracy of better than 1 %. For a drift space $L = 5.2$ cm, this implies measuring times of flight of magnitude 1.5 ms to an accuracy of 15 μs. An electrometer was built following the guide lines of Wing & Sanders (1967). A 0.6 to 6.0 pF capacitor was placed in parallel with a $10^9 \Omega$ resistor in the feedback loop of an Analog Devices 149 A operational amplifier, which provides a 30 μs rise time with the feedback capacitor adjusted to minimum.

The noise output is sufficiently great that signal averaging is required. Our 400 channel RIDL analyser has a minimum dwell time of 12.5 μs per channel and a switching time of 12.5 μs. The time resolution required in the experiment is obtained by averaging on a Princeton Applied Research TDH-9 Waveform Eductor which has a minimum resolving time of about 1 μs. The output of the operational amplifier electrometer is first fed into a Tektronix 1 A 7 A pre-amplifier. The signal stored in the Eductor can be averaged further in the RIDL analyser, using a Hewlett Packard 2212 A voltage-to-frequency converter which converts voltage levels stored on 100 capacitors in the Eductor to pulse times that can be counted and stored in the RIDL analyser. This transfer of data from the faster signal averager to the slower one can be accomplished without loss of time resolution because the Eductor can record the signal at one sweep rate and read out the signal at another (in this case, slower) sweep rate. By adjusting these sweep rates, the signal is spread out in time (the time axis is 'stretched') by a factor of 100. By repeating the sequence of storing on the Eductor and reading into the RIDL many times it is simple to improve the signal-to-noise ratio to the point where it is easier to analyse. Appropriate time delay circuitry makes it possible to use the 100 channels of the Eductor in the immediate time domain of the received pulse. These techniques have made possible the precise ion velocities needed in this investigation.

We show in figure 21 results of such measurements as a function of voltage V (between G 3 and C in figure 20) at $T = 0.60, 0.65$ and 0.70 K for negative ions and in figure 22 results at $T = 0.60, 0.65, 0.70$ and 0.75 K for positive ions. The solid lines represent equation (7.16). One can see that this relation provides a very useful interpolation formula for the data.

The next step is to measure the current as a function of field. This is done by using a relatively wide pulse which allows the current to equilibrate while it is on. Typical results are shown in figure 23 for negative ions at $T = 0.65$ K. Below 300 V the current is continuously rising in a manner which reflects the characteristics of the source of ions. We assume the curve would carry on as suggested by the extrapolation except for lifetime effects above 300 V. The current is measured on the ordinate in terms of the current, I_{260}, present at 260 V. This was done because amplitude measurements were plagued by drifts which appeared to be associated with the build-up of charge in the source region. Repeated comparisons with I_{260} helped compensate for this drift. From time to time the source voltages were 'retuned' to optimize the current. The data for the lifetime edge were taken as being proportional to the value of I/I_{260} at a given voltage on the lifetime edge, divided by the amplitude indicated by the solid curve at the same voltage. This yields N_1/N as a function of V and hence E.

The lifetime edge is now produced by combining the data for the measurements as outlined

in § 7 (*e*). (See figure 24.) Considering the difficulties and uncertainties in both the theory and experiment the agreement in magnitude is probably fortuitous. The slopes of the experimental points would appear to exceed slightly that of the theoretical curve. Three other examples are shown in figures 25 to 30, demonstrating again that the theory quite satisfactorily accounts for nucleation at the vapour pressure. We have already indicated in § 7 (*e*) that the situation at higher pressures for negative ions is qualitatively correct, but not yet satisfactory in magnitude (Strayer 1971).
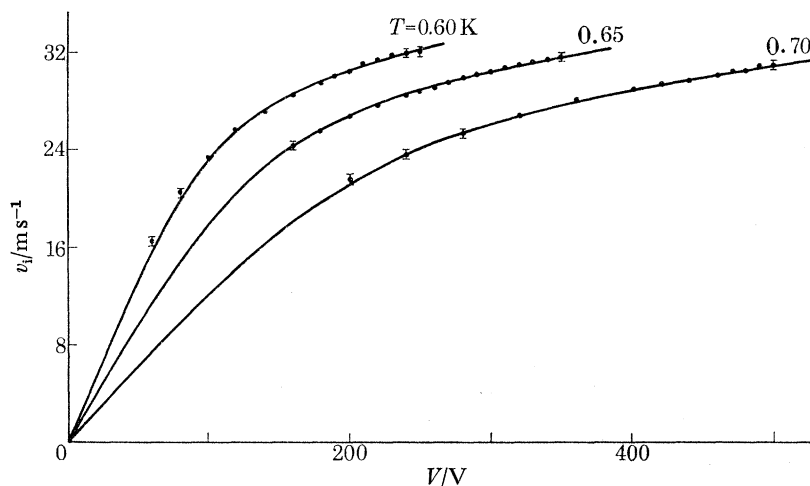

FIGURE 21. Velocities v_i for negative ions at the vapour pressure determined from time-of-flight experiments across the drift space of length $L = 5.2$ cm. The voltage difference V refers to the region G 3–C in figure 20. The solid curves come from equation (7.16).
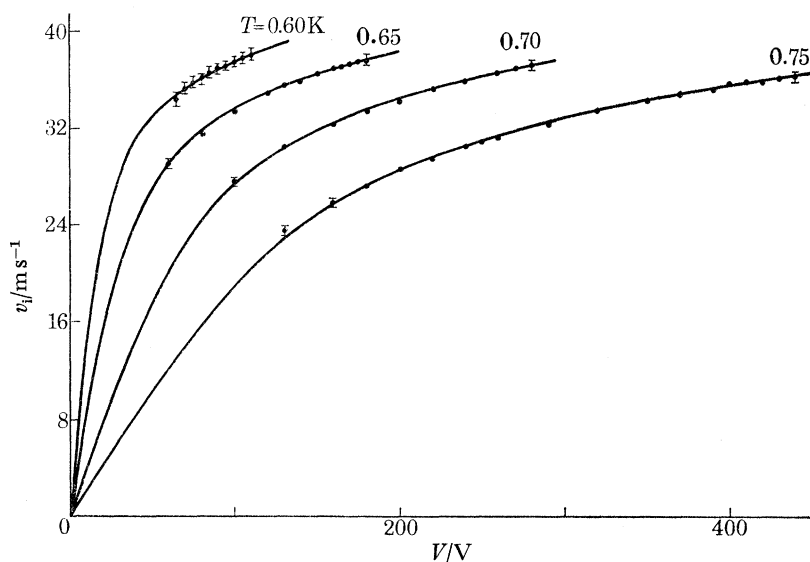
FIGURE 22. Results as in figure 21, but for positive ions.

Another characteristic of the present theory which can be seen experimentally is the random nucleation of rings as the ion traverses its flight path. We show in figure 31 *a* a sharp pulse corresponding to the arrival of a group of ions under conditions that the velocity is just short of the life-time edge. An increase in the drift space voltage of just a few volts produces the dramatic change seen in figure 31 *b*. Here the ion pulse amplitude has dropped considerably (it is indicated

by the small arrow) and a large irregular pulse owing to rings now follows it. One can see that the quickest rings move at about the same velocity as the ions, a circumstance made use of in § 7 (a). Higher resolution experiments confirm this more precisely.

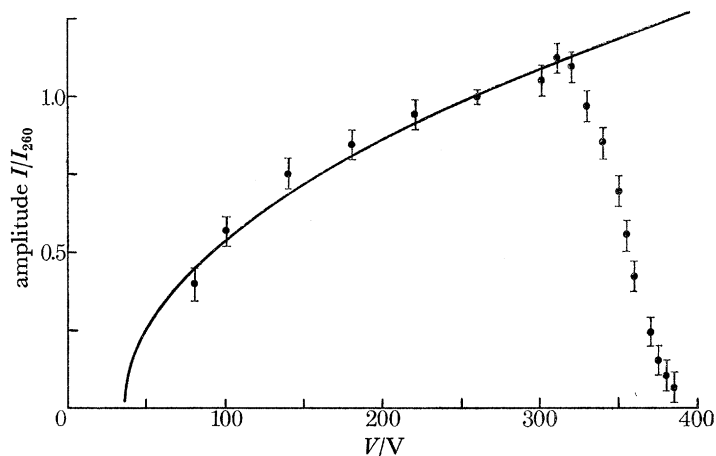FIGURE 23. Ion current amplitude as a function of drift space voltage. The amplitudes were continually referred to the current at 260 V to compensate for current drifts during the run. The solid curve is chosen to extrapolate the currents beyond the lifetime edge (here about 300 V). The probability N_i/N is taken as the ratio of the observed amplitudes to that represented by the solid curve.
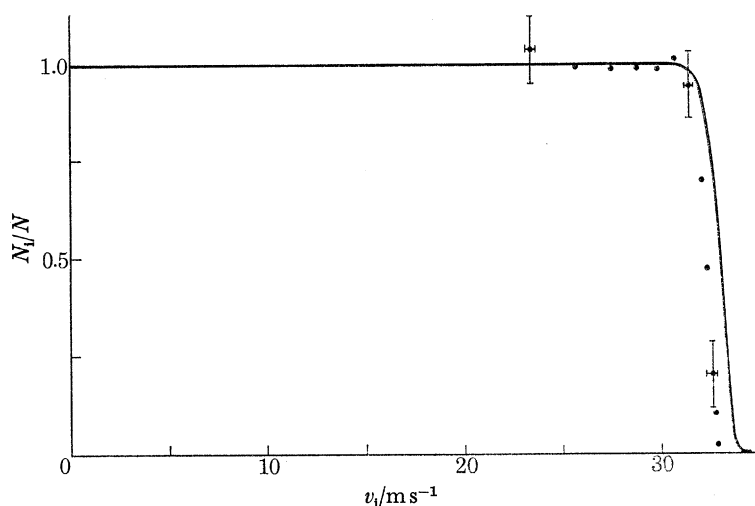
FIGURE 24. The experimental points represent the probability N_i/N as a function of v_i obtained by combining data such as in figure 23 with data such as in figures 21 and 22. The magnitude of the experimental uncertainties is indicated by bars on three representative points. The solid curve is calculated by the method outlined in § 7 (e). Here $T = 0.60$ K, $P = 0$, $R_1 = 1.6$ nm, $a = 0.128$ nm and the ions are negative.

A final comment should be made here. The gratifying agreement of the theory at the vapour pressure with experiment is *not* sufficient to justify the assumption that the smallest rings are rotons. Close inspection of the consequences of equation (7.43) reveals that the nucleation rate of an ion is independent of the gap Δ and varies only slowly with p_0. An assumption that the smallest rings have a different energy E_m and momentum p_m [presumably near (Δ, p_0)] would not substantially affect the results obtained here.
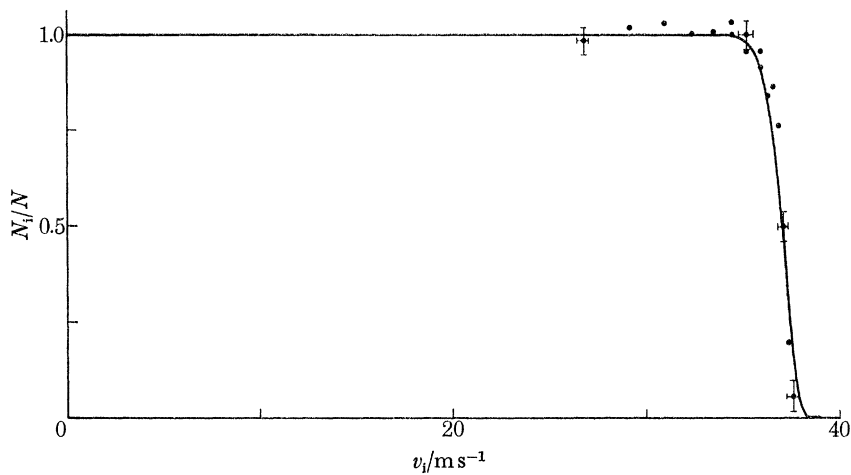
FIGURE 25. Results as in figure 24, except $T = 0.65\,\mathrm{K}$.
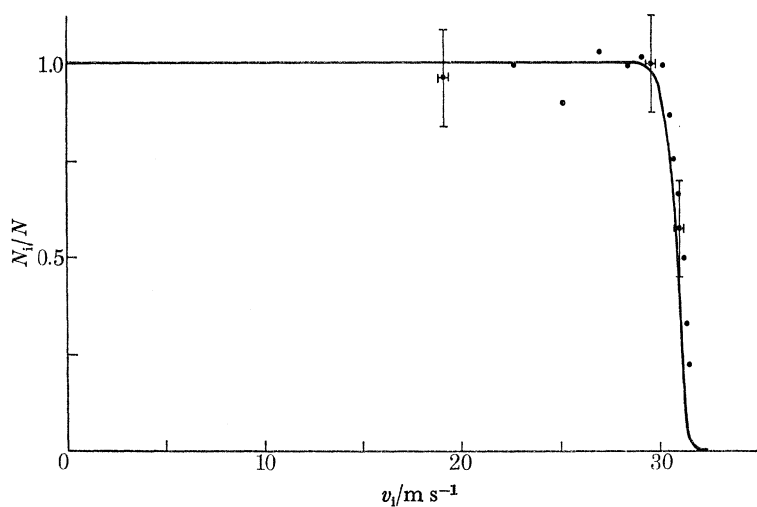
FIGURE 26. Results as in figure 24, except $T = 0.70\,\mathrm{K}$.
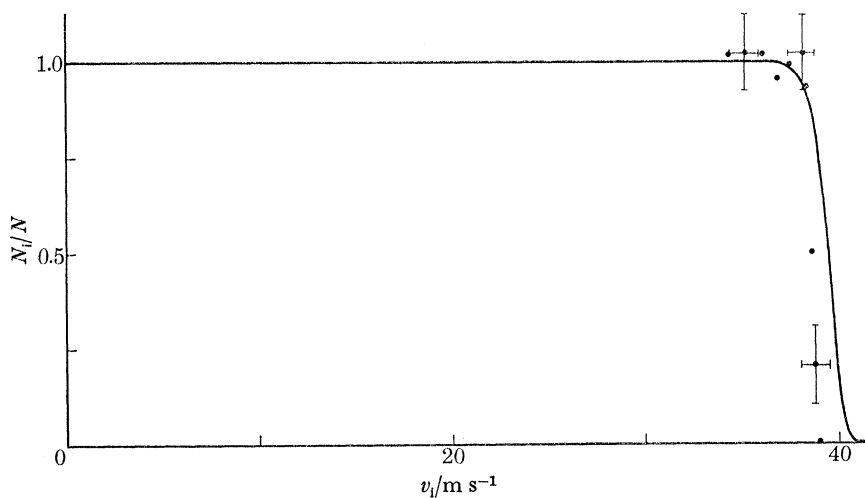
FIGURE 27. Results as in figure 24 but for positive ions, $T = 0.60\,\mathrm{K}$, $R_i = 0.65\,\mathrm{nm}$, $P = 0$, $a = 0.128\,\mathrm{nm}$.

R. J. DONNELLY AND P. H. ROBERTS
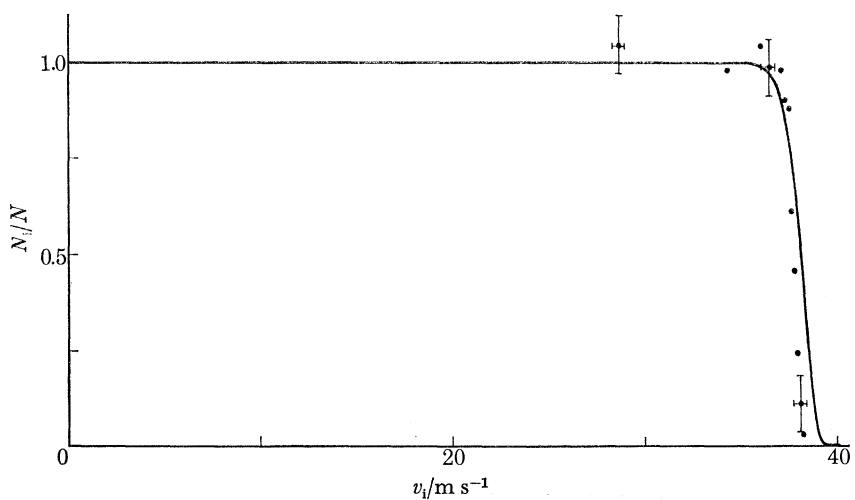
FIGURE 28. Results as in figure 27, except $T = 0.65$ K.
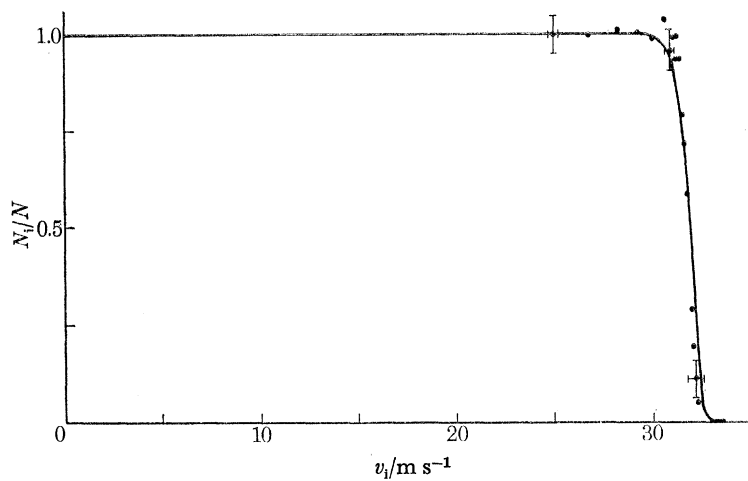
FIGURE 29. Results as in figure 27, except $T = 0.70$ K.
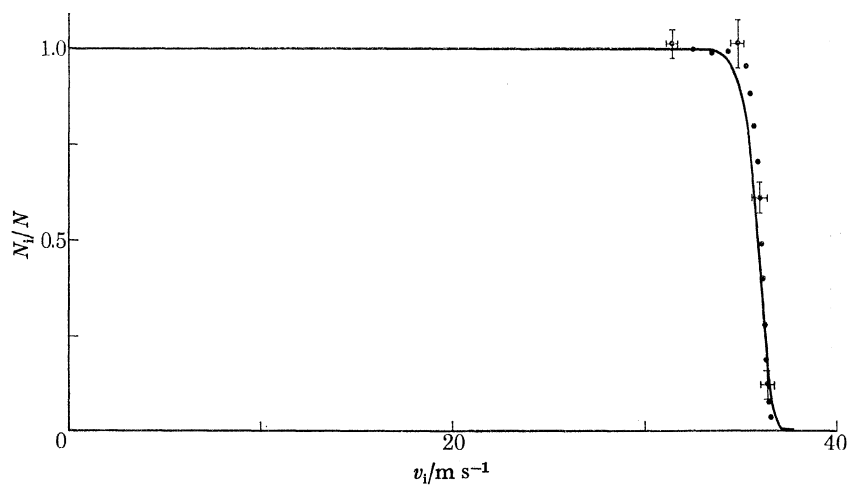
FIGURE 30. Results as in figure 27, except $T = 0.75$ K.

8. Roton–phonon relaxation times: the attenuation of sound

We referred at the end of § 2 to the adjustment of the population of rotons and phonons across the barrier B of figure 1. Consider the presence of a sound wave in otherwise quiescent liquid helium. On compressing the helium adiabatically, the value of Δ/k will be reduced, the velocity of sound will increase, and N_r and N_p will tend to adjust towards equilibrium values corresponding to these new conditions. The rate of redistribution of energy will depend on the details of the populations, and in general one would expect the phonon gas to adjust its population in some characteristic relaxation time, the roton gas in another, with yet a third accounting for the inter-conversion of phonons and rotons. If the frequency of the sound wave is comparable with the reciprocal of any of these relaxation times, one can, in general, expect absorption to occur.
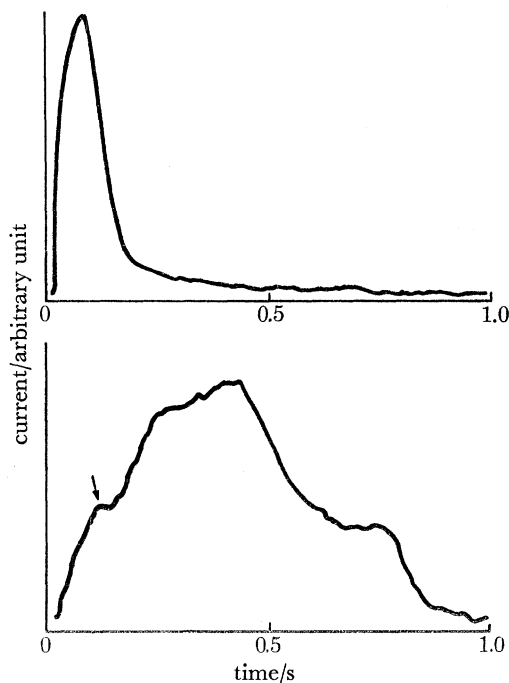
FIGURE 31. (a) Ion pulse produced by negative ions traversing a time-of-flight path of 5 cm at $T = 0.74$ K. The transit time is too rapid to resolve the arrival time. The voltage, 181.9 V, was just below the lifetime edge so that $N_i/N \cong 1$.   (b) Result of raising the voltage to 213.9 V, the lifetime edge region. The ion pulse, indicated by the arrow, can be seen with its peak at the same time as in (a), but its amplitude considerably reduced. The lost ions appear attached to rings which move much more slowly, and because they nucleate at random throughout the flight path, produce the large irregular pulse shown here.

The theory of these processes was pioneered by Khalatnikov. It is, of course, detailed, and may be consulted in various references, notably Khalatnikov (1965), Wilks (1967) and Keller (1969). Our discussion has to do only with the phonon–roton conversion process, and we shall have reference to the work of Dransfeld, Newell & Wilks (1958).

Khalatnikov considers the roton–phonon process

$$R_1 + P_1 \rightleftharpoons R_2 + R_3, \tag{8.1}$$

which will occur with appreciable probability only if the phonon on the left has an energy of the

order of Δ. Khalatnikov finds that if the rate of change of phonon and roton populations is written as

$$\dot{N}_p = \Gamma_{pr}(\mu_r - \mu_p), \quad \dot{N}_r = -\Gamma_{pr}(\mu_r - \mu_p), \tag{8.2}$$

then

$$\Gamma_{pr} \sim 4 \times 10^{49}\, e^{-2\Delta/kT}, \tag{8.3}$$

where the numerical coefficient is obtained by comparison with experiment. The corresponding relaxation time θ_{rp} is given by

$$\frac{1}{\theta_{rp}} = 4 \times 10^{49}\, e^{-2\Delta/kT} \left(\frac{\partial\mu_r}{\partial N_r} + \frac{\partial\mu_p}{\partial N_p}\right)_{\rho, S}. \tag{8.4}$$

In (8.3) and (8.4) the chemical potentials of roton (μ_r) and phonon (μ_p) and their variations are estimated by Dransfeld *et al.* in an appendix. Numerical values of $1/\theta_{rp}$ are given in table 12 using the (now slightly dated) numerical constants of the authors. One can see that sound of the order of 10 MHz will be affected by the phonon–roton conversion process at temperatures just below 1 K.

The theory considered in this paper offers an alternative view of this relaxation process. We can imagine that instead of the collision process (8.1), rotons can diffuse over the barrier B (of figure 1) as the result of many collisions. In doing the calculation we shall retain the view that the roton is a small ring in order to estimate the appropriate diffusion constants. Although this is a drastic assumption it leads to cross-sections near B of the order of those used by Khalatnikov.

If we imagine the roton and phonon populations are perturbed, equilibrium will be restored by conversion of rotons to phonons (P_{rp}) and phonons to rotons (P_{pr}) according to the relations

$$\dot{N}_r = -P_{rp}N_r + P_{pr}N_p, \tag{8.5}$$

and

$$\dot{N}_p = -P_{pr}N_p + P_{rp}N_r. \tag{8.6}$$

In the steady state

$$P_{pr} = (N_r/N_p)\, P_{rp}, \tag{8.7}$$

and it is an easy matter to show from (8.5) and (8.6) that the deviations from this state decay aperiodically at the e-folding rate of

$$\lambda = P_{rp} + P_{pr} = (1 + N_r/N_p)\, P_{rp}, \tag{8.8}$$

where we have used (8.7) in the last step.

The expression for P_{rp} for the escape of rotons from their well, or more precisely, their trough in three-dimensional momentum space, over the maximum point, or more precisely the rim, has been given in (3.40):

$$P_{rp} = \frac{\Lambda_c \omega_A \omega_C}{2\pi} \left(\frac{p_c}{p_0}\right)^2 e^{-\Delta E/kT}, \tag{8.9}$$

where ω_A^2 ($= 1/\mu_0$) is the curvature of the roton trough, ω_C^2 ($= 1/0.53m$) is the curvature of the rim, p_0 is the momentum of the trough, p_C ($\simeq 11.1\hbar\,\text{nm}^{-1}$) that of the rim and E_C ($= 13.97k\,\text{K}$) its energy. For Λ_C we use the expression we have employed in previous sections, obtaining $7.67 \times 10^{-5}\alpha\rho_s^{-\frac{1}{2}}\,\text{g/s}$ where α and ρ_s are the quantities listed in the appendix.

The results for λ are shown in table 12 compared with the results for $1/\theta_{rp}$ given by Dransfeld *et al.* One can see that λ and $1/\theta_{rp}$ are generally comparable in magnitude and temperature dependence—values of $1/\theta_{rp}$ are not considered to give quantitative agreement with experiment.

The present calculations may be easily extended to take into account the effects of pressure and added helium-3 as described in the appendix. Using equation (A 8) we have recomputed λ for a series of concentrations at $T = 1.2$ K. The results are shown in table 13, and they show that added ^{3}He increases λ substantially, the effect being in some ways equivalent to raising the temperature.

TABLE 12. COMPARISON OF RELAXATION TIMES ON KHALATNIKOV'S
AND THE PRESENT MODELS

T/K	$\theta_{\mathrm{rp}}^{-1}/\mathrm{s}^{-1}$	λ/s^{-1}
0.6	9.29×10^4	1.02×10^3
0.7	1.26×10^6	2.69×10^4
0.8	1.02×10^7	3.40×10^5
0.9	6.16×10^7	2.61×10^6
1.0	2.78×10^8	1.46×10^7
1.1	9.58×10^8	6.40×10^7
1.2	2.64×10^9	2.29×10^8
1.4	1.24×10^{10}	1.88×10^9
1.6	3.75×10^{10}	1.00×10^{10}

The methods described in this section are, in a sense, an opposite extreme to Khalatnikov's 'lucky collision' model of (8.1). In our model, which depends upon a diffusion process, and hence many collisions, a finite time of order $(p_C - p_0)^{\frac{3}{2}}/\beta_e kT$ (cf. remarks below 3.18) must elapse before a new population suddenly set up at the bottom of the roton trough can establish, by diffusion, the equilibrium current used in the calculation above. This time at $0.8\,\mathrm{K}$ is of order $2 \times 10^{-8}\,\mathrm{s}$. Were this not small compared with the period ($\approx 10^{-7}\,\mathrm{s}$) of the sound wave, our diffusion process could not operate. The process (8.1), however, would still be viable. The validity of the processes we have proposed would have to be resolved, in a given experimental situation, by investigating the number of phonon–roton and roton–roton collisions which occur during one cycle of the transducer.

TABLE 13. EFFECT OF ADDING ^{3}HE ON THE ROTON–PHONON RELAXATION TIME

%^{3}He	0	0.5	1.0	2.0	3.0	4.0	5.0
λ/s^{-1}	2.29×10^8	3.63×10^8	4.97×10^8	7.63×10^8	1.03×10^9	1.30×10^9	1.56×10^9

APPENDIX. DERIVATION OF NUMERICAL CONSTANTS USED
IN THE CALCULATIONS

The calculations described in the body of this paper cover a wide range of temperatures and involve the use of a number of constants whose experimental magnitudes are still subject to considerable uncertainty. We present, therefore, a short discussion of the origin of our estimates, and tables of their values.

Table A 1 presents values of ρ_n, ρ_s, ρ_s/ρ_λ and $\rho_\lambda T/\rho_s$ from $1.1\,\mathrm{K}$ to the λ-point. Values for ρ_n from $T = 1.1$ to $T = 1.98\,\mathrm{K}$ were calculated by Tough, McCormick & Dash (1963) from experimental specific heat and second sound data. Values of ρ_s in this range were calculated from $\rho_s = \rho_\lambda - \rho_n$, where $\rho_\lambda = 0.1459\,\mathrm{g\,cm^{-3}}$. Actually ρ varies from 0.1459 at T_λ to $0.1450\,\mathrm{g/cm^3}$ at $0\,\mathrm{K}$; this difference has been neglected throughout since using ρ_λ leads to the best agreement near T_λ where small differences are important, and gives less than 1 % error at lower temperatures. A number of experimental investigations have shown that near T_λ, $\rho_s/\rho_\lambda = A(T_\lambda - T)^{\frac{2}{3}}$. This is an asymptotic relation valid only very near T_λ; we have chosen a value of $A = 1.43$ (Tyson & Douglass 1966) which makes ρ_s agree fairly closely with the other estimate at $2\,\mathrm{K}$. The point where data from second sound is joined to oscillatory disk data is $T = 2\,\mathrm{K}$.

Table A 2 gives values of Δ/k. In the range 0 to $2\,\mathrm{K}$ we have used an expression due to Bendt, Cowan & Yarnell (1959)

$$\Delta/k = 8.68 - 0.0084\,T^7. \tag{A 1}$$

TABLE A1

T/K	ρ_n	ρ_s	$\Delta T/\mathrm{mK}$	$\rho_\mathrm{s}/\rho_\lambda$	$\rho_\lambda\, T/\rho_\mathrm{s}$
1.10	0.00212	0.1438	1072	0.986	1.12
1.20	0.00405	0.1419	972	0.973	1.23
1.30	0.00686	0.1390	872	0.953	1.36
1.40	0.0108	0.1351	772	0.926	1.51
1.45	0.0136	0.1323	722	0.907	1.60
1.50	0.0165	0.1294	672	0.887	1.69
1.55	0.0205	0.1254	622	0.859	1.80
1.60	0.0247	0.1212	572	0.831	1.93
1.65	0.0289	0.1170	522	0.802	2.06
1.70	0.0346	0.1113	472	0.763	2.23
1.75	0.0400	0.1059	422	0.726	2.41
1.80	0.0472	0.0987	372	0.676	2.66
1.82	0.0504	0.0955	352	0.655	2.78
1.84	0.0536	0.0923	332	0.633	2.91
1.86	0.0568	0.0891	312	0.611	3.04
1.88	0.0600	0.0859	292	0.589	3.19
1.90	0.0624	0.0835	272	0.572	3.32
1.92	0.0678	0.0781	252	0.535	3.59
1.94	0.0702	0.0757	232	0.519	3.74
1.96	0.0740	0.0719	212	0.493	3.98
1.98	0.0778	0.0681	192	0.467	4.24
2.00	0.0814	0.0645	172	0.442	4.52
2.02	0.0865	0.0594	152	0.407	4.96
2.04	0.0919	0.0540	132	0.371	5.50
2.06	0.0974	0.0485	112	0.332	6.20
2.08	0.1034	0.0425	92	0.291	7.15
2.10	0.1098	0.0361	72	0.247	8.50
2.11	0.1132	0.0327	62	0.224	9.42
2.12	0.1168	0.0291	52	0.199	10.7
2.13	0.1207	0.0252	42	0.173	12.3
2.14	0.1249	0.0210	32	0.144	14.9
2.15	0.1295	0.0164	22	0.112	19.2
2.16	0.1350	0.0109	12	0.0750	28.8
2.161	0.1356	0.0103	11	0.0707	30.6
2.162	0.1362	0.00968	10	0.0664	32.6
2.163	0.1369	0.00903	9	0.0619	34.9
2.164	0.1376	0.00835	8	0.0572	37.8
2.165	0.1383	0.00763	7	0.0523	41.4
2.166	0.1390	0.00689	6	0.0472	45.9
2.167	0.1398	0.00610	5	0.0418	51.8
2.168	0.1406	0.00526	4	0.0360	60.2
2.169	0.1416	0.00434	3	0.0297	73.0
2.170	0.1426	0.00331	2	0.0227	95.6
2.171	0.1438	0.00209	1	0.0143	152
2.172	0.1459	0	0	0	—

TABLE A2

(In this table the second figure in an entry indicates the power of 10, e.g. $2.18-15 \equiv 2.18 \times 10^{-15}$.)

T/K	Δ/k	α_r	α_3	α_p	α	N_r	αN_r
0.01	8.68	0	2.18 −15	5.59 −21	2.18 −15	0	0
0.02	8.68	0	3.08 −15	8.94 −20	3.08 −15	0	0
0.04	8.68	0	4.36 −15	1.43 −18	4.36 −15	6.10 −73	2.66 −78
0.06	8.68	2.94 −69	5.34 −15	7.24 −18	5.35 −15	1.94 −41	1.04 −55
0.08	8.68	1.50 −53	6.17 −15	2.29 −17	6.19 −15	1.14 −25	7.06 −40
0.10	8.68	3.97 −44	6.90 −15	5.59 −17	6.95 −15	3.38 −16	2.35 −30
0.15	8.68	1.46 −31	8.45 −15	2.83 −16	8.73 −15	1.52 −3	1.33 −17

TABLE A 2 *(cont.)*

T/K	Δ/k	α_r	α_3	α_p	α	N_r	αN_r
0.20	8.68	2.80 −25	9.75 −15	8.94 −16	1.06 −14	3.38 3	3.59 −11
0.25	8.68	1.65 −21	1.09 −14	2.18 −15	1.31 −14	2.22 7	2.91 −7
0.30	8.68	5.38 −19	1.19 −14	4.52 −15	1.65 −14	7.93 9	1.31 −4
0.35	8.68	3.35 −17	1.29 −14	8.38 −15	2.13 −14	5.34 11	1.14 −2
0.40	8.68	7.44 −16	1.38 −14	1.43 −14	2.88 −14	1.27 13	3.66 −1
0.45	8.68	8.30 −15	1.46 −14	2.29 −14	4.58 −14	1.50 14	6.87
0.50	8.68	5.71 −14	1.54 −14	3.49 −14	1.07 −13	1.09 15	1.17 2
0.55	8.68	2.77 −13	1.62 −14	5.11 −14	3.44 −13	5.53 15	1.90 3
0.60	8.68	1.03 −12	1.69 −14	7.24 −14	1.12 −12	2.15 16	2.41 4
0.65	8.68	3.14 −12	1.76 −14	9.97 −14	3.25 −12	6.81 16	2.22 5
0.67	8.68	4.67 −12	1.79 −14	1.13 −13	4.80 −12	1.03 17	4.95 5
0.70	8.68	8.14 −12	1.82 −14	1.34 −13	8.29 −12	1.83 17	1.52 6
0.75	8.68	1.86 −11	1.89 −14	1.77 −13	1.88 −11	4.34 17	8.16 6
0.80	8.68	3.84 −11	1.95 −14	2.29 −13	3.86 −11	9.24 17	3.57 7
0.85	8.68	7.26 −11	2.01 −14	2.92 −13	7.29 −11	1.80 18	1.32 8
0.90	8.68	1.28 −10	2.07 −14	3.66 −13	1.28 −10	3.27 18	4.20 8
1.00	8.67	3.39 −10	2.18 −14	5.59 −13	3.40 −10	9.14 18	3.11 9
1.10	8.66	7.53 −10	2.29 −14	8.18 −13	7.54 −10	2.13 19	1.60 10
1.20	8.65	1.46 −9	2.39 −14	1.18 −12	1.46 −9	4.32 19	6.33 10
1.30	8.63	2.59 −9	2.49 −14	1.62 −12	2.59 −9	7.95 19	2.06 11
1.40	8.59	4.28 −9	2.58 −14	2.22 −12	4.28 −9	1.36 20	5.84 11
1.45	8.57	5.36 −9	2.63 −14	2.55 −12	5.36 −9	1.74 20	9.32 11
1.50	8.54	6.66 −9	2.67 −14	2.92 −12	6.66 −9	2.20 20	1.46 12
1.55	8.50	8.21 −9	2.72 −14	3.39 −12	8.21 −9	2.75 20	2.26 12
1.60	8.45	1.00 −8	2.76 −14	3.85 −12	1.00 −8	3.43 20	3.45 12
1.65	8.40	1.22 −8	2.80 −14	4.43 −12	1.22 −8	4.21 20	5.12 12
1.70	8.34	1.46 −8	2.84 −14	5.08 −12	1.46 −8	5.14 20	7.52 12
1.75	8.26	1.76 −8	2.89 −14	5.80 −12	1.76 −8	6.28 20	1.11 13
1.80	8 17	2.11 −8	2.93 −14	6.61 −12	2.11 −8	7.63 20	1.61 13
1.82	8.12	2.28 −8	2.94 −14	6.91 −12	2.28 −8	8.29 20	1.89 13
1.84	8.08	2.48 −8	2.96 −14	7.21 −12	2.45 −8	8.95 20	2.19 13
1.86	8.03	2.64 −8	2.97 −14	7.66 −12	2.64 −8	9.69 20	2.55 13
1.88	7.98	2.84 −8	2.99 −14	8.00 −12	2.84 −8	1.05 21	2.97 13
1.90	7.93	3.04 −8	3.00 −14	8.49 −12	3.04 −8	1.13 21	3.44 13
1.92	7.87	3.28 −8	3.02 −14	8.86 −12	3.28 −8	1.22 21	4.02 13
1.94	7.81	3.53 −8	3.04 −14	9.23 −12	3.53 −8	1.32 21	4.67 13
1.96	7.75	3.79 −8	3.05 −14	9.79 −12	3.79 −8	1.43 21	5.42 13
1.98	7.68	4.09 −8	3.07 −14	1.02 −11	4.09 −8	1.55 21	6.33 13
2.00	7.63	4.36 −8	3.08 −14	1.08 −11	4.36 −8	1.66 21	7.23 13
2.02	7.57	4.66 −8	3.10 −14	1.12 −11	4.66 −8	1.78 21	8.32 13
2.04	7.51	4.98 −8	3.12 −14	1.17 −11	4.98 −8	1.92 21	9.54 13
2.06	7.46	5.29 −8	3.13 −14	1.26 −11	5.29 −8	2.04 21	1.08 14
2.08	7.39	5.66 −8	3.15 −14	1.31 −11	5.66 −8	2.20 21	1.25 14
2.10	7.33	6.03 −8	3.16 −14	1.41 −11	6.03 −8	2.35 21	1.42 14
2.11	7.29	6.24 −8	3.17 −14	1.44 −11	6.25 −8	2.44 21	1.53 14
2.12	7.26	6.44 −8	3.18 −14	1.49 −11	6.44 −8	2.52 21	1.63 14
2.13	7.22	6.67 −8	3.18 −14	1.55 −11	6.67 −8	2.62 21	1.75 14
2.14	7.17	6.93 −8	3.19 −14	1.60 −11	6.93 −8	2.73 21	1.89 14
2.15	7.12	7.21 −8	3.20 −14	1.63 −11	7.21 −8	2.85 21	2.05 14
2.16	7.06	7.53 −8	3.21 −14	1.67 −11	7.53 −8	2.98 21	2.24 14
2.161	7.05	7.57 −8	3.21 −14	1.67 −11	7.57 −8	3.00 21	2.27 14
2.162	7.05	7.58 −8	3.21 −14	1.67 −11	7.58 −8	3.01 21	2.28 14
2.163	7.04	7.63 −8	3.21 −14	1.67 −11	7.63 −8	3.02 21	2.31 14
2.164	7.03	7.68 −8	3.21 −14	1.68 −11	7.68 −8	3.04 21	2.34 14
2.165	7.02	7.72 −8	3.21 −14	1.71 −11	7.73 −8	3.06 21	2.36 14
2.166	7.01	7.77 −8	3.21 −14	1.71 −11	7.77 −8	3.08 21	2.39 14
2.167	7.00	7.82 −8	3.21 −14	1.72 −11	7.82 −8	3.10 21	2.42 14
2.168	7.00	7.83 −8	3.21 −14	1.72 −11	7.83 −8	3.10 21	2.43 14
2.169	6.98	7.91 −8	3.21 −14	1.72 −11	7.92 −8	3.14 21	2.49 14
2.170	6.97	7.96 −8	3.21 −14	1.73 −11	7.96 −8	3.16 21	2.52 14
2.171	6.96	8.01 −8	3.21 −14	1.73 −11	8.01 −8	3.18 21	2.55 14
2.172	6.93	8.14 −8	3.21 −14	1.77 −11	8.14 −8	3.23 21	2.63 14

Above 2 K no direct measurements of Δ/k have been made. Experiments by Henshaw & Woods (1961) valid near the roton minimum show that Δ/k falls as T_λ is approached, but the line width of the scattered neutrons becomes so broad that a large experimental uncertainty remains. We have, therefore, chosen Δ/k to be that value which, on the Landau theory of independent quasi-particles, gives the observed value of ρ_n near the λ-point, namely

$$\rho_n = \frac{2\mu^{\frac{1}{2}}p_0^4 \, e^{-\Delta/kT}}{3(2\pi)^{\frac{3}{2}}(kT)^{\frac{1}{2}}\hbar^3},\tag{A 2}$$

assuming $p_0/\hbar = 19.1\,\mathrm{nm}^{-1}$ and $\mu = 0.16m$ are independent of temperature. In the absence of better data, this seems to be the most consistent procedure we can follow, but it should be emphasized that the values of Δ/k above 2 K are, in fact, fictitious.

The roton densities in column seven of table A 2 are calculated from the values of Δ/k by the relation

$$N_r = 3kT\rho_n/p_0^2.\tag{A 3}$$

Although the preceding relation breaks down for high densities of excitations, it is interesting that N_r stays considerably lower than the atomic density $(= \rho/m)$ consistent with the notion that each roton involves a number of atoms in its motion. Values of N_r chosen in this way are reasonably consistent with experimental values of ρ_n down to 1 K. Below 1 K only theoretical values are available because of free path effects.

Table A 2 lists the vortex line energy loss coefficient α in column six, and the roton, ^{3}He, and phonon parts of that coefficient:

$$\alpha = \alpha_r + \alpha_3 + \alpha_p.\tag{A 4}$$

These coefficients were introduced by Rayfield & Reif (1964) in the following way. If $\mathscr{F}$ is the total drag force on a vortex ring and $\mathscr{F}'$ the drag force per unit length of line, then the relations among $\mathscr{F}$, $\mathscr{F}'$, D and β are given by

$$\begin{aligned}
\mathscr{F} &= 2\pi R\mathscr{F}'\\
&= 2\pi RDv\\
&= \beta p^{\frac{1}{2}}v\\
&= \tfrac{1}{2}D\kappa[\ln(8R/a) - \tfrac{1}{2}]\\
&= \alpha[\ln(8R/a) - \tfrac{1}{2}].
\end{aligned}\tag{A 5}$$

Thus
$$D = 2\alpha/\kappa \quad \text{and} \quad \beta = 4\alpha(\pi/\rho_s\kappa^3)^{\frac{1}{2}},\tag{A 6}$$

which relates Hall's (1960) drag coefficient and the dynamical friction constant of the present theory to α. Rayfield & Reif then consider the detailed kinetic evaluation of α_r, α_3 and α_p in an appendix to their work. They derive the expressions

$$\alpha_r = \frac{3\pi^2}{8}\frac{\kappa}{\hbar^3}p_0^4\, e^{-\Delta/kT}\,\sigma_{r0},\tag{A 7}$$

$$\alpha_3 = \tfrac{3}{8}\kappa(2\pi m^* kT)^{\frac{1}{2}}n_3\,\sigma_{30},\tag{A 8}$$

$$\alpha_p = \frac{\pi^6}{20}\frac{\kappa}{\hbar^3}\left(\frac{kT}{u_1}\right)^4\sigma_{p0}.\tag{A 9}$$

Analysis of their experiments produced the following values for the collision cross-sections:

$$\sigma_{r0} = 0.95\,\mathrm{nm}, \quad \sigma_{30} = 1.83\,\mathrm{nm}, \quad \sigma_{p0} = 0.03\,\mathrm{nm}.\tag{A 10}$$

The effective mass of a solvated ^{3}He atom is $m^* = 2.5m_{^3\text{He}}$ and n_3 is the number density of solvated ^{3}He atoms, which we have taken as $(n_3/n_4) = 1.4 \times 10^{-7}$, a typical concentration of ^{3}He present in well helium in the United States. The velocity of sound u_1 decreases slowly as T increases in the He II temperature region. An examination of the numbers in table A 2 shows that dissolved ^{3}He atoms dominate the drag below $0.4\,\text{K}$, rotons, phonons, and ^{3}He atoms are roughly equally important at $0.5\,\text{K}$, and above $0.7\,\text{K}$ rotons dominate.

The effects of doping by adding ^{3}He can be estimated by modifying n_3/n_4 in the relation for α_3 up to the point where the concentration may no longer be considered dilute, and phase separation effects occur.

Application of external pressure will modify these coefficients. The variation of parameters with pressure factors is known only roughly. We use

$$\mu_0 = 0.16(1 - 0.0217P)\, m, \tag{A 11}$$

$$p_0/\hbar = 19.1(1 + 0.0029P)\ \text{nm}^{-1}, \tag{A 12}$$

$$\Delta(T, P) = \Delta(T, 0)\,(1 - 0.0075P), \tag{A 13}$$

where P is the applied pressure in atmospheres. The velocity of sound is a function of pressure (see, for example, Donnelly 1967, p. 238); the effective mass m^* for ^{3}He also increases with pressure (see, for example, Wilks 1967, p. 471).

REFERENCES

Andreev, A. F. 1966 *Zh. éksp. teor. Fiz.* **50**, 1415; trans. *Sov. Phys. J.E.T.P.* **23**, 939.

Arms, R. J. & Hama, F. R. 1965 *Phys. Fluids* **8**, 553.

Basset, A. B. 1888 *A treatise on hydrodynamics with numerous examples.* Cambridge: Deighton, Bell and Co.

Bendt, P. J., Cowan, R. D. & Yarnell, J. L. 1959 *Phys. Rev.* **113**, 1386.

Bruschi, L., Mazzoldi, P. & Santini, M. 1968 *Phys. Rev. Lett.* **21**, 1738.

Chandrasekhar, S. 1943 *Rev. Mod. Phys.* **15**, 1.

Clow, J. R. & Reppy, J. D. 1967 *Phys. Rev. Lett.* **19**, 291.

Cowley, R. A. & Woods, A. D. B. 1971 *Can. J. Res.* **49**, 177.

Cunsolo, S. & Maraviglia, B. 1969 *Phys. Rev.* **187**, 292.

Dahm, A. J. 1969 *Phys. Rev.* **180**, 259.

Dahm, A. J. & Sanders, T. M. 1966 *Phys. Rev. Lett.* **17**, 126.

Donnelly, R. J. 1967 *Experimental superfluidity.* Chicago and London: University of Chicago Press.

Donnelly, R. J. & Roberts, P. H. 1969a *Proc. R. Soc. Lond.* A **312**, 519.

Donnelly, R. J. & Roberts, P. H. 1969b *Phys. Lett.* **30** A, 468.

Donnelly, R. J. & Roberts, P. H. 1969c *Phys. Rev. Lett.* **23**, 1491.

Dransfeld, K., Newell, J. A. & Wilks, J. 1958 *Proc. R. Soc. Lond.* A **243**, 500.

Feynman, R. P. 1955 *Progress in low temperature physics*, vol. 1 (ed. C. J. Gorter), ch. 2. Amsterdam: North Holland Publishing Co.

Fineman, J. C. & Chase, C. E. 1963 *Phys. Rev.* **129**, 1.

Fisher, M. E. 1968 *Conference on Fluctuations in Superconductors*, Asilomar, Calif. 13–15 March; edited by W. S. Goree and F. Chilton (Stanford Research Institute, Menlo Park, Calif.).

Fokkens, K., Taconis, K. W. & De Bruyn Ouboter, R. 1966 *Physica* **32**, 2129.

Fraenkel, L. E. 1970 *Proc. R. Soc. Lond.* A **316**, 29.

Gamota, G. & Barmatz, M. 1969 *Phys. Rev. Lett.* **22**, 874.

Gamota, G. & Sanders, T. M. 1968 *Proceedings of LT 11.* (ed. J. F. Allen, D. M. Finlayson & D. M. McCall), vol. 1, p. 261. University of St. Andrews Press.

Glaberson, W. I. & Donnelly, R. J. 1966 *Phys. Rev.* **141**, 208.

Glaberson, W. I., Strayer, D. M. & Donnelly, R. J. 1968 *Phys. Rev. Lett.* **21**, 1740.

Gopal, E. S. R. 1963 *Ann. Phys.* **25**, 196.

Guyon, E. & Rudnick, I. 1969 *J. Phys. Radium* **29**, 1081.

Hall, H. E. 1960 *Phil. Mag. Suppl.* **9**, 89.

Harling, O. K. 1970 *Phys. Rev. Lett.* **24**, 1046.

Henshaw, D. G. & Woods, A. D. B. 1961 *Phys. Rev.* **121**, 1266.

Hill, M. J. M. 1894 *Phil. Trans. R. Soc. Lond.* A **185**, 213.

Huang, K. & Olinto, C. 1965 *Phys. Rev.* **139**, A 1441.

Huggins, E. R. 1966 *Phys. Rev. Lett.* **17**, 1284.

Iordanskiĭ, S. V. 1965 *J. Expt. Theor. Phys. U.S.S.R.* **48**, 708; transl. *Sov. Phys. J.E.T.P.* **21**, 467.

Kawatra, M. P. & Pathria, R. K. 1966 *Phys. Rev.* **151**, 132.

Keller, W. E. 1969 *Helium-3 and helium-4.* New York: Plenum Press.

Khalatnikov, I. M. 1965 *An introduction to the theory of superfluidity*; transl. P. C. Hohenberg. New York, Amsterdam: W. A. Benjamin, Inc.

Kramers, H. A. 1940 *Physica* **7**, 284.

Kukich, G., Henkel, R. P. & Reppy, J. D. 1968 *Phys. Rev. Lett.* **21**, 197.

Langer, J. S. & Fisher, M. E. 1967 *Phys. Rev. Lett.* **19**, 560.

Langer, J. S. & Reppy, J. D. 1970 *Progress in low temperature physics*, vol. VI (ed. C. J. Gorter), p. 1. Amsterdam: North Holland Publishing Co.

Mehl, J. B. & Zimmermann, W., Jr. 1968 *Phys. Rev.* **167**, 214.

Neeper, D. A. & Meyer, L. 1969 *Phys. Rev.* **182**, 223.

Notarys, H. A. 1969 *Phys. Rev. Lett.* **22**, 1240.

Rayfield, G. W. 1967 *Phys. Rev. Lett.* **19**, 1371.

Rayfield, G. W. 1968 *Phys. Rev.* **168**, 222.

Reppy, J. D. 1965 *Phys. Rev. Lett.* **14**, 733.

Rayfield, G. W. & Reif, F. 1964 *Phys. Rev.* **136**, A 1194.

Roberts, P. H. & Donnelly, R. J. 1970*a Phys. Lett.* **31** A, 137.

Roberts, P. H. & Donnelly, R. J. 1970*b Phys. Rev. Lett.* **24**, 367.

Roberts, P. H. & Donnelly, R. J. 1971 (to be published).

Roberts, P. H. & Grant, J. 1971 *J. Phys.* A 4, 55.

Schwarz, K. W. & Stark, R. W. 1969 *Phys. Rev. Lett.* **22**, 1278.

Strayer, D. M. 1971 Structure and nucleation of quantized vortices in helium II. Thesis. Department of Physics, University of Oregon, Eugene.

Strayer, D. M., Donnelly, R. J. & Roberts, P. H. 1971 *Phys. Rev. Lett.* **26**, 165.

Tough, J. T., McCormick, W. D. & Dash, J. G. 1963 *Phys. Rev.* **132**, 2373.

Tyson, J. A. & Douglass, D. H., Jr. 1966 *Phys. Rev. Lett.* **17**, 472.

Vinen, W. F. 1963 *Liquid helium*, Course 21, International School of Physics, 'Enrico Fermi' (ed. G. Careri), p. 336. New York and London: Academic Press.

Vinen, W. F. 1966 *Quantum fluids* (ed. D. F. Brewer), p. 104. Amsterdam: North Holland Publishing Co.

Wilks, J. 1967 *Liquid and solid helium.* Oxford: Clarendon Press.

Wing, W. H. & Sanders, T. M. 1967 *Rev. scient. Instrum.* **38**, 1341.

Woods, A. D. B. 1966 *Quantum fluids* (ed. D. F. Brewer). Amsterdam: North Holland Publishing Co.

Zinovyeva, K. N. & Bolarev, S. T. 1968 *Proceedings of LT 11* (ed. J. F. Allen, D. M. Finlayson & D. M. McCall), vol. I, p. 367. University of St Andrews Press.